Theoretical Simulation of Nonlinear Spectroscopy in the Liquid Phase

Thomas la Cour Jansen

Front cover: The calculated fifth-order Raman response $\chi^{(5)}_{mmzzzz}$ with three different polarizability models. (Chapter 7)

Thomas la Cour Jansen,

Theoretical Simulation of Non-linear Spectroscopy in the Liquid Phase,

Proefschrift Rijksuniversiteit Groningen.

RIJKSUNIVERSITEIT GRONINGEN

Theoretical Simulation of Nonlinear Spectroscopy in the Liquid Phase

PROEFSCHRIFT

ter verkrijging van het doctoraat in de
Wiskunde en Natuurwetenschappen
aan de Rijksuniversiteit Groningen
op gezag van de
Rector Magnificus, dr. F. Zwarts,
in het openbaar te verdedigen op
vrijdag 13 september 2002
om 16.00 uur

door

Thomas la Cour Jansen

geboren op 25 november 1974
te Gentofte (Denemarken)

voor Sara en Frida

Contents

Chapter 1

General Introduction

The vast majority of chemical reactions of everyday life, organic synthesis, biochemistry and medicine takes place in the liquid phase. Most of these reactions are dominated by the dynamics of the liquid instead of the direct reactivity of the reacting species. For example, it might be more important what time it takes for two reactants to get close together, than what time it takes to break and form new bonds. Furthermore, the interaction of a transition state with the surrounding liquid directly affects the reaction pathway and this interaction cannot always be taken into account correctly by assuming only one reaction coordinate. Nevertheless, the effects of friction and diffusion on chemical reactions has often been taken into account in effective approximate ways using one effective reaction coordinate in a traditional transition state picture. [1–12] In Figure 1.1 this picture is shown. The wavy line above the transition state illustrates the friction originating from the interaction between the reactants and the surrounding liquid. In order to improve the understanding of complex reactions in the liquid phase our knowledge about liquid structure and dynamics has to be extended.

The first experimental studies on liquid dynamics were performed by Brown, [13, 14] who observed irregular motion of particles floating in liquids. This phenomenon was later attributed to the impact of the molecules in the liquid on the particles by Gouy. [15] In the beginning of the last century Einstein and Smoluchowski developed quantitative theories for the Brownian motion [16] and derived the diffusion equation. [17] These theories treat the liquid as a collection of infinitely small particles, an assumption that breaks down when the motion of molecules in the liquid is studied in a detailed way. On short timescales the dynamics depends on the detailed molecular interaction while on longer timescales the motion can still be described effectively by the diffusion law. Langevin extended the

FIGURE 1.1: *The transition state picture of a chemical reaction with solvent effects as friction illustrated with the wavy line.*
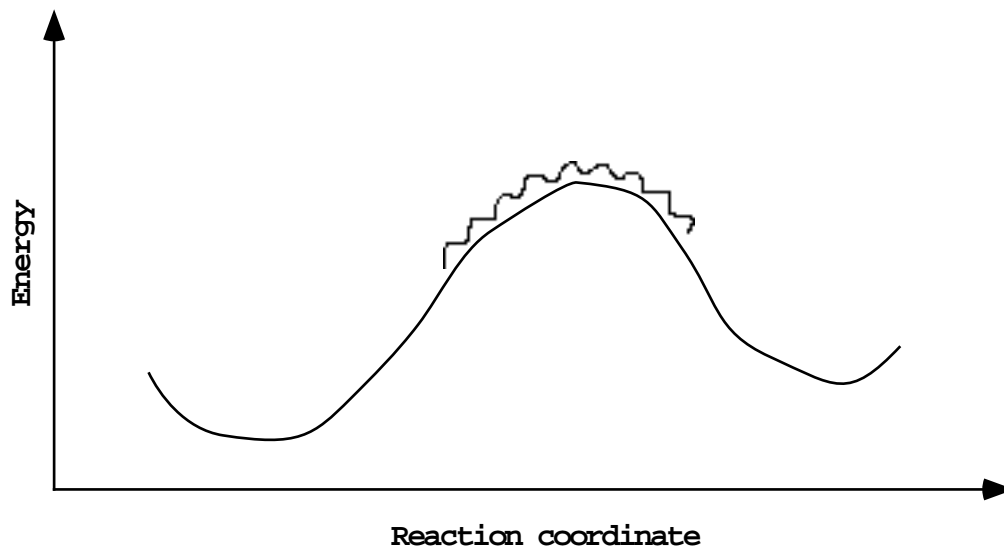
theories to include forces introduced by interaction between the molecules giving rise to damping. [1, 18]

Later models of liquids on a 'microscopic' level were constructed by Morrell and Hildebrand, using large numbers of gelatine balls to respresent the molecules. [19] The development of the computer allowed using abstract numerical models of liquids on the microscopic level. [20] Using the early computers, studies of liquids were performed using Monte Carlo simulations [21] and later hardsphere [22, 23] and soft-particle [24] Molecular Dynamics simulations in which Newtons equations of motion are solved numerically. Computers and simulation methods have improved a lot since then, allowing simulation of more complex liquids as well as proteins and other macromolecules in solution. [25] Even interactions and motion of quantum nature can be taken into account. [26]

1.1   Multi dimensional spectroscopy

Experimentally the interactions and dynamics in liquids manifest themself in various types of traditional one-dimensional spectroscopies (as Nuclear Magnetic Resonance (NMR), Infrared spectroscopy (IR), Raman spectroscopy etc.). Phenomena such as line broadening and spectral shifts of the spectra contain information on both the dynamics of the liquid

and intermolecular interactions. However, the information obtained in this way is not very clear, since different physical phenomena give rise to very similar effects in the observed response. More information can be obtained using multi-dimensional spectroscopies.

In 1950 the NMR spin echo experiment for the first time allowed the determination of different line broadening mechanisms. [27] With two sets of radio frequency pulses it was possible first to induce Larmor precession of the nuclear spins with their individual Larmor frequencies and later revert the precession to produce a spin echo. In this way it was possible to distinguish beween line broadening caused by slightly different Lamor frequencies due to different static environments around the nuclei and line broadening caused by interactions and motion on a timescale faster than the precession. This was the first example of a two-dimensional spectroscopy and developments in two-dimensional NMR now allows techniques with names such as COSY and NOESY to study complicated structures as those of proteins and even following protein folding processes on μs time scales. [28–30]

Theoretically, Feynman and coworkers showed that the concepts of NMR can be transfered to optical spectroscopies. [31] This leads to the photon echo experiment, [32] which in particular with the use of two color pulses allows a full analysis of the optical dynamics analogous to that of two-dimensional NMR techniques. [33, 34] In 1993 Tanimura and Mukamel suggested the use of 2D Raman response to resolve the low frequency modes found in liquids [35] and a lot of effort was put into measuring this response [36–45]. Both one- and two-dimensional Raman response will be treated from a theoretical point of view in this thesis. In recent years also two-dimensional versions of IR spectroscopy were developed. [46–48] The advantage of these methods is that they are able to probe motion on a much shorter timescales than NMR. The different nature of the methods means that they probe different kinds of motion and structural dynamics and hence the various multi-dimensional spectroscopies should rather been seen as complementing each other than competing.

1.2   Outline

In this thesis the work on developing a new method for theoretical simulation of the nonlinear Raman response of liquids will be presented together with theoretical and experimental achievements gained on the way. In chapter 2 the fundamental theory behind nonlinear optical response in general [49–51] and time-resolved stimulated Raman scattering in par-

ticular [52] will be outlined. Furthermore, considerations about polarization directions and symmetry [53–56] will be presented. In this chapter the problems with cascaded processes contaminating the experimentally observed response will also be treated. [41, 55, 56]

The finite field method, [55, 56] developed in this work, will be described in chapter 3 and compared with methods based on classical time correlation functions. [50, 57–59] The advantages and disadvantages of the different methods will be considered.

In chapter 4 the local field effects in the polarizability, giving rise to response from intermolecular motion, will be discussed and a model to take these effects into account in the simulations will be described. [60–62] Additionally the way to find the forces exerted in the liquid when a pair of optical pump pulses are applied will be treated together with some computational tricks used in the implementation. [56, 62]

Time-dependent density functional theory (TDDFT [63]) calculations, performed to calculate polarizabilities and optimize the polarizability model described in chapter 4, are treated in chapter 5. [62] Calculations on both the monomer and dimers of carbon disulfide are presented. The importance of different types of effects on the many-body polarizability are analysed.

In chapter 6 the conditions for the molecular dynamics (MD) simulations on carbon disulfide are described as well as some of the properties found for liquid CS_2 in these simulations. It is also discussed how these simulations can eventually be improved.

The simulated one-dimensional spectrum using the finite field method is presented in chapter 7 and compared with the results obtained with the time correlation function method. [55] Furthermore, the importance of local field effects is investigated [62] and the one-dimensional response is compared with experiments. The two-dimensional response is also calculated and the intensity ratio between the cascaded response and the true two-dimensional response is estimated for different polarization directions. [56]

In chapter 8 simulations of the one-dimensional response from an idealized mixture are performed and the results are compared with experimental results on carbon disulfide / alkane mixtures obtained by Audrius Pugzlys and Gheorghe Dan Crînguş at the Ultrafast Laser Laboratory, Rijksuniversiteit Groningen, in connection with this study. [64] Changes made in the idealized simulations are used to interpret the experimentally observed spectra which provides insight unto the microscopic structural changes and dynamics when mixing carbon disulfide with different alkane compounds.

Finally in chapter 9 the study of electron overlap effects in the one-dimensional spectrum of liquid xenon is presented. Liquid xenon is especially suited for studying these effects

since xenon does not give rise to either single molecules response or induced multipole effects that together dominate the carbon disulfide response. [65]

Chapter 2

Nonlinear optical response

More than 70 years after C.V. Raman discovered Raman scattering [66,67], Raman spectroscopy has become a widespread technique that is used in many areas of science. In the last decade, the conventional methods, based on determining the characteristics of the spontaneous light scattering spectrum, have been supplemented by a number of femtosecond techniques, relying on stimulated light scattering. In these experiments, that have been extensively applied in experimental studies of the intra- and intermolecular dynamics of liquids and solutions, a short optical pulse perturbs a sample in equilibrium through a Raman interaction. After a period of free evolution another, variably delayed optical pulse is employed to probe the state of the sample. Examples of experiments that are aimed at the low frequency, intermolecular part of the Raman spectrum, are the (heterodyned) optical Kerr effect [68,69] and transient grating scattering [70,71]. The main advantage of these time domain methods is that for short enough pulses the excitation occurs impulsively, so that it is possible to observe the induced motions in real time, rather than as a resonance. In particular the initial, short time dynamics can be clearly followed, while that information is hidden in the wings of frequency domain spectra. Despite these operational advantages, however, it should be realized that the information content of time and frequency domain experiments is, in principle, identical. They are both determined by the accessible Raman modes of the liquid and are simply related by Fourier transforms.

Recently, the use of two-dimensional (2D-) Raman spectroscopy has been suggested [35]. In these experiments there are two Raman perturbations of the sample, separated by a variable period of free evolution, before the state of the sample is probed after a second independently variable delay. Such experiments are expected to yield considerably more information on the structural dynamics of liquids than the one-dimensional (in either

time- or frequency-domain) experiments discussed above. The 2D-experiments do not just depend on the overall Raman spectrum of the liquid, but also on dynamical details that give rise to this spectrum. For instance, it should be possible to determine whether the spectra are dominated by ultrafast fluctuations on a local, molecular scale, or by density fluctuations on a much larger length scale [35, 72]. In limiting cases this may be described as homogeneous line broadening, arising from the interaction of a system with a fast heat bath, and inhomogeneous line broadening, due to a slowly fluctuating distribution of local environments, respectively. Also, the experiments are expected to be sensitive to mode coupling effects, similar to the well-known coupling effects between spins in 2D-NMR [36, 37].

In the last few years, the two-dimensional off-resonant Raman response has been measured experimentally by various groups [38–41]. The shape of these spectra was not understood until very recently, when Blank *et al.* [41] demonstrated experimentally that the two-dimensional Raman spectrum is dominated by third-order cascade processes. The true fifth-order response that contains all the information about the line broadening and the mode coupling mechanisms, is apparently much weaker than these cascading lower order processes. More recently new experimental methods were developed. These use heterodyne detection [42] or two-color interactions [43–45] to improve the discrimination against the cascading processes.

In this chapter the theory behind the third- and fifth-order Raman response will be treated. First a brief review of the perturbation treatment of nonlinear optics will be given [49–51, 72]. This treatment is not only valid for the third- and fifth-order Raman response, but also for many other type of experiments. In section 2.1 the general quantum mechanical response functions will be derived. In section 2.2 the first-, third- and fifth-order Raman response functions will be found, assuming that the Born-Oppenheimer approximation [73] holds and that the nuclear and electronic dynamics can be separated.

In section 2.3 the third- and fifth-order Raman processes, which are the main topic in this thesis, will be described and the symmetry of the polarization directions will be considered. Finally in section 2.4 the cascade processes that have been shown to contaminate the measured fifth-order response [41, 55, 56, 74, 75] are treated. A way to estimate the intensity ratio between the true fifth-order response and the cascaded processes will be presented together with considerations about how this ratio can be optimized to suppress the cascaded response.

2.1   Quantum mechanical response functions

When exposing a material to an electromagnetic field a polarization will be induced in the material. The polarization of the material can in general be expanded in parts depending on different powers of the perturbing electric field. [50, 72]

$$P(t) = P^{(0)}(t) + P^{(1)}(t) + P^{(2)}(t) + P^{(3)}(t) + P^{(4)}(t) + P^{(5)}(t) + \cdots \tag{2.1}$$

Here $P^{(0)}(t)$ is independent of the applied field, $P^{(1)}(t)$ is the linear response and in general $P^{(n)}(t)$ depends on the perturbing electric field to the power n. When one or more time-dependent electric fields E are present, these polarizations are given by the time-dependent response functions $R^{(n)}$ as

$$P_p^{(n)}(t) = \int\limits_{-\infty}^{t} dt_n \int\limits_{-\infty}^{t_n} dt_{n-1} \cdots \int\limits_{-\infty}^{t_2} dt_1 \, R_{pp_n\cdots p_1}^{(n)}(t, t_n, \cdots, t_1) E_{p_n}(t_n) \cdots E_{p_1}(t_1). \tag{2.2}$$

The time-dependent response functions $R_{pp_n\cdots p_1}^{(n)}(t, t_n, \cdots, t_1)$ determine the induced polarization in the direction p at time t if the n electric fields with polarization directions p_1 to p_n where applied instantaneously at times t_1 to t_n. The integrals over the different times take into account that the electric fields might not be applied instantaneously in reality, leading to a convolution of the response function with the electric field shapes.

Since the response does in general depend on the time intervals between perturbations and measurement and not on the absolute times, the response functions can be written as functions of the time intervals τ_1 to τ_n, where $\tau_n = t - t_n$ and $\tau_i = t_{i+1} - t_i$, for $i < n$. This allows us to rewrite the nth order polarization as

$$P_p^{(n)}(t) = \int\limits_{0}^{\infty} d\tau_n \cdots \int\limits_{0}^{\infty} d\tau_1 \, R_{pp_n\cdots p_1}^{(n)}(\tau_n, \cdots, \tau_1) E_{p_n}(t-\tau_n) \cdots E_{p_1}(t-\tau_n-\tau_{n-1}-\cdots-\tau_1). \tag{2.3}$$

The polarization of a material at a given time is given by the expectation value of the dipole operator p per unit volume, V. The dipole operator is associated with the charge q and position r of all charged particles in the material. [50, 72]

$$P(t) \equiv \frac{1}{V} \langle p\rho(t) \rangle \equiv \frac{1}{V} Tr\left(p\rho(t)\right) \tag{2.4}$$

$$\mathbf{p} = \sum_i q_i(r - r_i) \quad (2.5)$$

Here the expectation value is expressed in a density operator/matrix $\rho(t)$ formulation. Denoting $P_n(t)$ the probability of the system being in the state $| n \rangle$, the density operator can be expressed

$$\rho(t) \equiv P_n(t) \, | n \rangle \langle n | \, . \quad (2.6)$$

To find the polarization at a given time t, we must know the density operator at this time, so the evolution of the polarization is determined by the evolution of the density operator. The density operator evolves according to the Liouville-Von Neumann equation.

$$\frac{\partial \rho(t)}{\partial t} = \frac{1}{i\hbar}[H_0 + H_I(t), \rho(t)] \quad (2.7)$$

Here H_0 is the time independent Hamiltonian for the unperturbed system, while $H_I(t)$ is the Hamiltonian describing the interaction between the system and the electric fields. In the electric dipole approximation this interaction is given by:

$$H_I(t) = -p \cdot E(t). \quad (2.8)$$

This approximation holds if the wavelength of the electric field is much larger than the size of the chromophores so that the electric field can be considered to be independent of the position. At the same time this approximation also allows to separate the propagation of the applied electric field and generation of the signal field, described by Maxwell Equations, from the calculation of the response function on the microscopic level.

When the Hamiltonian is time independent the time evolution of the density operator is known and the time-dependent density can be expressed in terms of a time independent density operator ρ_0 and a simple time evolution operator.

$$\rho(t) = \exp\left(\frac{1}{i\hbar}(t - t_0)H_0\right) \rho_0 \exp\left(-\frac{1}{i\hbar}(t - t_0)H_0\right) \quad (2.9)$$

Time-dependent problems can be simplified by transforming from the usual Schrödinger picture, where all observables correspond to time independent operators, to the interaction picture. This is done by applying the unitary transformation [51]

$$A(t) = \exp\left(-\frac{1}{i\hbar}(t - t_0)H_0\right) A_S \exp\left(\frac{1}{i\hbar}(t - t_0)H_0\right) \quad (2.10)$$

to all the Schrödinger picture operators (A_S). When the Hamiltonian is time independent the density operator in the interaction picture will also be time independent and all time evolution is in the operators. In that case the interaction picture coincides with the Heisenberg picture.

If the Hamiltonian is time dependent, the density operators will also become time dependent in the interaction picture. In the interaction picture the Liouville-Von Neumann equation is

$$\frac{\partial \rho(t)}{\partial t} = \frac{1}{i\hbar}[H_I(t), \rho(t)] \tag{2.11}$$

and the density operator only evolves under the influence of the perturbation, while the unperturbed dynamics is hidden in the operators.

The first-order change in the density at time t due to one time dependent perturbation H_I at an earlier time can be found [51] assuming that the unperturbed density is perturbed once and integrating over all possible moments, where the perturbation could have taken place.

$$\rho^{(1)}(t) = \frac{1}{i\hbar} \int_{-\infty}^{t} dt_1 \, [H_I(t_1), \rho(-\infty)]. \tag{2.12}$$

Here $\rho(-\infty)$ is the density operator for the system in equilibrium determined by the Hamiltonian for the unperturbed system.

The nth order change in the density due to the same or with other perturbations at later times can be expressed by assuming that the nth order perturbation acts on the $(n-1)$th order density.

$$\rho^{(n)}(t) = \left(\frac{1}{i\hbar}\right)^n \int_{-\infty}^{t} dt_n \int_{-\infty}^{t_n} dt_{n-1} \cdots \int_{-\infty}^{t_2} dt_1 \Big[H_I(t_n), \big[H_I(t_{n-1}) \cdots , [H_I(t_1), \rho(-\infty)] \cdots \big]\Big] \tag{2.13}$$

The nth order polarization can be found by substituting this expression into Eq. (2.4) and using the interaction Hamiltonian given in Eq. (2.8).

$$P_p^{(n)}(t) = \frac{1}{V}\left(\frac{1}{i\hbar}\right)^n \int_{-\infty}^{t} dt_n \int_{-\infty}^{t_n} dt_{n-1} \cdots \int_{-\infty}^{t_2} dt_1 \tag{2.14}$$

$$\left\langle p_p(t) \Big[p_{p_n}(t_n), \big[p_{p_{n-1}}(t_{n-1}) \cdots , [p_{p_1}(t_1), \rho] \cdots \big]\Big] \right\rangle E_{p_n}(t_n) \cdots E_{p_1}(t_1). \tag{2.15}$$

Here $p_p(t)$ is the dipole moment operator at time t in the direction parallel to the polarization direction of the electric field E_p. Comparing this equation with Eq. (2.2) allows identifying the response function $R^{(n)}$.

$$R_{pp_n\cdots p_1}^{(n)}(t, t_n, \cdots, t_1) = \frac{1}{V}\left(\frac{1}{i\hbar}\right)^n \left\langle p_p(t) \Big[p_{p_n}(t_n), \big[p_{p_{n-1}}(t_{n-1}) \cdots , [p_{p_1}(t_1), \rho] \cdots \big]\Big] \right\rangle \tag{2.16}$$

Using the time intervals as in Eq. (2.3) leaves us with the final equation for the quantum mechanical response function.

$$
\begin{aligned}
R^{(n)}_{pp_n \cdots p_1}(\tau_n, \cdots, \tau_1) \;=\; & \frac{1}{V}\left(\frac{1}{i\hbar}\right)^n \Big\langle p_p(\tau_n + \cdots + \tau_1)\Big[p_{p_n}(\tau_{n-1} + \cdots + \tau_1), \\
& \Big[p_{p_{n-1}}(\tau_{n-2} + \cdots + \tau_1)\cdots, [p_{p_1}(0), \rho]\cdots\Big]\Big]\Big\rangle
\end{aligned}
\tag{2.17}
$$

This expression is very general and is in principle valid for all types of response to electric fields as long as the electric dipole approximation holds. The expression in principle includes the response of both electrons and nuclei on the same level of theory. In practice this is not an advantage and in the following section the Born-Oppenheimer approximation will be introduced to allow treating electrons and nuclei in different manners.

2.2   Response functions in the Born-Oppenheimer approximation

The fact that nuclei are more than three orders of magnitude heavier than electrons means that while nuclear motion often takes place on a femtosecond timescale the electronic motion occurs on an attosecond time scale. This means that the electrons adjust to the nuclear framework virtually instantaneously in most situations and that the nuclear motion can be seen as motion of the nuclei on an electronic ground state potential. When the nuclear and electronic motions take place on different timescales the Born-Oppenheimer approximation [73] can be applied to decouple the nuclear and electronic motion. This allows writing the total energy of a system as the sum of the kinetic energy of the nuclei $H^{\mathrm{nuc}}_{\mathrm{kin}}$, the electrostatic repulsion between the nuclei $H^{\mathrm{nuc}}_{\mathrm{pot}}$ and the ground state energy of the electrons with a given set of nuclear coordinates H^{el}_0.

$$
H_0 = H^{\mathrm{nuc}}_{\mathrm{kin}} + H^{\mathrm{nuc}}_{\mathrm{pot}} + H^{\mathrm{el}}_0
\tag{2.18}
$$

In this expression it is assumed that all nuclear motion takes place on the electronic ground state potential. Therefore the integration over the electronic variables have already been performed and the operators only work on nuclear coordinates.

In the presence of an electric field the electronic energy can be expanded in powers of the electric field. The first term is the ground state energy in absence of an external field

and the remaining terms are the electronic part of the interaction energy H_I.

$$
\begin{aligned}
H^{\text{el}} \;=\; & H_0^{\text{el}} - \Big(\mu_a E_a + \frac{1}{2}\alpha_{ab}E_a E_b + \frac{1}{3}\beta_{abc}E_a E_b E_c + \frac{1}{4}\gamma_{abcd}E_a E_b E_c E_d \\
& + \; \frac{1}{5}\epsilon_{abcde}E_a E_b E_c E_d E_e + \frac{1}{6}\zeta_{abcdef}E_a E_b E_c E_d E_e E_f + \cdots \Big)
\end{aligned}
\tag{2.19}
$$

here a to f are the polarization directions of the field. The prefactors 1/2, 1/3, 1/4 are chosen in such a way that they will disappear later in the dipole operator. An alternative definition of the (hyper)polarizabilities (α, β, etc.) uses the prefactors 1/2!, 1/3!, 1/4! and so on. The electronic (hyper)polarizabilities account for the electronic response to the elctric field that is instantaneous in the Born-Oppenheimer approximation compared to the nuclear response. The (hyper)polarizabilities depend only on the nuclear cooriditates.

The interaction energy between the nuclei and the electric field is given by

$$
H_I^{\text{nuc}} = -\sum_i q_i(r - r_i) \cdot E.
\tag{2.20}
$$

The sum is now only over nuclei and not over all particles as in Eq. (2.5), therefore the reference position vector r is used. Defining m as $\sum_i q_i(r - r_i) + \mu$ we can write the interaction energy between the system and the field

$$
H_I = -\Big(m_a E_a + \frac{1}{2}\alpha_{ab}E_a E_b + \frac{1}{3}\beta_{abc}E_a E_b E_c + \cdots \Big).
\tag{2.21}
$$

Multiple interactions with the perturbing fields are introduced. This gives rise to a different power dependence in the perturbation and in the electric field.

The dipole moment operator in the electric fields is then given by

$$
p_a = -\frac{d\,H_I}{d\,E} = m_a + \alpha_{ab}E_b + \beta_{abc}E_b E_c + \gamma_{abcd}E_b E_c E_d + \cdots .
\tag{2.22}
$$

For molecules possessing inversion symmetry the hyperpolarizabilities of uneven order (β, ϵ etc.) vanish. This is the case for carbon disulfide that will be studied here. Therefore these hyperpolarizabilities will be neglected in the following. The response functions R, for molecules with less symmetry can be found in the paper by Steffen *et al.* [72] Using the interaction energy in Eq. (2.21), the dipole operator in Eq. (2.22) and the expansion in Eq. (2.13) in the expression for the expectation value of the polarization in Eq. (2.4) the first-order response for molecules with inversion symmetry is:

$$
R_{ab}^{(1)}(\tau_1) = \frac{1}{V} \left\langle \alpha_{ab}(0)\rho(-\infty) \right\rangle \delta(\tau_1)
\tag{2.23}
$$

The first-order response is just the constant average (electronic) polarizability. The argument of the polarizability denotes the time.

The third-order response is given by:

$$
\begin{aligned}
R^{(3)}_{abcd}(\tau_3, \tau_2, \tau_1) &= \frac{1}{V} \left\langle \gamma_{abcd}(0)\rho(-\infty) \right\rangle \delta(\tau_1)\delta(\tau_2)\delta(\tau_3) \\
&- \frac{1}{i\hbar} \frac{1}{V} \left\langle \alpha_{ab}(\tau_2)[\frac{1}{2}\alpha_{cd}(0), \rho(-\infty)] \right\rangle \delta(\tau_1)\delta(\tau_3)
\end{aligned}
\tag{2.24}
$$

The third-order response consist of two contributions. One instantaneous (electronic) contribution depending on the hyper-polarizability γ but not on the nuclear dynamics. The other contribution depends on one time variable τ_2 and on the polarizabilities. This contribution does probe the nuclear motion.

The fifth-order response is given by:

$$
\begin{aligned}
R^{(5)}_{abcdef}(\tau_5, \tau_4, \tau_3, \tau_2, \tau_1) &= \frac{1}{V} \left\langle \zeta_{abcdef}(0)\rho(-\infty) \right\rangle \delta(\tau_1)\delta(\tau_2)\delta(\tau_3)\delta(\tau_4)\delta(\tau_5) \\
&- \frac{1}{i\hbar} \frac{1}{V} \left\langle \gamma_{abcd}(\tau_2)[\frac{1}{2}\alpha_{ef}(0), \rho(-\infty)] \right\rangle \delta(\tau_1)\delta(\tau_3)\delta(\tau_4)\delta(\tau_5) \\
&- \frac{1}{i\hbar} \frac{1}{V} \left\langle \alpha_{ab}(\tau_4)[\frac{1}{4}\gamma_{cdef}(0), \rho(-\infty)] \right\rangle \delta(\tau_1)\delta(\tau_2)\delta(\tau_3)\delta(\tau_5) \\
&+ \left(\frac{1}{i\hbar}\right)^2 \frac{1}{V} \left\langle \alpha_{ab}(\tau_4+\tau_2)[\frac{1}{2}\alpha_{cd}(\tau_2), [\frac{1}{2}\alpha_{ef}(0), \rho(-\infty)]] \right\rangle \delta(\tau_1)\delta(\tau_3)\delta(\tau_5)
\end{aligned}
\tag{2.25}
$$

This response consist of four contributions. One of those is purely electronic (ζ) and is only found when all time delays are zero. Two contributions depend on the γ hyper-polarizability and have one time delay different from zero. The last contribution depends on two time delays and polarizabilities at three different times. This contribution is the one of most interest, since it possibly contains information about mode coupling and line broadening mechanisms [35] as discussed in the introduction.

When applying Eqs. (2.23) to (2.25) to macroscopic systems, the (hyper-)polarizabilities α, γ and ζ, should be replaced by the instantaneous electronic susceptibilities (polarizabilities pr. unit volume) $\chi^{(1)}$, $\chi^{(3)}$ and $\chi^{(5)}$. [56, 76, 77] The macroscopic response functions, which are respectively first-, third- and fifth-order (time-dependent) susceptibilities, are then denoted $\boldsymbol{\chi}^{(1)}_{ab}$, $\boldsymbol{\chi}^{(3)}_{abcd}$ and $\boldsymbol{\chi}^{(5)}_{abcdef}$ throughout this thesis.

For the macroscopic response functions a notation will be adopted that only applies, when the hyper-polarizabilities of uneven order can be neglected and all interactions involve one or more pairs of optical fields. The first-order response is time independent and will be denoted $\boldsymbol{\chi}^{(1)}_{ab}$. Since the third-order response considered here will only depend on one time delay (τ_2) this response will be denoted $\boldsymbol{\chi}^{(3)}_{abcd}(t_1)$. The fifth order response will

be denoted $\boldsymbol{\chi}^{(5)}_{abcdef}(t_1, t_2)$, where t_1 and t_2 are the two time delays (τ_2 and τ_4). For the instantaneous (electronic) susceptibilities a notation with one relative time will be applied. These susceptibilities depending on the structure at time t will be denoted $\chi^{(1)}_{ab}(t)$, $\chi^{(3)}_{abcd}(t)$ and $\chi^{(5)}_{abcd}(t)$.

In this notation the first-order response is

$$\boldsymbol{\chi}^{(1)}_{ab} = \left\langle \chi_{ab}(0)\rho(-\infty) \right\rangle, \tag{2.26}$$

which is just the constant average first-order susceptibility. The third-order response is

$$\boldsymbol{\chi}^{(3)}_{abcd}(t_1) = \left\langle \chi^{(3)}_{abcd}(0)\rho(-\infty) \right\rangle \delta(t_1) \tag{2.27a}$$

$$- \frac{V}{i\hbar} \left\langle \chi^{(1)}_{ab}(t_1)[\frac{1}{2}\chi^{(1)}_{cd}(0), \rho(-\infty)] \right\rangle \tag{2.27b}$$

and the fifth-order response

$$\boldsymbol{\chi}^{(5)}_{abcdef}(t_1, t_2) = \left\langle \chi^{(5)}_{abcdef}(0)\rho(-\infty) \right\rangle \delta(t_1)\delta(t_2) \tag{2.28a}$$

$$- \frac{V}{i\hbar} \left\langle \chi^{(3)}_{abcd}(t_1)[\frac{1}{2}\chi^{(1)}_{ef}(0), \rho(-\infty)] \right\rangle \delta(t_2) \tag{2.28b}$$

$$- \frac{V}{i\hbar} \left\langle \chi^{(1)}_{ab}(t_2)[\frac{1}{4}\chi^{(3)}_{cdef}(0), \rho(-\infty)] \right\rangle \delta(t_1) \tag{2.28c}$$

$$+ \left(\frac{V}{i\hbar}\right)^2 \left\langle \chi^{(1)}_{ab}(t_1 + t_2)[\frac{1}{2}\chi^{(1)}_{cd}(t_1), [\frac{1}{2}\chi^{(1)}_{ef}(0), \rho(-\infty)]] \right\rangle \tag{2.28d}$$

2.3   Time-resolved stimulated Raman scattering

In a time-domain one-dimensional Raman experiment an initial laser pulse pair perturbs the sample and after a delay t_1 the nuclear dynamics (Eq. (2.27b)), following the impact of the initial pulse pair, is probed by a third laser pulse. If the delay is zero a pure electronic response (Eq. (2.27a)) will also arise. This is illustrated in the energy diagrams of Figure 2.1. Typical experimental techniques are the (heterodyned) optical Kerr effect [68,69] and transient grating scattering [70,71]. The signal is governed by the third-order response function $\boldsymbol{\chi}^{(3)}_{abcd}$ (Eq. (2.27)), where b, c and d are the polarization directions of the driving fields and a is the polarization direction of the emitted Rayleigh/Raman radiation. The possible polarization directions for the third-order response are limited by symmetry. [53] Because the liquid phase is isotropic, the only tensor elements of polarization with nonzero response are $\boldsymbol{\chi}^{(3)}_{zzzz}$, $\boldsymbol{\chi}^{(3)}_{zzyy}$, $\boldsymbol{\chi}^{(3)}_{zyzy}$ and $\boldsymbol{\chi}^{(3)}_{zyyz}$. All permutations of x, y and z and linear combinations of these response functions are possible.
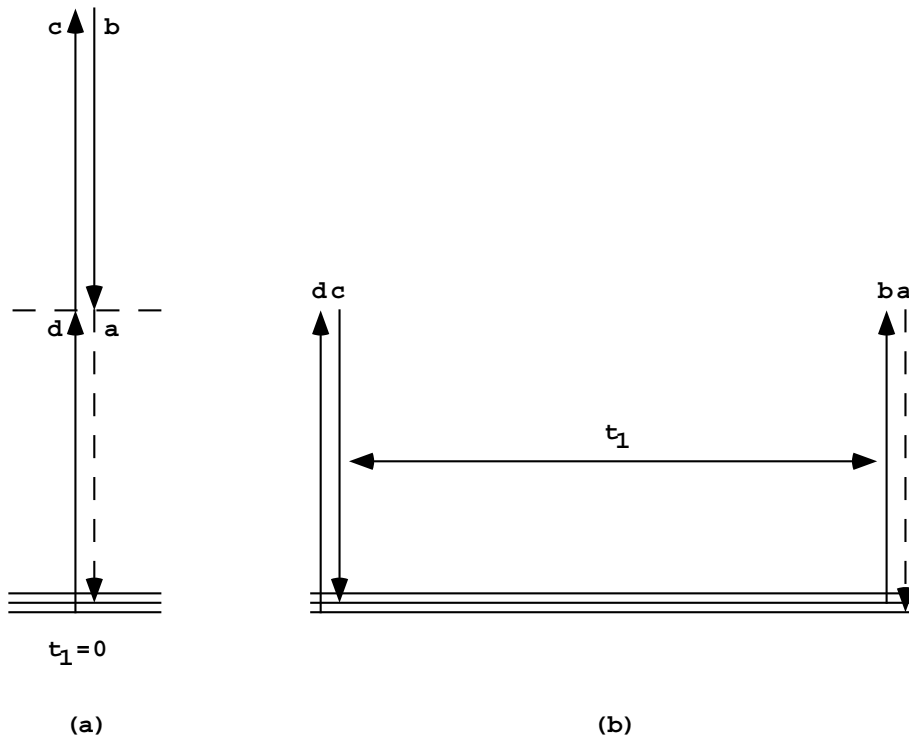
FIGURE 2.1: *Energy level diagrams of the electronic (a) and nuclear (b) third-order response as in Eq. (2.27a) and (2.27b). The driving fields (full lines) have polarization directions d, c and b. The signal field (dashed line) have polarization direction a.*

The susceptibilities are symmetric in permutation of the polarization directions ($\chi^{(1)}_{ab} = \chi^{(1)}_{ba}, \chi^{(3)}_{abcd} = \chi^{(3)}_{cbad} = \ldots$ etc.), this is called Kleinman symmetry [78]. For the nuclear part of the response given in Eq. (2.27b) the Kleinman symmetry [78] in the first-order susceptibilities introduces a relation between the nonzero elements. Furthermore, in an isotropic medium the response function is invariant under any rotation of space, this introduces another relation between the nonzero elements [79] that will not be discussed in detail here. The four nuclear response functions are then related by the two expressions [53]:

$$
\begin{aligned}
\boldsymbol{\chi}^{(3)}_{zyyz}(t) &= \boldsymbol{\chi}^{(3)}_{zyzy}(t), \\
\boldsymbol{\chi}^{(3)}_{zzyy}(t) &= \boldsymbol{\chi}^{(3)}_{zzzz}(t) - 2\boldsymbol{\chi}^{(3)}_{zyzy}(t)
\end{aligned}
\tag{2.29}
$$

Hence, finding two of these response functions will provide all the information we can obtain. Usually $\boldsymbol{\chi}^{(3)}_{zzzz}$ and $\boldsymbol{\chi}^{(3)}_{zyzy}$ are the functions determined experimentally. They are denoted as the polarized and the depolarized components of the response. Alternatively a separation into a part due to fluctuations of the anisotropic part of the susceptibility and another due to fluctuations of the isotropic part of the susceptibility can be used. The depolarized component and the anisotropic component are identical. The linear combination with equal weight of $\boldsymbol{\chi}^{(3)}_{zzxx}$, $\boldsymbol{\chi}^{(3)}_{zzyy}$ and $\boldsymbol{\chi}^{(3)}_{zzzz}$ is equivalent with the isotropic response function $\boldsymbol{\chi}^{(3)}_{zzmm}$, where m denotes an axis forming an angle of $54.74°$ with the z-axis (the magic angle). The electronic part of the response given in Eq. (2.27a) shows Kleinman symmetry [78] in the third-order susceptibility $\chi^{(3)}_{abcd}$ and only one independent component is found. Using that the isotropic and anisotropic first-order susceptibilities can be expressed as irreducible tensor operators of rank 0 and 2 respectively and that the third-order susceptibility is a rank 4 irreducible tensor operator, [80] the same symmetry restrictions can be obtained.

Any response component $\boldsymbol{\chi}^{(3)}_{zzkk}$, where k denotes an axis forming an angle of θ with respect to the z-axis, can be expressed as [53]

$$
\boldsymbol{\chi}^{(3)}_{zzkk} = \cos^2\theta \times \boldsymbol{\chi}^{(3)}_{zzzz} + \sin^2\theta \times \boldsymbol{\chi}^{(3)}_{zzyy}.
\tag{2.30}
$$

This can for example be used to calculate the magic angle (isotropic) response. Later a choice of θ at $60°$ will be considered. The axis connected with this angle, will be denoted l. It should be realized that using an angle of $120°$ gives exactly the same response as with $60°$. It will be shown that this property can effectively be used to suppress the cascaded response. In Figure 2.2 the polarization directions of the $\boldsymbol{\chi}^{(3)}_{zzzz}$ and $\boldsymbol{\chi}^{(3)}_{zzll}$ components are illustrated.
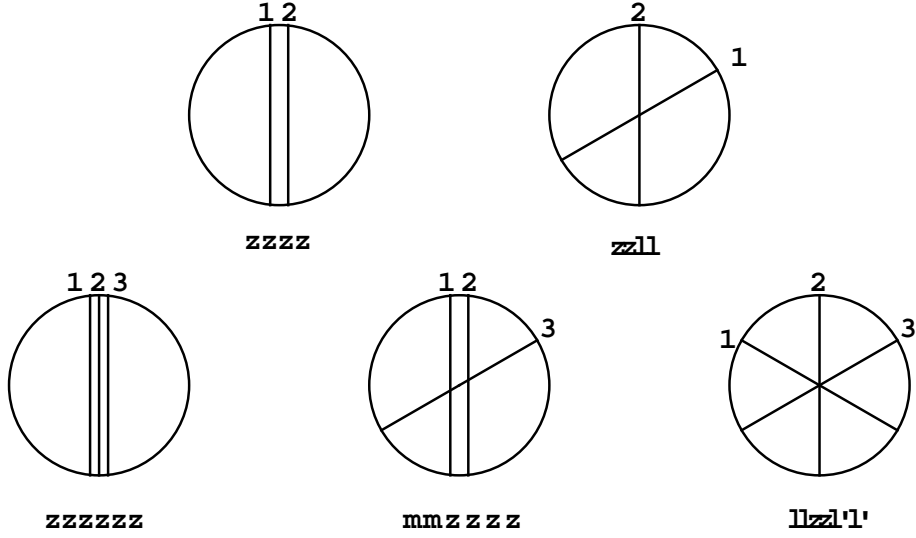
FIGURE 2.2: *In the upper line the polarization directions of the $\chi^{(3)}_{zzzz}$ and $\chi^{(3)}_{zzll}$ tensor components are illustrated. The circle is the unit circle in the plane perpendicular to the propagation direction of the laser beams. The lines symbolizes the polarization alignment of the pulse pairs and the probe and signal fields. Since the pulses in the considered experiments come in aligned pairs and the Raman events depend on the product of the aligned fields, the orientation of the polarization vector of each individual field is not important. In the third-order case line 1 is the driving field pulse pair and line 2 is the probe and signal fields. In the lower line the polarization directions of the fifth-order tensor components $\chi^{(5)}_{zzzzzz}$, $\chi^{(5)}_{mmzzzz}$ and $\chi^{(5)}_{llzzl'l'}$ are illustrated. Line 1 and 2 are driving field pulse pairs and line 3 is the probe and signal fields.*

In the time-domain two-dimensional Raman experiment two initial laser pulse pairs with a relative time delay t_1 are followed by a Raman probe pulse after an additional time delay t_2. If both time delays are zero a pure electronic response will arise (Eq. (2.28a)). If one of the time delays is zero, responses depending on both the first-order and the third-order electronic susceptibility will arise (Eqs. (2.28b) and (2.28c)). If none of the delays are zero only the pure nuclear response (Eq. (2.28d)) will be present. In Figure 2.3 all these processes are illustrated. Most of the fifth-order experiments performed till now [38–42, 74, 75, 81–83] have been performed with the same optical frequency for all fields, as illustrated in the figure. Recent experiments have utilized different frequencies for the probe (E_b) and signal fields (E_a) than for the other fields (E_c, E_d, E_e and E_f) [43–45] to help suppressing the third-order cascaded response that will be described in the following section. When only elecronically off-resonant Raman response is considered, the use of different frequencies is not expected to affect the response function appreciably since then the first-order susceptibilities do not change to any great extend when changing the frequency.

The two-dimensional nuclear response function is governed by the fifth-order response function given in Eq. (2.28d) $\chi^{(5)}_{abcdef}$, where b, c, d, e and f are the polarization directions of the driving fields and a is the polarization direction of the measured signal. For the nuclear fifth-order response similar symmetry considerations hold as those made for the third-order response. [54] For the nuclear response given in Eq. (2.28d) there are five linearly independent tensor elements [54]. Two linearly independent tensor elements exist for each of the one-dimensional responses involving both $\chi^{(1)}$ and $\chi^{(3)}$. These response functions, given in Eqs. (2.28b) and (2.28c), are found along the axes of the full two-dimensional spectrum. Only one linearly independent tensor element exists for the pure electronic response given in Eq. (2.28a). This response is confined to the origin of the full two-dimensional spectrum.

Different fifth-order tensor elements have been measured experimentally. Among these are the $\chi^{(5)}_{yzzzyz}$ [42–45], $\chi^{(5)}_{zzzyyz}$, [38, 41, 45, 82, 84] $\chi^{(5)}_{zzzzzz}$ [41, 45, 74, 85] and three magic angle tensor elements. [74, 75] Calculations have been done on the tensor elements $\chi^{(5)}_{yzzzyz}$, [58] $\chi^{(5)}_{zzzzzz}$ [56, 58, 59, 86, 87] and three magic angle tensor elements. [56, 87] Furthermore calculations have been performed on the tensor element $\chi^{(5)}_{llzzl'l'}$, [56] which will be discussed further in the following section.
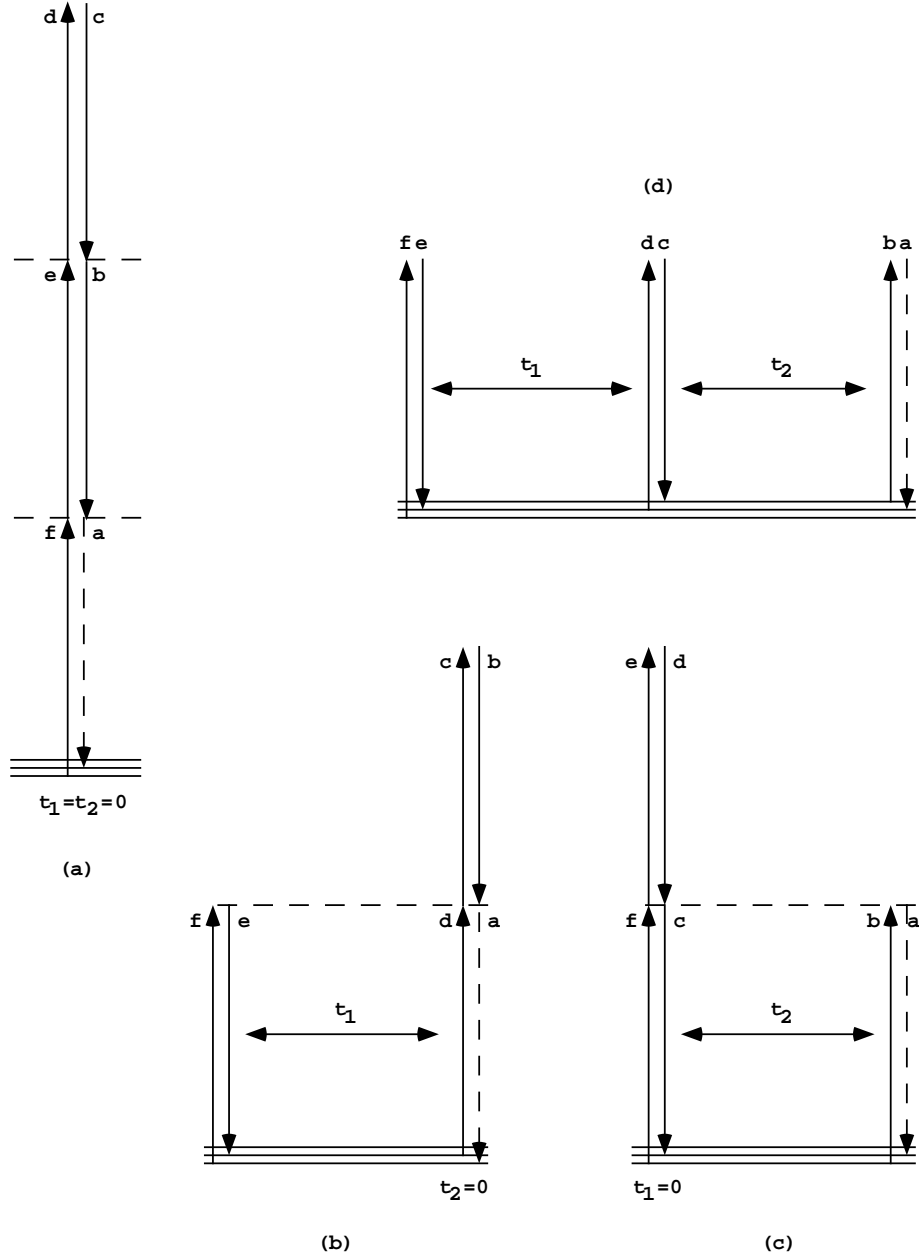
19

FIGURE 2.3*: Energy level diagrams of the pure electronic (a), mixed nuclear electronic (b), (c), and pure nuclear (d) fifth-order response as in Eq. (2.28a), (2.28b), (2.28c) and (2.28d). The driving fields (full lines) have polarization directions f, e, d, c and b. The signal field (dashed line) have polarization direction a.*

2.4   Direct vs. cascaded response

In 1999 Blank *et al.* [41] showed that the all earlier experimental spectra were dominated by third-order cascaded response. The existence of these processes were already reported earlier [88, 89].

This artificial fifth-order response consist of two third-order processes that together generate signals with exactly the same power dependence as the true fifth-order signals. The two third-order processes are connected by an intermediate field E_i that is generated by one of of the third-order processes and acts as pump or probe field in a second third-order process. The cascaded processes are induced by the exact same fields that give rise to the fifth-order response and the signal is therefore emitted in the same direction as the true fifth-order response possibly contaminating this response. Two types of cascading processes exists, sequential and parallel cascades, these are illustrated in Figure 2.4 [41]. It is important to understand these processes to avoid contamination of the experiments. In the following the theory behind the cascaded processes will be outlined and a method to estimate the intensity ratio between the cascaded response and the true fifth-order response will be described. This will later be applied in chapter 7.
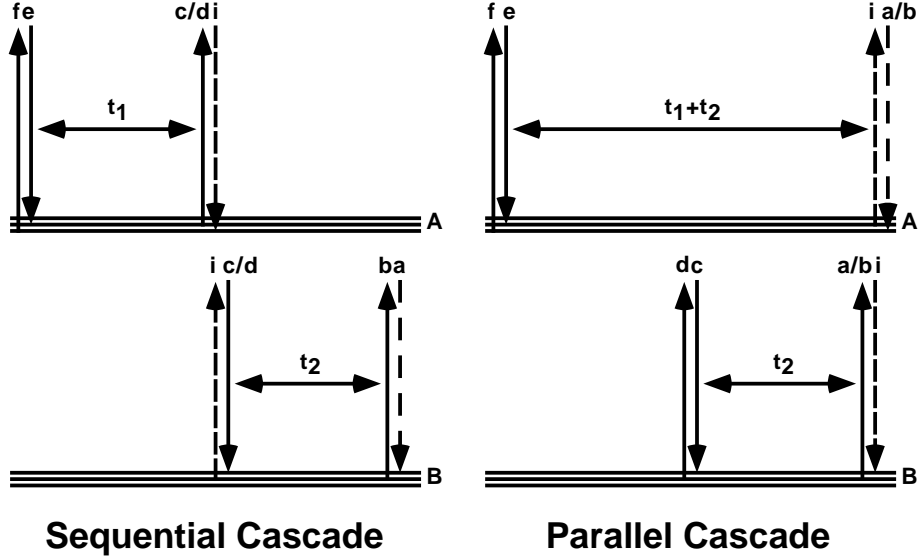

Sequential Cascade   **Parallel Cascade**

FIGURE 2.4*: Energy level diagrams of the third-order cascaded response. The driving fields (full lines) have polarization directions f, e, d, c and b. The signal field (dashed line) has polarization direction a. The intermediate field (long dashed line) has polarization direction i.*

Taking the polarization direction combinations into account, two possibilities exist for each type of cascading process. The time and polarization dependence of the sequential processes of Figure 2.4 are

$$
\begin{aligned}
\boldsymbol{\chi}^{(5)}_{\text{seq},1}(t_1, t_2) &= \boldsymbol{\chi}^{(3)}_{abci}(t_2)\boldsymbol{\chi}^{(3)}_{idef}(t_1) \\
\boldsymbol{\chi}^{(5)}_{\text{seq},2}(t_1, t_2) &= \boldsymbol{\chi}^{(3)}_{abid}(t_2)\boldsymbol{\chi}^{(3)}_{cief}(t_1).
\end{aligned}
\tag{2.31}
$$

Similarly the time and polarization dependence of the two parallel cascading processes of Figure 2.4 are

$$
\begin{aligned}
\boldsymbol{\chi}^{(5)}_{\text{par},1}(t_1, t_2) &= \boldsymbol{\chi}^{(3)}_{aicd}(t_2)\boldsymbol{\chi}^{(3)}_{ibef}(t_1 + t_2) \\
\boldsymbol{\chi}^{(5)}_{\text{par},2}(t_1, t_2) &= \boldsymbol{\chi}^{(3)}_{ibcd}(t_2)\boldsymbol{\chi}^{(3)}_{aief}(t_1 + t_2).
\end{aligned}
\tag{2.32}
$$

Each cascading process is connected with a unique phase mismatch given by the experimental conditions. The polarization direction of the intermediate field is determined by the polarization directions of the applied fields and the polarization of the measured signal. In Table 2.1 the polarization and time dependence are given for the same components of the direct fifth-order response, considered here. There is no difference between the polarization and time dependence in the two kinds of sequential processes for the considered components and the same is true for the two parallel responses. Hence, the ratio between the intensities of the true fifth-order signal and cascading processes can be of two types: sequential and parallel. The intensity ratio in the homodyne detection experiment between each of the third-order cascading processes and the direct fifth-order response can be estimated from the peak intensities as [41, 55]

$$
\frac{I_{\text{cas}}}{I_{\text{5th}}} \approx \left(\frac{\pi\omega l}{nc}\right) f^2(\Delta k l)\frac{\mid \boldsymbol{\chi}^{(3)}\boldsymbol{\chi}^{(3)} \mid^2}{(4\pi\epsilon_0)^2 \mid \boldsymbol{\chi}^{(5)} \mid^2}.
\tag{2.33}
$$

Here, the polarization dependence is omitted for simplicity and $f(\Delta k l)$ is a number smaller than one that is determined by the phase matching conditions.

Typical experimental wavelengths $2\pi c/\omega$ are 620 [38,40,81] and 800 nm [39]. In the two color experiments [45] 400 nm and 800 nm were used. Sample thicknesses $l = $ 1-2 mm are typically used, [38–40,81] but in the recent two color experiments a thickness of 0.1 mm was used. The refractive index n of pure CS_2 is 1.628 [90]. The intensity ratio can be divided into a ratio independent of the experimental conditions R_{abcdef} that is used to compare different calculations and an experimental factor F_{ex} that depends on the experimental conditions. The experiment independent ratio is defined as

$$
R = \frac{\mid \boldsymbol{\chi}^{(3)}\boldsymbol{\chi}^{(3)} \mid^2}{(4\pi\epsilon_0)^2 \mid \boldsymbol{\chi}^{(5)} \mid^2},
\tag{2.34}
$$

Table 2.1: *In fifth-order experiments, with the polarization directions given in the first column, competing sequential and parallel cascaded processes can show up. The time and polarization dependence of these processes are given in the second and third column. m is an axis forming the magic angle with the z-axis, l is an axis forming an angle of 60° with the z-axis and l′ is an axis forming an angle of 120° with the z-axis.*

$\chi^{(5)}_{abcdef}$	$\chi^{(5)}_{\text{seq}} = \chi^{(3)}(t_2)\chi^{(3)}(t_1)$		
$\chi^{(5)}_{zzzzzz}$	$\chi^{(3)}_{zzzz}(t_2)\chi^{(3)}_{zzzz}(t_1)$	$+$	$\chi^{(3)}_{zzzx}(t_2)\chi^{(3)}_{xzzz}(t_1)$
$\chi^{(5)}_{mmzzzz}$	$\chi^{(3)}_{zzmm}(t_2)\chi^{(3)}_{zzzz}(t_1)$	$+$	$\chi^{(3)}_{xzmm}(t_2)\chi^{(3)}_{zxzz}(t_1)$
$\chi^{(5)}_{zzmmzz}$	$\chi^{(3)}_{zzmz}(t_2)\chi^{(3)}_{zzmz}(t_1)$	$+$	$\chi^{(3)}_{zzmx}(t_2)\chi^{(3)}_{zzmx}(t_1)$
$\chi^{(5)}_{zzzzmm}$	$\chi^{(3)}_{zzzz}(t_2)\chi^{(3)}_{zzmm}(t_1)$	$+$	$\chi^{(3)}_{zxzz}(t_2)\chi^{(3)}_{xzmm}(t_1)$
$\chi^{(5)}_{llzzl'l'}$	$\chi^{(3)}_{zzll}(t_2)\chi^{(3)}_{zzll}(t_1)$	$+$	$\chi^{(3)}_{zxll}(t_2)\chi^{(3)}_{xzl'l'}(t_1)$

$\chi^{(5)}_{abcdef}$	$\chi^{(5)}_{\text{par}} = \chi^{(3)}(t_2)\chi^{(3)}(t_1 + t_2)$
$\chi^{(5)}_{zzzzzz}$	$\chi^{(3)}_{zzzz}(t_2)\chi^{(3)}_{zzzz}(t_1 + t_2) + \chi^{(3)}_{zxzz}(t_2)\chi^{(3)}_{xzzz}(t_1 + t_2)$
$\chi^{(5)}_{mmzzzz}$	$\chi^{(3)}_{zzzm}(t_2)\chi^{(3)}_{zzmz}(t_1 + t_2) + \chi^{(3)}_{zzxm}(t_2)\chi^{(3)}_{zzmx}(t_1 + t_2)$
$\chi^{(5)}_{zzmmzz}$	$\chi^{(3)}_{zzmm}(t_2)\chi^{(3)}_{zzzz}(t_1 + t_2) + \chi^{(3)}_{zxmm}(t_2)\chi^{(3)}_{xzzz}(t_1 + t_2)$
$\chi^{(5)}_{zzzzmm}$	$\chi^{(3)}_{zzzz}(t_2)\chi^{(3)}_{zzmm}(t_1 + t_2) + \chi^{(3)}_{zxzz}(t_2)\chi^{(3)}_{xzmm}(t_1 + t_2)$
$\chi^{(5)}_{llzzl'l'}$	$\chi^{(3)}_{zzlz}(t_2)\chi^{(3)}_{lzl'l'}(t_1 + t_2) + \chi^{(3)}_{zzlx}(t_2)\chi^{(3)}_{lxl'l'}(t_1 + t_2)$

where the polarization directions and time dependencies are given in Table 2.1. The experimental factor F_{ex} is the part of Eq. (2.33) not accounted for in Eq. (2.34) and given by

$$F_{ex} = \left(\frac{\pi \omega l}{nc} \right) f^2(\Delta k l). \tag{2.35}$$

These considerations do not apply directly to the heterodyne detected experiments that were recently performed, [42,45] since the measured intensity in these experiments is linear and not quadratic in the response function.

Chapter 3

Calculation methods

Two fundamentally different approaches exist to calculate the third- and fifth-order Raman responses. Of these the simplest to understand intuitively is the Finite Field approach, where the experiments are simulated on a microscopic level by applying laser fields in MD simulations [55, 56]. In principle this approach can be generalized to any order of the Raman response, but in practice the method is limited to the lower order responses where the signals have a reasonable intensity compared to a background response. This approach, developed by us and described in this work, will be treated in section 3.1.

Alternatively the response can be calculated using the time correlation function method, where the response functions are related to time correlation functions [50, 57, 58] which are directly related to the quantum mechanical response functions derived in chapter 2. This approach will be described in section 3.2. These time correlation functions can then be evaluated using Brownian oscillator type models for the liquid motion [35, 50, 91–94] or by using molecular dynamics data. Either the full MD data [57, 59, 77, 95–101] or snapshots of the potential surface extracted from MD simulations can be used. The later method, called instantaneous normal modes (INM) analysis [58, 102–108], is only valid for short times, so that, for instance, diffusion cannot be described properly. In section 3.3 a brief description of the analytical models for the response will be given and in section 3.4 the INM approach will be treated.

A mode-coupling theory projecting the dynamics of an atomic liquid onto bilinear pairs of fluctuating density variables also exists [86, 100, 108–110] as well as a quasi-crystal model [111–113] in which the molecular movements are approximated by the motion in short lived quasi-crystalline structures. These will not be treated extensively here.

3.1   The finite field method

The nuclear part of third-order response function can be calculated using the finite field method (FF) [55], where the actual experiment is simulated using non-equilibrium molecular dynamics. Here the forces, due to the optical fields at time zero, are actually applied in the simulation and the response is measured by calculating the susceptibility at later time steps. This procedure is repeated for numerous trajectories to produce sufficient statistical material. The noisy background response from calculations without the applied forces, is subtracted to improve the accuracy.

The forces exerted on the molecular coordinates are determined by the derivative of the optical interaction energy with respect to the molecular coordinate (x) considered.

$$F_x^{ab} = -\frac{\partial H_{\text{int}}^{ab}}{\partial x} \tag{3.1}$$

Thus, the third-order response function is calculated from the difference between the susceptibility in the calculation, where electric fields E_c and E_d, are applied in a time step of duration Δt, and the background calculation where no fields are applied. The ab tensor element of the susceptibility, calculated with applied pump fields with polarization directions c and d, is denoted $\chi_{ab;cd}^{(1)}$, while the same tensor element from the background calculation is denoted $\chi_{ab;00}^{(1)}$. The third-order response function is then given by

$$\boldsymbol{\chi}_{abcd}^{(3)}(t) = \frac{\chi_{ab;cd}^{(1)}(t) - \chi_{ab;00}^{(1)}(t)}{E_c E_d \Delta t}. \tag{3.2}$$

When averaging over a large (infinite) number of trajectories the background ($\chi_{ab;00}^{(1)}(t)$) will be constant in time and can be discarted, but in most practical calculations this will not be the case.

Instead of calculating the third-order response using a background calculation, it can also be done by inverting the forces excerted by the pump pulse pair. This is equivalent to turning the polarization direction of one of the pump fields 180°. In many other type of finite field calculations this is a well known approach. The calculated components will be $\chi_{ab;cd}^{(1)}$ and $\chi_{ab;c\overline{d}}^{(1)}$, where $\overline{d}$ denotes the field turned 180°. The third-order response is then given by

$$\boldsymbol{\chi}_{abcd}^{(3)}(t) = \frac{\chi_{ab;cd}^{(1)}(t) - \chi_{ab;c\overline{d}}^{(1)}(t)}{2 E_c E_d \Delta t}. \tag{3.3}$$

In Figure 3.1 the two different approaches to calculate the third-order response are illustrated. The first method has been used in all calculations presented in this thesis. The

advantage of the second method is that in both the $\chi_{ab;cd}^{(1)}$ and $\chi_{ab;c\overline{d}}^{(1)}$ calculation the third-order response is present, but with opposite sign. This doubles the amount of statistical data and eliminates the background at the same time. Furthermore, some of the possible higher-order (order $4n+1$, $n \in \mathbb{N}$) contributions are eliminated allowing the use of stronger laser fields in the calculations.

FIGURE 3.1: *Left the parallel field ($\chi_{ab;cd}^{(1)}$) and background ($\chi_{ab;00}^{(1)}$) calculations are illustrated. The difference between these gives the third-order response. Right the alternative set of parallel field ($\chi_{ab;cd}^{(1)}$) and anti-parallel ($\chi_{ab;c\overline{d}}^{(1)}$) calculations are illustrated. The difference between these calculations gives twice the third-order response.*
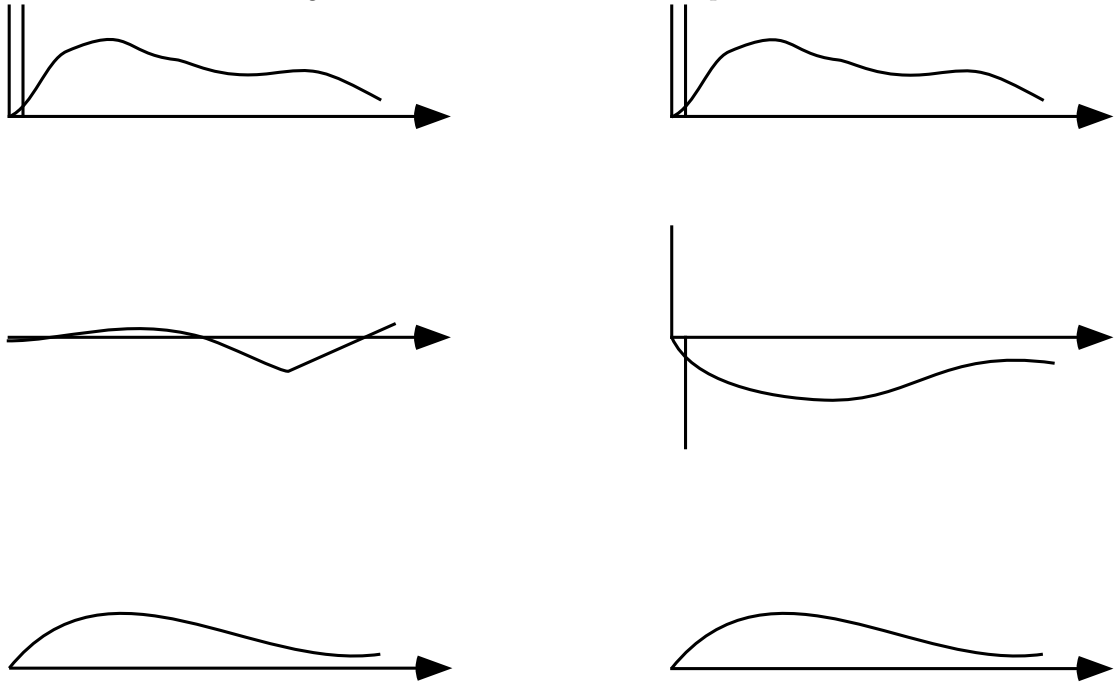
Both the anisotropic and the isotropic response can be obtained from one third-order calculation, where the applied optical fields during the initial excitation are polarized in the z direction. This is because the full first-order susceptibility matrix can be calculated at the time of the probeing. The anisotropic response is calculated using the last symmetry relation in Eq. (2.29).

$$\boldsymbol{\chi}_{zyzy}^{(3)}(t) = \frac{1}{2}\left(\boldsymbol{\chi}_{zzzz}^{(3)}(t) - \boldsymbol{\chi}_{zzyy}^{(3)}(t)\right) \tag{3.4}$$

Similarly the isotropic response can be calculated.

$$\boldsymbol{\chi}_{mmzz}^{(3)}(t) = \frac{1}{3}\left(\boldsymbol{\chi}_{zzzz}^{(3)}(t) + \boldsymbol{\chi}_{yyzz}^{(3)}(t) + \boldsymbol{\chi}_{xxzz}^{(3)}(t)\right) \tag{3.5}$$

The accuracy of the calculations can be tested by examining the $\boldsymbol{\chi}^{(3)}_{xyzz}(t)$, $\boldsymbol{\chi}^{(3)}_{xzzz}(t)$ and $\boldsymbol{\chi}^{(3)}_{yzzz}(t)$ components of the calculated response. These should be zero in an isotropic liquid, as discussed in section 2.3, but in the molecular dynamics simulations this result will only be obtained when averaging over a sufficiently large ensemble. These components of the response should therefore be found to vanish in comparison with the anisotropic and isotropic repsonses.

The nuclear part of the fifth-order response corresponding to Eq. (2.28d) can be determined from four trajectories: one background trajectory without any applied fields $\chi^{(1)}_{ab;00;00}$, a trajectory with the field applied at time zero $\chi^{(1)}_{ab;00;ef}$, a trajectory with the field applied at time t_1 $\chi^{(1)}_{ab;cd;00}$, and one with fields applied at both times zero and t_1 $\chi^{(1)}_{ab;cd;ef}$. The fifth-order response function then is

$$\boldsymbol{\chi}^{(5)}_{abcdef}(t_1, t_2) = \frac{\chi^{(1)}_{ab;cd;ef} + \chi^{(1)}_{ab;00;00} - \chi^{(1)}_{ab;cd;00} - \chi^{(1)}_{ab;00;ef}}{E_c E_d E_e E_f (\Delta t)^2}. \tag{3.6}$$

This treatment can in principle easily be generalized to higher order response functions.

Just as for the third-order response, the fifth-order signals can also be calculated using inverted forces. This requires the calculation of four different components $\chi^{(1)}_{ab;cd;ef}$, $\chi^{(1)}_{ab;\overline{cd};ef}$, $\chi^{(1)}_{ab;cd;\overline{ef}}$ and $\chi^{(1)}_{ab;\overline{cd};\overline{ef}}$ as also illustrated in Figure 3.2. The fifth-order response is then calculated through the expression

$$\boldsymbol{\chi}^{(5)}_{abcdef}(t_1, t_2) = \frac{\chi^{(1)}_{ab;cd;ef} + \chi^{(1)}_{ab;\overline{cd};\overline{ef}} - \chi^{(1)}_{ab;\overline{cd};ef} - \chi^{(1)}_{ab;cd;\overline{ef}}}{4 E_c E_d E_e E_f (\Delta t)^2}. \tag{3.7}$$

The fifth-order response, presented in this thesis except the final calculations in section 7.5, was calculated with the first method with a background calculation. In fifth-order, this has the advantage that it almost halves the number of calculations, since only the $\chi^{(1)}_{ab;cd;ef}$ and $\chi^{(1)}_{ab;cd;00}$ calculations have to be repeated when changing t_1, whereas the $\chi^{(1)}_{ab;00;00}$ and $\chi^{(1)}_{ab;00;ef}$ calculations are independent of t_1. In the alternative inverse force method all calculations depend on t_1. On the other hand, this method provides better statistics, and as in the third-order case, some of the higher-order (order $4n + 3, n \in \mathbb{N}$) contributions are eliminated. Among the contributions eliminated are the seventh-order signals that can be expected to contaminate the fifth-order response quite significantly, when too strong laser fields are used.

Since the finite field method is essentially simulating the real experiment at a microscopic level, some of the problems encountered in the experiment will also arise in the simulations. If the intensity of the applied laser fields is too high one risks boiling the sample, a problem that can also arise in the laboratory. It is therefore important to keep an

FIGURE 3.2: *Left the parallel four field ($\chi^{(1)}_{ab;cd;ef}$), two parallel three field ($\chi^{(1)}_{ab;00;ef}$, $\chi^{(1)}_{ab;cd;00}$) and background ($\chi^{(1)}_{ab;00;00}$) calculations are illustrated. The combination of these given in Eq. (3.6) provides the fifth-order response. Right the alternative set of double parallel field ($\chi^{(1)}_{ab;cd;ef}$), two single anti-parallel ($\chi^{(1)}_{ab;\overline{cd};ef}$, $\chi^{(1)}_{ab;cd;\overline{ef}}$) and double anti-parallel ($\chi^{(1)}_{ab;\overline{d};\overline{ef}}$) calculations are illustrated. The combination of these calculations given in Eq. (3.7) provides the fifth-order response.*
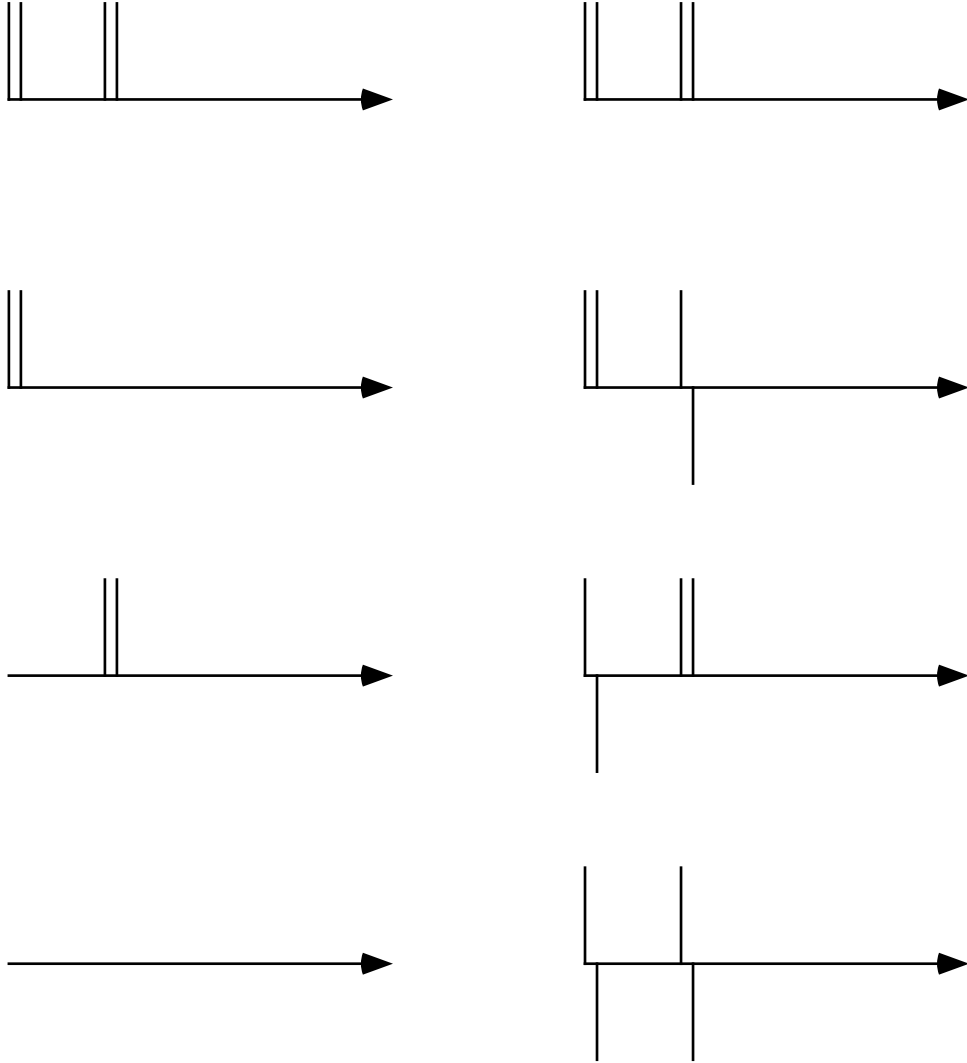
eye on the effects of the laser fields on the properties of the liquid during the simulations. The fact that the simulations mimic the experiment, provides important insight into the physics of these experiments.

3.2   Time correlation functions

The nuclear parts of the 3rd- and 5th-order nonlinear optical response functions $\boldsymbol{\chi}^{(3)}$ (Eq. (2.27b)) and $\boldsymbol{\chi}^{(5)}$ (Eq. (2.28d)) are related to the quantum mechanical correlation functions of the first-order electronic susceptibility tensor elements $\chi_{ab}^{(1)}$ [50, 57] here given in the density matrix formulation:

$$\boldsymbol{\chi}_{abcd}^{(3)}(t_1) = -\frac{1}{2}\frac{V}{i\hbar}Tr\left(\chi_{ab}^{(1)}(t_1)[\chi_{cd}^{(1)}(0), \rho(-\infty)]\right) \tag{3.8}$$

$$\boldsymbol{\chi}_{abcdef}^{(5)}(t_1, t_2) = \frac{1}{4}\left(\frac{V}{i\hbar}\right)^2 Tr\left(\chi_{ab}^{(1)}(t_1+t_2)[\chi_{cd}^{(1)}(t_1), [\chi_{ef}^{(1)}(0), \rho(-\infty)]]\right), \tag{3.9}$$

where $\rho(-\infty)$ is the phase space density of the system at equilibrium, which is the classical analogue to the quantum mechanical density matrix.

In classical mechanics the time development of the density of a system in phase space is determined by [50, 114]

$$\frac{\partial \rho(t)}{\partial t} = \left(\sum_i \frac{\partial H}{\partial q_i}\frac{\partial \rho(t)}{\partial p_i} - \frac{\partial H}{\partial p_i}\frac{\partial \rho(t)}{\partial q_i}\right) \equiv \{H, \rho(t)\} \tag{3.10}$$

instead of the Liouville-Von Neumann equation (Eq. 2.11) and the time derivative of a function A of the phase space cooridinates and time is [114]

$$\frac{\partial A}{\partial t} = \{A, H\}. \tag{3.11}$$

The time development in the classical limit is thus described replacing the commutator $[A, B]$ by the Poisson bracket $i\hbar\{A, B\}$. The quantum-mechanical response functions (Eqs. (3.8) and (3.9)) can therefore in the classical limit be written as the classical ensemble averages involving the classical equilibrium density instead of the quantum mechanical density matrix:

$$\boldsymbol{\chi}_{abcd}^{(3)}(t_1) = -\frac{V}{2}\langle\chi_{ab}^{(1)}(t_1)\{\chi_{cd}^{(1)}(0), \rho(-\infty)\}\rangle \tag{3.12}$$

$$\boldsymbol{\chi}_{abcdef}^{(5)}(t_1, t_2) = \frac{V^2}{4}\langle\chi_{ab}^{(1)}(t_1+t_2)\{\chi_{cd}^{(1)}(t_1), \{\chi_{ef}^{(1)}(0), \rho(-\infty)\}\}\rangle. \tag{3.13}$$

This can be simplified by using the fact that the classical equilibrium density is given by the Boltzman distribution and can be written

$$\rho(-\infty) = \frac{\exp(-H/k_BT)}{\int\int \exp(-H/k_BT)dp\,dq}. \tag{3.14}$$

Here k_B is Boltzmann's constant and T the temperature.

Since the Poisson bracket $\{A, \rho\}$ only contains first derivatives and the density is a function of the classical Hamiltonian the Poisson bracket is

$$\{A, \rho\} = \frac{\partial\rho(-\infty)}{\partial H}\{A, H\} = -\frac{1}{k_BT}\rho(-\infty)\{A, H\}, \tag{3.15}$$

where the last Poisson bracket is just the time derivative of A according to Eq. (3.11). The Poisson bracket can therefore be expressed in terms of the temperature and the time derivative of the function A [50].

$$\{A, \rho\} = -\frac{1}{k_BT}\rho(-\infty)\dot{A} \tag{3.16}$$

This using this identity the response functions can be written as:

$$\boldsymbol{\chi}^{(3)}_{abcd}(t_1) = \frac{V}{2}\frac{1}{k_BT}\langle\chi^{(1)}_{ab}(t_1)\dot{\chi}^{(1)}_{cd}(0)\rho(-\infty)\rangle \tag{3.17}$$

$$\boldsymbol{\chi}^{(5)}_{abcdef}(t_1, t_2) = -\frac{V^2}{4}\frac{1}{k_BT}\langle\chi^{(1)}_{ab}(t_1+t_2)\{\chi^{(1)}_{cd}(t_1), \dot{\chi}^{(1)}_{ef}(0)\rho(-\infty)\}\rangle. \tag{3.18}$$

Using the general relation $\{A, B\rho\} = B\{A, \rho\} + \{A, B\}\rho$ and moving the time differentiation in the third-order expression we get the classical correlation function expressions:

$$\boldsymbol{\chi}^{(3)}_{abcd}(t_1) = -\frac{V}{2k_BT}\langle\dot{\chi}^{(1)}_{cd}(t_1)\chi^{(1)}_{ef}(0)\rho(-\infty)\rangle \tag{3.19}$$

$$\begin{aligned}
\boldsymbol{\chi}^{(5)}_{abcdef}(t_1, t_2) &= \left(\frac{V}{2k_BT}\right)^2\langle\chi^{(1)}_{ab}(t_1+t_2)\dot{\chi}^{(1)}_{cd}(t_1)\dot{\chi}^{(1)}_{ef}(0)\rho(-\infty)\rangle \\
&\quad -\frac{V^2}{4k_BT}\langle\chi^{(1)}_{ab}(t_1+t_2)\{\chi^{(1)}_{cd}(t_1), \dot{\chi}^{(1)}_{ef}(0)\}\rho(-\infty)\rangle.
\end{aligned} \tag{3.20}$$

The Poisson bracket, $\{\cdots, \cdots\}$, in the second term of the fifth-order expression can be written in terms of the differentials with respect to the phase space coordinates, p and q.

$$\{\chi^{(1)}_{cd}(t_1), \dot{\chi}^{(1)}_{ef}(0)\} = \sum_i \frac{\partial\chi^{(1)}_{cd}(t_1)}{\partial q_i(0)}\frac{\partial\dot{\chi}^{(1)}_{ef}(0)}{\partial p_i(0)} - \frac{\partial\chi^{(1)}_{cd}(t_1)}{\partial p_i(0)}\frac{\partial\dot{\chi}^{(1)}_{ef}(0)}{\partial q_i(0)} \tag{3.21}$$

These differentials of the polarizabilities at one time with respect to a phase space coordinate at another time pose a problem, since they cannot be calculated straightforwardly from Molecular Dynamics data. However, they can be rewritten using the chain rule for derivatives, where x can be any phase space coordinate, both momentum and position, and the summation over k runs over all possible phase space coordinates.

$$\frac{\partial \chi_{cd}^{(1)}(t_1)}{\partial x_i(0)} = \sum_k \frac{\partial \chi_{cd}^{(1)}(t_1)}{\partial x_k(t_1)} \frac{\partial x_k(t_1)}{\partial x_i(0)} \tag{3.22}$$

It is possible to calculate this expression, if one knows how a change in the phase space coordinates at one time affects the phase space coordinates at a later time. [57, 58, 115] The $\partial x_k(t_1)/\partial x_i(0)$ derivatives can be collected in the so called stability matrix [57].

$$M_{jk}(t_1, 0) \equiv \left\{ \frac{\partial x_k(t_1)}{\partial x_j(0)} \right\} \tag{3.23}$$

This stability matrix contains N^2 numbers, where N is the number of phase space coordinates. Using Molecular Dynamics all these numbers have to be updated every time step, [57] which is very time consuming unless the number of phase space coordinates is very limited.

Mukamel *et al.* [57] and Saito *et al.* [58] described how a general stability matrix $M_{jk}(t_a, t_b)$ can be calculated from a single molecular dynamics trajectory. The derivatives $\frac{\partial q_j(t_1)}{\partial q_i(0)}$ and $\frac{\partial q_j(t_1)}{\partial p_i(0)}$ can be calculated using the time development of the derivatives and the trivial values of the derivatives at $t_1 = 0$. Using the classical equation of motion in Eq. (3.11) [114] the time derivatives are expressed:

$$\frac{\partial}{\partial t} \begin{pmatrix} \frac{\partial q(t_1)}{\partial q(0)} & \frac{\partial q(t_1)}{\partial p(0)} \\ \frac{\partial p(t_1)}{\partial q(0)} & \frac{\partial p(t_1)}{\partial p(0)} \end{pmatrix} = \begin{pmatrix} -\frac{\partial^2 H(t_1)}{\partial q(t_1)\partial p(t_1)} & \frac{\partial^2 H(t_1)}{\partial p(t_1)\partial p(t_1)} \\ -\frac{\partial^2 H(t_1)}{\partial q(t_1)\partial q(t_1)} & \frac{\partial^2 H(t_1)}{\partial p(t_1)\partial q(t_1)} \end{pmatrix} \begin{pmatrix} \frac{\partial q(t_1)}{\partial q(0)} & \frac{\partial q(t_1)}{\partial p(0)} \\ \frac{\partial p(t_1)}{\partial q(0)} & \frac{\partial p(t_1)}{\partial p(0)} \end{pmatrix} \tag{3.24}$$

This can also be written more compact using the stability matrix notation:

$$\frac{\partial M}{\partial t} = \begin{pmatrix} -\frac{\partial^2 H(t_1)}{\partial q(t_1)\partial p(t_1)} & \frac{\partial^2 H(t_1)}{\partial p(t_1)\partial p(t_1)} \\ -\frac{\partial^2 H(t_1)}{\partial q(t_1)\partial q(t_1)} & \frac{\partial^2 H(t_1)}{\partial p(t_1)\partial q(t_1)} \end{pmatrix} M. \tag{3.25}$$

This is simplified by the fact that the second order derivatives of the Hamiltonian $\frac{\partial^2 H(t_1)}{\partial q(t_1)\partial p(t_1)}$ and $\frac{\partial^2 H(t_1)}{\partial p(t_1)\partial q(t_1)}$ under normal circumstances are zero and $\frac{\partial^2 H(t_1)}{\partial p(t_1)\partial p(t_1)}$ is diagonal. This allows splitting the equation into two independent parts. One part is related to the derivatives with respect to positions and the other is related to derivatives with respect to momentum.

$$
\begin{aligned}
\frac{\partial}{\partial t}\frac{\partial q_j(t_1)}{\partial q_i(0)} &= \frac{\partial p_j(t_1)}{\partial q_i(0)}\frac{\partial^2 H(t_1)}{\partial p_j(t_1)\partial p_j(t_1)}\\
\frac{\partial}{\partial t}\frac{\partial p_j(t_1)}{\partial q_i(0)} &= \sum_k \frac{\partial q_k(t_1)}{\partial q_i(0)}\frac{\partial^2 H(t_1)}{\partial q_k(t_1)\partial q_j(t_1)}
\end{aligned}
\tag{3.26}
$$

$$
\begin{aligned}
\frac{\partial}{\partial t}\frac{\partial q_j(t_1)}{\partial p_i(0)} &= \frac{\partial p_j(t_1)}{\partial p_i(0)}\frac{\partial^2 H(t_1)}{\partial p_j(t_1)\partial p_j(t_1)}\\
\frac{\partial}{\partial t}\frac{\partial p_j(t_1)}{\partial p_i(0)} &= \sum_k \frac{\partial q_k(t_1)}{\partial p_i(0)}\frac{\partial^2 H(t_1)}{\partial q_k(t_1)\partial q_j(t_1)}
\end{aligned}
\tag{3.27}
$$

The stability matrix $M(t_a, 0)$, with one time fixed at the beginning of the simulation, can then be found by means of numerical integration. And the general stability matrix $M(t_a, t_b)$ can be found using the chain rule.

$$
\frac{\partial x_k(t_a)}{\partial x_j(t_b)} = \sum_i \frac{\partial x_k(t_a)}{\partial x_i(0)}\frac{\partial x_i(0)}{\partial x_j(t_b)}
\tag{3.28}
$$

In matrix notation this is simply:

$$
M(t_a, t_b) = M(t_a, 0)M^{-1}(t_b, 0).
\tag{3.29}
$$

Recently studies on the $\chi^{(5)}_{zzzzzz}$ response of liquid xenon using variants of this approach [59, 99, 100] have been published. Due to the complications, related to the evaluation of the stability matrix at every timestep, only 32 atoms could be included in these simulations. Simulations on carbondisulfide and water systems with 32 molecules have later been reported. [101] The finite field method, discussed in section 3.1, is computationally much more efficient in calculating higher order multi-dimensional response.

3.3   Analytical models

Often phenomenological models have been used to interpret vibrational line shapes in liquids. This is usually done by assuming that the motion takes place in a harmonic potential and that the Placzek approximation holds for the Raman response. [103, 116] In this approximation it is assumed that the polarizability changes linearly with the displacement in each coordinate. When coupling the motion in the harmonic potential to a heat bath [50],

models can be obtained interpreting the response in terms of homogeneous and inhomogeneous line broadening mechanisms. The homogeneous line broadening is then related to the interaction between the system and the heat bath, while the inhomogeneous line broadening is related to the slowly fluctuating distribution of local environments. [35, 50, 72, 91, 92] More complicated models, including anharmonicity, mode coupling and more complicated expressions for the polarizability dependency on the coordinates, can be constructed in similar ways. [35, 91, 92]

Tanimura and Mukamel [35] used such phenomenological models when they first suggested the use of fifth-order Raman spectroscopy. They showed that if the motion is harmonic and the polarizability dependency on the coordinates is linear, no fifth-order response arises. This suggests that the fifth-order response will be sensitive to anharmonicity and non-linear dependence of the polarizability on the coordinates. Furthermore it was shown that motion in the homogeneous and inhomogeneous line broadening limits can, in principle, be clearly distinguished in two-dimensional Raman spectroscopy. In the homogeneous limit the signal can be expected to be rather symmetric in the two time dimensions, while in the inhomogeneous limit ridges are found along the diagonal and the t_2 axis but not along the t_1 axis. It is not possible to distinguish between the homogeneous and inhomogeneous line broadening limits in the third-order response.

Unfortunately the analytical models are difficult to interpret in microscopic molecular terms. They are either too simple to describe a real liquid, assuming one harmonic frequency and damping process or too complicated to allow for a unique interpretation of the response. They also lack the power of predicting spectra and spectral intensities.

In the following a few of the simplest analytical models that have been used in the interpretation of third-order spectra will be described. [68, 69, 82, 117–122] The following function describes the experimental CS_2 results rather well. [117, 118]

$$\chi^{(3)}(t) \propto \left(1 - \exp(-t/\tau_R) + A_R \sin(\Omega_R t)\exp(-w_R t^2/2)\right)\exp(-t/\tau_D) \qquad (3.30)$$

Here, the constant τ_D is the diffusive picosecond relaxation time and the other constants are related to the initial subpicosecond part of the response. The Gaussian damped sine function is taken from the work by Kalpouzos *et al.* [117, 118], where it was related to single-molecule librational motion.

Bucaro and Litovitz derived an expression for the spontaneous Raman scattering (frequency domain) due to interaction induced effects, based on an atomic collision model. [119] This is related by a Fourier transform to the stimulated third-order Raman response (time

domain).

$$\boldsymbol{\chi}^{(3)}(t) \propto \frac{\tau_C^n \sin(n \tan^{-1}(t/\tau_C))}{(t^2 + \tau_C^2)^{n/2}} \tag{3.31}$$

The factor of τ_C^n was added here to eliminate the time unit dependence. The frequency domain response was originally given as

$$\boldsymbol{\chi}^{(3)}(\omega) \propto \omega^{2[(m-7)/7]} \exp(-\omega/\omega_0), \tag{3.32}$$

where ω_0 is the inverse of τ_C and $2[(m-7)/7]$ is equal to $n-1$ ($m = [7n+7]/2$). In the paper by Bucaro and Litovitz [119] the time constant τ_C was related to molecular and thermodynamical properties in an approximate way.

$$\tau_C \approx \frac{1}{6} \pi r_0 (\mu/kT)^{1/2} \left[1 - (2/\pi) \tan^{-1}(2\epsilon/kT)^{1/2} \right] \tag{3.33}$$

Here ϵ and r_0 are the potential depth and the distance in a supposed Lennard-Jones potential and μ is the reduced mass. The constant m was related to the polarizability dependence on the interatomic distance r.

$$\alpha(r) - \alpha(\infty) \propto r^{-m} \tag{3.34}$$

It should be emphasized that one should be very careful using these functions for a microscopic interpretation of the liquid motion. The long time diffusive decay τ_D is the only constant that can be directly related to a dynamical property of the liquid. The description of the interaction induced effects, derived in an approximative way for atomic collisions, should be taken very cautiously or rather be avoided completely. Interaction induced effects will be discussed more extensively in chapter 4. The single molecule response is directly related to the time correlation function of the single molecule orientation tensor. This single molecule response is very difficult to isolate from experiments and fitting the results to a linear combination of Eqs. (3.30) and (3.31) will be likely to fail because of the similarity in shape between the Gaussian damped sine part of the single molecule response and the interaction induced response. In this way Kalpouzos *et al.* [117, 118] succeeded in fitting the whole anisotropic response function to Eq. (3.30), while Hattori *et al.* [120] succeeded in fitting the anisotropic response function to the same equation, but leaving out the Gaussian damped sine part and including a contribution from Eq. (3.31) instead. McMorrow *et al.* [122] recently presented an interpretation based on the classical and quantum models by Steffen *et al.* [69, 72]

For the fifth-order response the phenomenological models are much more complicated and they will not be treated here. [35, 72, 91, 92]

3.4 Instantaneous normal modes

At sufficiently short time scales the motion in liquids can be approximated as motion in
instantaneous harmonic potentials. [102] The instantaneous normal modes of the liquid
can be found by diagonalisation of the mass-weighted Hessian (G) using mass-weighted
coordinates y.

$$G_{ij} = \frac{1}{\sqrt{m_i m_j}} \frac{\partial^2 H}{\partial x_i \partial x_j} = \frac{\partial^2 H}{\partial y_i \partial y_j} \qquad (3.35)$$

The harmonic frequencies will then be related to the eigenvalues $(\omega_i = \sqrt{\lambda_i})$ and the normal
coordinates will be given by the eigenvectors. [123] The time dependence of the normal
mode coordinate q_i is given by [58]

$$q_i(t) = q_{i,0} \cos(\omega_i t + \phi_i), \qquad (3.36)$$

when supposing that the eigenvalues are positive. In this expression $q_{i,0}$ is the amplitude
of the motion and ϕ_i gives the initial displacement.

The first-order susceptibility can be expanded in the normal mode coordinates

$$
\begin{aligned}
\chi^{(1)} &= \chi_0^{(1)} + \sum_i \left(\frac{\partial \chi^{(1)}}{\partial q_i} \right) q_i + \frac{1}{2} \sum_{i,j} \left(\frac{\partial^2 \chi^{(1)}}{\partial q_i \partial q_j} \right) q_i q_j + \cdots \\
&= \chi_0^{(1)} + \sum_i \chi_i' q_i + \frac{1}{2} \sum_{i,j} \chi_{ij}'' q_i q_j + \cdots,
\end{aligned}
\qquad (3.37)
$$

allowing the expression of the third-order time correlation function (Eq. (3.19)) in the
normal mode coordinates.

$$
\begin{aligned}
\boldsymbol{\chi}^{(3)}(t) &= -\frac{1}{2} \frac{V}{k_B T} \langle \dot{\chi}^{(1)}(t) \chi^{(1)}(0) \rho(-\infty) \rangle \\
&= -\frac{1}{2} \frac{V}{k_B T} \frac{\partial}{\partial t} \Big(\chi_0^{(1)} \chi_0^{(1)} + \chi_0^{(1)} \sum_i \chi_i' \langle q_i(t) + q_i(0) \rangle \\
&\quad + \sum_{i,j} \chi_i' \chi_j' \langle q_i(t) q_j(0) \rangle + \frac{1}{2} \sum_{i,j,k} \chi_i' \chi_{jk}'' \langle q_j(t) q_k(t) q_i(0) + q_i(t) q_j(0) q_k(0) \rangle \\
&\quad + \frac{1}{4} \sum_{i,j,k,l} \chi_{ij}'' \chi_{kl}'' \langle q_i(t) q_j(t) q_k(0) q_l(0) \rangle + \cdots \Big)
\end{aligned}
\qquad (3.38)
$$

The first term is independent of time and vanishes when the derivative is taken (see Eq.
(3.19)) with respect to time. Furthermore all terms depending on the normal mode co-
ordinates in uneven powers vanish when averaging (integrating) over all possible initial

phases ϕ_i. The time correlation functions left over can be calculated using the expression for the normal mode coordinates (Eq. (3.36)), when keeping in mind that the normal mode coordinates are uncorrelated.

$$
\begin{aligned}
\sum_{i,j} \chi_i' \chi_j' \langle q_i(t) q_j(0) \rangle &= \sum_i (\chi_i')^2 q_{i,0}^2 \cos(\omega_i t) \\
\sum_{i,j,k,l} \chi_{ij}'' \chi_{kl}'' \langle q_i(t) q_j(t) q_k(0) q_l(0) \rangle &= \sum_{i,j} (\chi_{ij}'')^2 q_{i,0}^2 q_{j,0}^2 \cos\left((\omega_i + \omega_j)t\right)
\end{aligned}
\tag{3.39}
$$

The normal mode amplitudes $q_{i,0}$ are related to the temperature (average energy) in the system.

$$
E_i = \frac{\omega_i^2 q_{i,0}^2}{2} \approx \frac{1}{2} k_B T
\tag{3.40}
$$

Combining this with the correlation function expressions in Eq. (3.39) the third-order response given in Eq. (3.38) reads:

$$
\boldsymbol{\chi}^{(3)}(t) = \frac{V}{2} \sum_i (\chi_i')^2 \frac{\sin(\omega_i t)}{\omega_i} + \frac{V k_B T}{2} \sum_{i,j} (\chi_{ij}'')^2 \frac{\sin(\omega_i t)}{\omega_i} \frac{\cos(\omega_j t)}{\omega_j^2} + \cdots
\tag{3.41}
$$

Similarly the fifth-order expression can be found analytically avoiding the problems of numerical evaluation of the stability matrix (Eq. 3.23). The fifth-order INM expression is: [58]

$$
\begin{aligned}
\boldsymbol{\chi}^{(5)}(t_1, t_2) &= \frac{V^2}{4} \sum_{i,j} \chi_i' \chi_{ij}'' \chi_j' \frac{\sin(\omega_i t_2) \sin(\omega_j t_1)}{\omega_i \omega_j} & (3.42) \\
&+ \frac{V^2}{4} \sum_{i,j} \chi_{ij}'' \chi_i' \chi_j' \frac{\sin(\omega_i t_2) \sin(\omega_j (t_1 + t_2))}{\omega_i \omega_j} & (3.43) \\
&+ \frac{V^2 k_B T}{4} \sum_{i,j,k} \chi_{ij}'' \chi_{ik}'' \chi_{jk}'' \frac{\sin(\omega_i t_2)}{\omega_i} \left[\frac{\sin(\omega_j (t_1 + t_2))}{\omega_j} \frac{\cos(\omega_k t_1)}{\omega_k^2} \right. & (3.44) \\
&\left. + \frac{\cos(\omega_j (t_1 + t_2))}{\omega_j^2} \frac{\sin(\omega_k t_1)}{\omega_k} \right] + \cdots & (3.45)
\end{aligned}
$$

The mass-weighted Hessian (G) will under normal circumstances have a number of zero and negative eigenvalues resulting in imaginary frequencies. The normal modes related to these eigenvalues can be related to barriers crossings, transition states or diffusive motion. [102, 104, 124–126] Some discussion is found in literature on how these modes should be treated to be taken correctly into account. [58, 102, 104, 124–126] Claims have been made that including these modes in an approximate way takes diffusional motion into account [104, 125], while the imaginary frequencies have just been discarded in other studies. [58]

3.5   Discussion

The calculation methods mentioned in this chapter all have their advantages and drawbacks. Which method to use depends on what one wants to do. In fifth-order finite field calculations, first the distortion of the phase space coordinates caused by the applied laser fields is calculated. Subsequently, the field-free evolution of the system is followed, which is equivalent to calculating only the part of the stability matrix that corresponds to the initial distortion. In contrast, the whole stability matrix that takes arbitrary distortions into account has to be calculated in the correlation function method.

When the full MD data are used, the stability matrix has to be calculated numerically. This process, updating an N^2 matrix where N is the number of phase space coordinates, is much slower than the finite field method, where only a single vector of phase space coordinates is evaluated. Therefore the finite field method must be the preferred method, when one wants to calculate the fifth-order Raman response using the full MD trajectories as illustrated by the fact that the fifth-order time correlation function method has only been applied to a small system containing 32 atoms [59,99] or 32 triatomic molecules [101], whereas the finite field method has been applied to systems with 192 and 768 atoms (chapter 7). If one wants to calculate response due to other types of interactions (e.g. IR) simultaneously, it might turn out to be advantageous to calculate the full stability matrix. For third-order Raman response calculations the two methods are comparable when it comes to computational costs; they provide complementary ways to look at and think about the Raman response of liquids. The analytical models are all based on relatively simple assumptions and allow interpretation of the response within the framework of these assumptions. They give an idea about the kind of response that can be expected under different conditions. Unfortunately these phenomenological models are not related to microscopic or molecular properties and they are not able to predict the spectrum of a given liquid.

In the methods based on instantaneous normal modes the evaluation of the Poisson bracket is not a major problem. On the other hand, one should realize that this method is based on snapshots of the liquid and the method cannot be expected to be reliable for long time or even intermediate time response. One should also be aware that the potential surface in a real liquid changes on the same timescale as the dynamics one tries to describe. This fact means that the Instantaneous Normal Modes method is a rather bad approach and full MD approaches should be prefered.

Chapter 4

Local field effects

The first-order susceptibility is needed in order to calculate the third- and fifth-order Raman response described in the previous chapters. The microscopic counterpart to the susceptibility, i.e. the polarizability, can be calculated using quantum mechanical response methods such as time-dependent density functional theory (TDDFT). Unfortunately this method is far too time consuming to be used on large numbers of molecules as found in a molecular dynamics (MD) simulation. Alternatively, polarizability models based on interacting molecular or atomic polarizabilities can be employed. In these models the physical interaction between the individual entities should be properly taken into account. The importance of different kinds of interaction can be studied theoretically by examining molecule dimers or small clusters of molecules.

Physical interactions between molecules such as the dipole-induced dipole effect, induced multipole effects and electron cloud overlap effects give rise to a polarizability deviating from the simple sum of the single molecule polarizabilities. The dipole-induced dipole effects arise from the fact that two molecules in a macroscopic electric field do not only feel the macroscopic field but also the local field generated by the dipole induced by the electric field on the other molecule. The induced multipole effects arise because the molecules cannot be considered as point-like polarizabilities. Due to their extended atomic structure the local field from induced dipoles on neighboring molecules does not need to be felt equally strong in both ends of a molecule. The electron cloud overlap effects arise from molecules so close to each other that their electron clouds overlap. The interaction between the overlapping electron clouds will also affect the polarizability.

As a first approximation the susceptibility can be considered as being the sum of the molecular polarizabilities only valid in the limit of infinite dilution. Since the isotropic

part of the molecular polarizability is constant as long as the influence from intramolecular vibrations is neglected, the isotropic third-order response will be exactly zero in this approximation. Only anisotropic response exists, originating from molecular reorientation and therefore molecules belonging to the cubic symmetry groups will show no response at all at this level of approximation.

Inclusion of the dipole-induced dipole (DID) effects, arising from local fields generated by induced dipoles on neighboring molecules, will make the first-order susceptibility depend on the local structure in the liquid. Fluctuations in the local structure will then lead to fluctuations in the isotropic first-order susceptibility and hence to isotropic third-order response and changes in the anisotropic response as well. Thus, the isotropic third-order response provides a measure of the local structure dynamics.

Inclusion of the multipole and electron overlap effects will not change the symmetry considerations discussed above, but the exact structure dependence of the first-order susceptibility will be altered by smearing out the polarizability and by close encounters of molecules. These effects can be taken into account using the direct reaction field (DRF) model. [60, 61, 127, 128] Independent molecule and dipole-induced dipole models can be seen as simplifications of this model, omitting the multipole and electron overlap or even the dipole-induced dipole effects. In the next section it will be described how the first-order susceptibility can be calculated using the direct reaction field model. Then it will be explained how this model can be simplified to the other models, among others the DID model. In section 4.3 it will be considered how to calculate the forces within the DRF model and in section 4.4 some computational tricks will be given.

4.1   The direct reaction field model

Local field effects can be included in the calculation of the susceptibility by using the dipole-induced dipole correction to the electric field. An individual atom does not only feel the macroscopic field inside the sample, but also the electric fields generated by the induced dipole moments on molecules in the local surroundings. The surroundings can be divided into two areas: the nearby surroundings with distinct local structure and the surroundings far away that can be described by a continuous dielectric medium. Here the structured surroundings will be considered to be inside a spherical cavity around the individual molecule. The electric field generated by the induced dipoles in the dielectric medium is taken into account by using the macroscopic electric field instead of the external

electric field. The macroscopic field is the electric field inside a continuous dielectric sample, due to an externally field, applied outside the sample in vacuum. The relation between the macroscopic and the external field depends on the shape of the material, which is unknown. As long as no particular shape is considered the macroscopic electric field has te be used in order to keep the considerations general. The local electric field on each atom arises from the macroscopic field and the induced dipole moments on the nearby atoms within the spherical cavity, which are taken into account through a dipole interaction term. Using a modified dipole interaction term the electron overlap effect is also taken into account. [60] The contribution from the continuous dielectric medium inside the cavity is eliminated by subtracting a term due to the polarization of a spherical dielectric medium [50, 76, 127]. This term depends on the constant average susceptibility $\boldsymbol{\chi}^{(1)}$ (Eq. (2.26)). The approach is depicted schematically in Figure 4.1.

The local electric field on atom p is in this model given by:

$$E_p^{\text{local}} = E^{\text{mac}} + \sum_{q \neq p} \mathcal{T}_{pq} \mu_q + \frac{4\pi \boldsymbol{\chi}^{(1)}}{3} E^{\text{mac}} \tag{4.1}$$

Here $\mathcal{T}_{pq}$ is a modified dipole field tensor defined as:

$$\mathcal{T}_{pq} = \frac{3 f_{pq}^T (\hat{r}_{pq} : \hat{r}_{pq}) - f_{pq}^E}{r_{pq}^3} \tag{4.2}$$

The modification is present in the screening functions f_{pq}^T and f_{pq}^E representing the damping due to overlapping charge densities. These are functions of the distance r_{pq} and they have to approach one as r_{pq} goes to infinity, leaving us with the unmodified dipole tensor suitable to describe only dipole-induced dipole effects. Various models for these screening functions have been suggested. [60] Assuming an exponentially decaying electron density around the atoms, one gets the following expressions for the screening functions:

$$f_{pq}^E = 1 - \left(\frac{1}{2} \nu_{pq}^2 + \nu_{pq} + 1 \right) \exp(-\nu_{pq}) \tag{4.3}$$

$$f_{pq}^T = f_{pq}^E - \frac{\nu_{pq}^3}{6} \exp(-\nu_{pq}) \tag{4.4}$$

$\nu_{pq} = \frac{\mathbf{a} r_{pq}}{(\alpha_p \alpha_q)^{1/6}}$ (4.5) The empirical screening factor $\mathbf{a}$, and the atomic polarizabilities are usually optimized to give as good a description of the molecular polarizability as possible for a wide variety of molecules. [128]
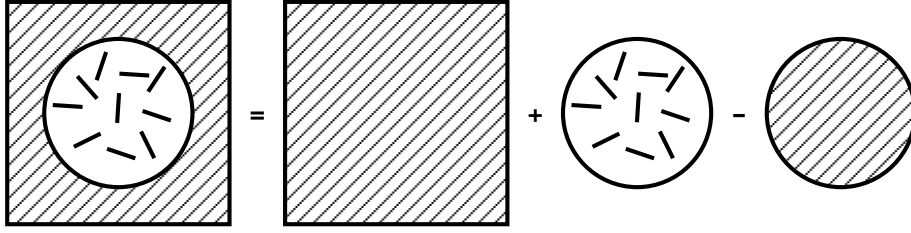
FIGURE 4.1*: The local fields acting on a molecule in a medium with local structure, inside a cavity surrounded by a continuous dielectric medium, can be divided into the contributions from the dielectric medium, and from the molecules inside the cavity. The contribution from the dielectric medium inside the cavity has to be subtracted in order to avoid counting the influence of this region twice.*

Solving a linear set of equations for the independent molecules, [95] the susceptibility can be found as well as the index of refraction and the dielectric constant. Both are related to the first-order susceptibility. An effective polarizability $\Pi_n^{(1)}$, reproducing the same induced-dipole moment from the macroscopic field as generated by polarizability α_n in the local field, is defined for simplicity:

$$\mu_p = \alpha_p E_p^{\text{local}} \equiv \Pi_p E^{\text{mac}}. \tag{4.6}$$

Combining Eq. (4.1) and (4.6) gives

$$\Pi_p E^{\text{mac}} = \alpha_p \left(1 + \frac{4\pi\boldsymbol{\chi}^{(1)}}{3} \right) E^{\text{mac}} + \alpha_p \sum_{q \neq p} \mathcal{T}_{pq} \Pi_q E^{\text{mac}}. \tag{4.7}$$

Since this relation is valid for macroscopic fields with any polarization direction, the macroscopic field can be left out giving the matrix equation:

$$\Pi_p = \alpha_p + \alpha_p \sum_{q \neq p} \mathcal{T}_{pq} \Pi_q + \frac{4\pi\boldsymbol{\chi}^{(1)}}{3} \alpha_p \tag{4.8}$$

When the equation is multiplied with the inverse molecular polarizability and the terms containing the effective polarizability are isolated on the left side of the equation, the following expression is obtained:

$$\alpha_p^{-1} \Pi_p - \sum_{q \neq p} \mathcal{T}_{pq} \Pi_q = 1 + \frac{4\pi\boldsymbol{\chi}^{(1)}}{3} \tag{4.9}$$

Introducing Kronecker deltas, the summation over q can be taken over all terms on the left side. When at the same time the index of the effective polarizability is changed from p to q, the effective polarizability can be isolated.

$$\sum_q (\alpha_p^{-1}\delta_{pq} - \mathcal{T}_{pq}(1 - \delta_{pq}))\Pi_q = 1 + \frac{4\pi\boldsymbol{\chi}^{(1)}}{3} \tag{4.10}$$

This linear set of equations can be written as

$$\sum_q B_{pq}\Pi_q = L, \tag{4.11}$$

where the B matrix is defined:

$$B_{pq} \equiv \alpha_p^{-1}\delta_{pq} - \mathcal{T}_{pq}(1 - \delta_{pq}). \tag{4.12}$$

L is the Lorentz factor, which in the isolated molecule case without surrounding liquid is one, and else given by:

$$L = 1 + \frac{4\pi\boldsymbol{\chi}^{(1)}}{3}. \tag{4.13}$$

The effective polarizability can then be calculated from Eq. (4.11) using Cholesky decomposition, [129] which is a special form of LU decomposition [129] that can be applied when the B matrix is symmetric and positive definite.

From the induced macroscopic polarization density $\mathbf{P}$, the first-order susceptibility can be identified.

$$\chi^{(1)}E^{\text{mac}} \equiv \mathbf{P} = \frac{1}{V}\sum_p \mu_p = \left(\frac{1}{V}\sum_p \Pi_p\right)E^{\text{mac}} \tag{4.14}$$

Similarly the polarizability of a molecule or an isolated cluster of molecules can be identified from the induced polarization P.

$$\alpha E^{\text{mac}} \equiv P = \sum_p \mu_p = \sum_p \Pi_p E^{\text{mac}} \tag{4.15}$$

The dielectric constant and the diffractive index can be found from the mean value of the susceptibility (when c.g.s. units are applied), $\boldsymbol{\chi}^{(1)} = \langle\chi^{(1)}\rangle$.

$$\begin{aligned} \epsilon &= 1 + 4\pi\boldsymbol{\chi}^{(1)} \\ n &= \sqrt{1 + 4\pi\boldsymbol{\chi}^{(1)}} \end{aligned} \tag{4.16}$$

4.2   Different local field effect models

The first-order susceptibility has been approximated in several other ways in literature. A few studies have left out the electron overlap effect. [87, 103, 104, 106, 126, 130–132] This is done by setting the screening functions equal to one (or letting the screening factor **a** go toward infinity). Optimizing this model for the single molecule also gives slightly different polarizabilities on the atoms than the DRF model resulting in a change in the induced multipole contributions. This artefact can be avoided by using the DRF screening factors for interactions within the molecules but not in intermolecular interactions. This model, in which the DRF induced multipoles are retained, will be called the Multipole model (POL). Computationally almost nothing is gained by using this simpler model since the calculation of the screening factors is not a time limiting computation. On the other hand this model allows an investigation of the role of electron overlap effects, by comparing the results with a model in which these effects are properly taken into account.

Using polarizabilities located only on the center of mass of a molecule, the computations can be made faster. Solving the set of linear equation is practically a N^3 process. [129] Carbon disulfide contains 3 atoms and in a molecular model N will be 3 times smaller resulting in an approximate speed-up of a factor 27. The calculation is slightly more complicated since the molecular polarizability need not be isotropic and taking the inverse is slightly more complicated than in the isotropic atom model. In section 4.4.1 a simple procedure to find the inverse of the polarizability of a randomly oriented linear molecule is given. When the screening functions are equal to one this approach is the molecular dipole-induced dipole model (DID) used in most early studies [56, 59, 77, 95–98].

Solving the full linear set of equations can be avoided by applying the first-order dipole-induced dipole approximation. In this model the effective polarizability of molecule p does not depend on the effective polarizabilities of the other molecules Π_q as in the second term of Eq. (4.8), but is instead approximated to depend only on the initial molecular polarizabilities α_q. This gives closed expressions for all effective polarizabilities. However, when large molecular polarizabilities are encountered as in the carbon disulfide this approach was shown to be incorrect [95, 96].

Even simpler is the approximation of the effective polarizabilities by the molecular polarizabilities which amounts to the independent molecule model (MOL). Since the isotropic part of the molecular polarizability is constant as long as intramolecular vibrations are not taken into account, the isotropic (magic angle) response is zero in this model. [55, 133] The

four local field effect models outlined in this section are summarised in Table 4.1. The importance of the different physical phenomena taken into account in these models will be examined using time dependent density functional theory in chapter 5 and 9 and they will be applied in the calculations of the response in chapter 7 and 9 using the methods described in chapter 2.

TABLE 4.1: *The physical phenomena included by the four local field effect models.*

Model	Molecular Anisotropy	Dipole-induced dipole	Multipoles	Electron overlap
MOL	yes	no	no	no
DID	yes	yes	no	no
POL	yes	yes	yes	no
DRF	yes	yes	yes	yes

4.3   Calculating the forces

The interaction energy between a laser pulse pair and the liquid is given by the macroscopic laser fields E_a^{mac} and E_b^{mac} and the effective polarizabilities of the atoms [56, 134]

$$H_{\mathrm{int}}^{ab} = -\frac{1}{2} \sum_p E_a^{\mathrm{mac}} \Pi_p E_b^{\mathrm{mac}} \tag{4.17}$$

The forces exerted by the laser fields in a given atomic coordinate x, is given by the derivative of the interaction energy with respect to that particular coordinate.

$$
\begin{aligned}
F_x^{ab} &= -\frac{\partial H_{\mathrm{int}}^{ab}}{\partial x} & (4.18)\\
&= \frac{1}{2} \sum_q E_a^{\mathrm{mac}} \frac{\partial \Pi_q}{\partial x} E_b^{\mathrm{mac}} & (4.19)
\end{aligned}
$$

The forces can be found if the derivatives of the effective atomic polarizabilities are known. These derivatives can be obtained by differentiating Eq. (4.11), which gives the linear set of equations

$$\sum_q B_{pq} \frac{\partial \Pi_q}{\partial x} = \sum_q \frac{\partial \mathcal{T}_{pq}}{\partial x} (1 - \delta_{pq}) \Pi_q. \tag{4.20}$$

To find the derivatives of the effective polarizabilities as given in Eq. (4.20) the derivatives of the modified dipole tensor must be known. This derivative includes contributions depending on the derivatives of the screening functions. The modified dipole tensor is given by:

$$\mathcal{T}_{pq} = \frac{3f_{pq}^{T}\left(\hat{r}_{pq} : \hat{r}_{pq}\right) - f_{pq}^{E}}{r_{pq}^{3}} \tag{4.21}$$

with the distance vector r_{pq} defined to be the vector from atom q to atom p. When r_i is the Cartesian component i of the distance vector, the Cartesian components of the modified dipole tensor can be written as:

$$\left(\mathcal{T}_{pq}\right)_{ij} = \frac{3f_{pq}^{T}\left(\hat{r}_{pq;i} : \hat{r}_{pq;j}\right) - f_{pq}^{E}\delta_{ij}}{r_{pq}^{3}} \tag{4.22}$$

The derivative of the modified dipole tensor with respect to the coordinate $r_{p;k}$ is then given by: [62]

$$\left(\frac{\partial \mathcal{T}_{qp}}{\partial r_{p;k}}\right)_{ij} = \frac{3}{r_{pq}^{7}}\left(5r_i r_j r_k - r^2 r_i \delta_{jk} - r^2 r_j \delta_{ki}\right)f_{pq}^{T} - \frac{3}{r_{pq}^{5}}r_k \delta_{ij}f_{pq}^{E} \tag{4.23}$$

$$+ \quad \frac{1}{2}\left(\frac{r_i r_j r_k \nu}{r_{pq}^{7}} - \frac{r_k \delta_{ij}}{r_{pq}^{5}}\right)\nu^3 \exp(-\nu) \tag{4.24}$$

The similarity between Eq. (4.20) and Eq. (4.11) should be noticed, because the Cholesky decomposed B matrix first used to find the susceptibility in Eq. (4.11) can be used directly to find the derivatives in Eq. (4.20) saving computer time. [129]

4.4   Computational tricks

In the following subsections some mathematical tricks that can be used, when performing calculations with the molecular polarizability models given in the previous sections are described. Furthermore, a method to smoothen the boundary between the part of space where the local structure is taken explicitly into account and the part where the molecules are regarded as a continuous dielectric medium (see Figure 4.1), is described.

4.4.1   The inverse molecular polarizability

The polarizability tensor elements of a linear molecule p, is given by

$$\alpha_{p,ij} = \left(\alpha - \frac{1}{3}\gamma\right)\delta_{ij} + \gamma x_i^p x_j^p. \tag{4.25}$$

Here α is the isotropic polarizability, γ is the anisotropy, and x_i^p is the i component of the orientational unit-vector of molecule p. The tensor elements of the inverse polarizability are then given in the same form by

$$\alpha_{p,ij}^{-1} = \left(\epsilon - \frac{1}{3}\lambda\right)\delta_{ij} + \lambda x_i^p x_j^p. \tag{4.26}$$

Here ϵ is $3/(3\alpha - \gamma)$ and λ is $3/(3\alpha - 2\gamma) - \epsilon$. The validity of the relation is easily verified by matrix multiplication of the polarizability tensor and the inverse, using that the orientational vector is a unit-vector.

4.4.2 The derivative of the molecular polarizability

The derivative of the polarizability of a linear molecule, as given in subsection 4.4.1, with respect to a coordinate of the orientational unit-vector pointing along the molecular axis with the condition that the change is perpendicular to the molecular axis is given by

$$\left(\frac{\partial \alpha_n}{\partial x_i^n}\right)_{jk} = \gamma(x_j^n \delta_{ik} + x_k^n \delta_{ij} - 2x_i^n x_j^n x_k^n). \tag{4.27}$$

The derivative of the inverse molecular polarizability is found from the same expression simply by substituting γ by λ from subsection 4.4.1.

4.4.3 Soft cut-off

In the paper on the finite field method, based on the DID model, [56] we noted that noise was generated due to the fact that a molecule in the calculation with applied forces and in the calculation of the background polarizability at certain times could be on different sides of the cut-off boundary. Therefore its contribution to the local structure is taken explicitly into account in one calculation but not in the other. This was overcome by making the cut-off radius so large that the contribution from the molecules near the cut-off on the polarizability of the central molecule was vanishing. The problem can be overcome in a more elegant way that also allows using shorter cut-off distances without introducing artifacts due to boundary crossing. By introducing a soft cut-off the noise can be reduced. This is done by multiplying the dipole tensor with a weight function that is one at short distances and vanishes beyond the cut-off radius, but is continuous and differentiable.

In a paper on the calculation of susceptibilities of solids F. Kootstra *et al.* [135] introduced such a function. They suggested using the form:

$$w(x) = [1 + \exp(\beta[x - 1/x])]^{-1} \quad : \quad \beta > 0. \tag{4.28}$$

This function is nicely continuous and differentiable. However, it is rather costly to evaluate computationally since it includes both an exponential function and the inverse twice.

We will use a function that is faster to compute and has clear boundaries. The function is exactly one within the distance $x_c - \Delta x$, where x_c is the cut-off distance and Δx is the cut-off width. Outside the distance $x_c + \Delta x$ the function is defined to be exactly zero, allowing to skip calculations on molecules separated by such distances. In between the function is defined by a polynomial that ensures that both the weight function and its derivative are continuous.

$$w(x) = \begin{cases} 1 & : \quad x < x_c - \Delta x \\ \frac{1}{4}\left(\frac{x - x_c}{\Delta x}\right)^3 - \frac{3}{4}\frac{x - x_c}{\Delta x} + \frac{1}{2} & : \quad x_c - \Delta x \leq x \leq x_c + \Delta x \\ 0 & : \quad x > x_c + \Delta x \end{cases} \qquad (4.29)$$

The derivative is given by:

$$w^{(1)}(x) = \begin{cases} 0 & : \quad x < x_c - \Delta x \\ \frac{3}{4}\left(\left(\frac{x - x_c}{\Delta x}\right)^2 - 1\right) & : \quad x_c - \Delta x \leq x \leq x_c + \Delta x \\ 0 & : \quad x > x_c + \Delta x \end{cases} . \qquad (4.30)$$

Soft cut-offs like this is usual in many MD codes.

Chapter 5

TDDFT calculations

Time dependent density functional theory (TDDFT) has been shown to be a reliable quantum mechanical method for calculation of molecular response properties such as excitation energies, [136–139] dynamic polarizabilities [137, 140, 141] and van der Waals dispersion coefficients. [142] TDDFT has also been used to calculate the first-order susceptibility of solids. [135, 143] Here translation symmetry of an often small unit cell allows a quantum description of the whole (infinite) crystal using Bloch functions. This method is not practically applicable for liquids that on a macroscopic scale are isotropic systems, but on a local microscopic scale are characterized by a lack of symmetry. In molecular dynamics calculations (MD) liquids are usually simulated using periodic boundary conditions giving both a unit cell and the same translational symmetry as for a solid. Artefacts arising from applying periodic boundary conditions are avoided by using as big a unit cell as possible. If one wants to apply TDDFT to a liquid configuration one has to make sure that the size of the unit cell is so big that no interaction between any molecule with another molecule and the translated image of that other molecule in the neighbouring unit cells exists. This will require the use of very large unit cells for which TDDFT calculations are practically impossible.

Instead the liquid first-order susceptibility can be calculated effectively using local field effect models as described in chapter 4. Such a calculation for a liquid configuration typically takes a few seconds in contrast to precise quantum calculations that can take hours for just one molecule. By using quantum calculations on dimers, the accuracy of the simple models can be investigated and the models might even be optimized to give a description as close to the quantum description as possible.

In this chapter TDDFT calculations of the polarizability have been performed on the

CS_2 monomer and on various dimer conformations. In a study on liquid xenon the same methods has been used on xenon dimers, [144] as will be described in chapter 9. Other quantum methods as Coupled Cluster (CC) and Møller-Plesset perturbation theory (MP) could in principle have been used as well. For example CC studies on Helium and Argon dimers [145, 146] and MP studies on dimers of carbon dioxide and the noble gases [147] are found in the literature. The advantage of TDDFT compared to most other quantum methods is that TDDFT has a high accuracy, is time efficient and can be applied to large systems.

5.1   Polarizability calculations

TDDFT calculations have been performed on the carbon disulfide monomer as well as on dimers using the Amsterdam Density Functional Program Package (ADF). [136, 148– 152] The LB94 potential [153] was used for the response calculations to ensure correct asymptotic behavior in the diffuse region. A Slater-type orbital function basis set of triple zeta quality with polarization and diffuse functions was employed (ADF basis set VIII constructed for polarization calculations). All calculations were done using an electric field frequency corresponding to a wavelength of 514.5 nm. For the calculations a C-S bondlength of 1.5704 Å was used.

The monomer polarizability was found to be 8.95 Å^3 while the anisotropy was found to be 10.05 Å^3. These values coincide with the experimental numbers reported by Bogaard *et al.* [154] This exact agreement is a matter of coincidence rather than evidence of the general accuracy of the method. In calculated polarizabilities using the TDDFT method absolute average deviations of 3.6 % compared with experiment have been reported for a series of molecules. [137] In Table 5.1 the monomer polarizability is also given at other wavelengths and using the PW91 exchange correlation functional [155] that does not have the correct asymptotic behavior in the diffuse region.

Four representative dimer configurations were selected for investigation. These are shown in Figure 5.1. The polarizabilities were calculated with TDDFT for these config- urations at various intermolecular separations. The polarizabilities calculated with the dipole-induced dipole approach and the DRF model, described in chapter 4, were also calculated for comparison. In the DID model the molecular isotropic polarizability was 8.95 Å^3 and the molecular anisotropic polarizability was 10.05 Å^3. For the DRF model the screening factor was set to 2.5568 and the atomic polarizabilities were set to 1.197024 and

TABLE 5.1: *The polarizability of carbon disulfide calculated at different wavelengths, using the PW91 exchange correlation functional [155] or the LB94 potential. [153]*

Wavelength / nm	488.0	514.5	632.8	∞
Polarizability				
Calculated (PW91) / Å^3	9.32	9.23	8.98	8.54
Calculated (LB94) / Å^3	9.03	8.95	8.71	8.32
Experimental / Å^3	9.04	8.95	8.67	-
Anisotropy				
Calculated (PW91) / Å^3	9.99	9.82	9.32	8.50
Calculated (LB94) / Å^3	10.23	10.05	9.57	8.73
Experimental / Å^3	10.25	10.05	9.46	-

3.00098 Å^3 for carbon and sulfur respectively. This choice gives the correct polarizability for the monomer and the chosen screening factor gives an optimal description of the polarizability in the B and D configurations in the second solvation shell, as will be described later.

FIGURE 5.1: *The four considered CS_2 dimer configurations, A, B, C and D. The intermolecular (centre of mass) distances are marked with double arrows. The sloping line in configuration D indicates a molecule perpendicular to the paper plane.*
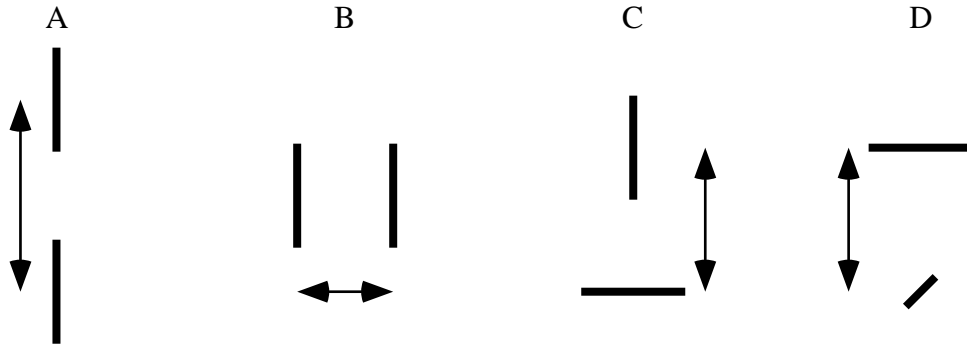
The relative importance of the different configurations of Figure 5.1 in the simulated liquid was estimated by calculating the radial distribution function (RDF), using molecular dynamics as will be described in chapter 6. All dimer configurations in the liquid were attributed to the configuration that they closest resemble. The RDFs for the dimer

configurations and the total RDF are shown in Figure 5.2.

FIGURE 5.2: *The radial distribution functions between the centers of mass (C-C) for A (full), B (long dashed), C (dashed) and D (dashed dotted) like dimer configurations (see Figure* 5.1*) and the total radial distribution function (thick full). The separation distance is given in Ångstrøm.*
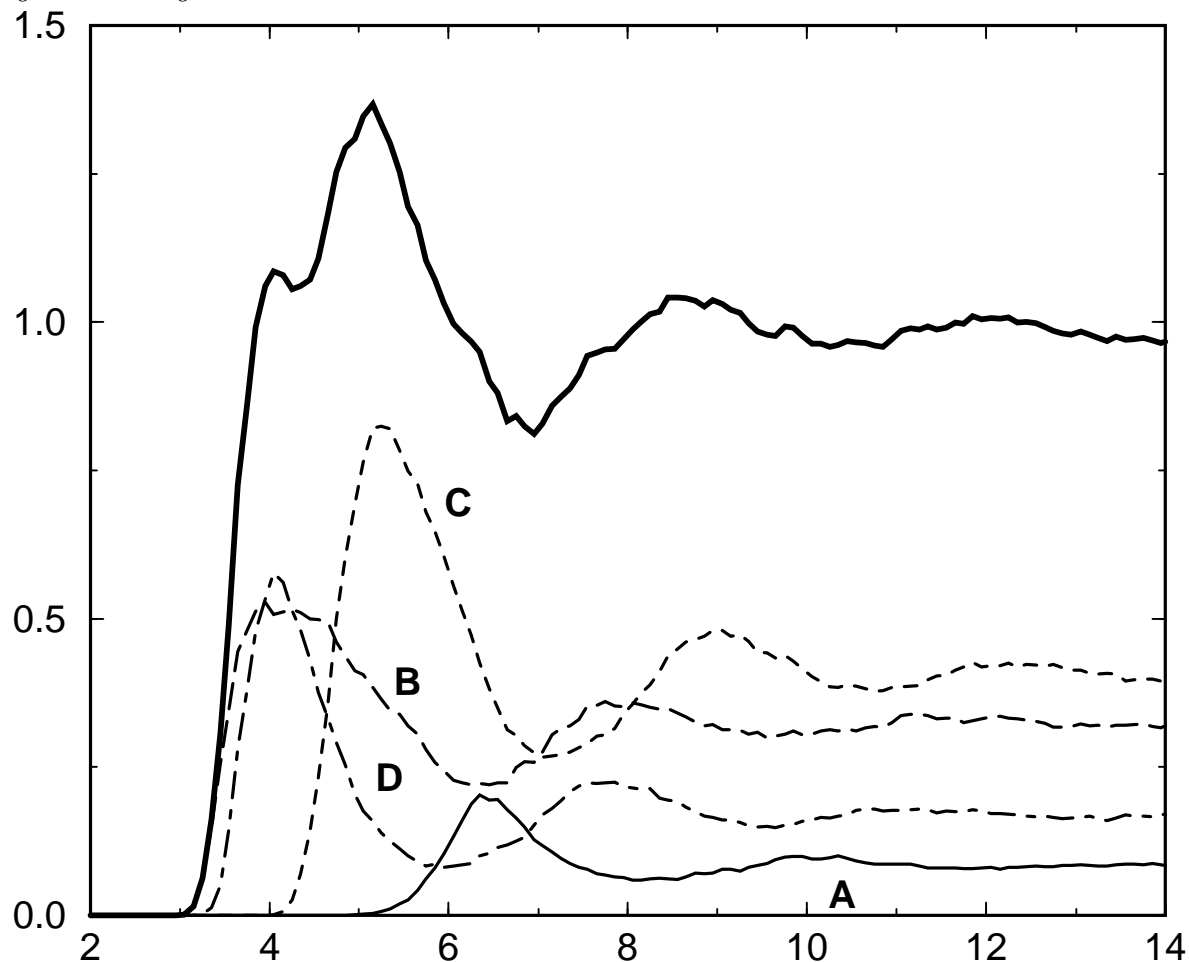
The dimer polarizabilities were calculated at distances found realistic by examining the RDFs. For each dimer configuration the distances covering the two first peaks (solvation shells) in the RDF were included. Furthermore in all configurations the polarizability is calculated in one point with shorter distance between the molecules than the shortest distance found in the RDF for that configuration. In Table 5.2 to 5.5 the polarizabilities obtained using the DID model and the DRF model are compared with the dimer polarizabilities calculated with TDDFT. The dimer polarizability is listed for the principal axes

a, *b* and *c* of the polarizability tensor. For configuration A, B and D the DRF model is clearly better than the DID approach. For configuration C no improvement is found in the dimer polarizability using the DRF model. For this configuration the results even seem a bit worse than the DID result. In general the errors in both the DID and the DRF are less than 1 % for distances in the order of the second solvation shell. In the first solvation shell the errors for the DID model are larger: up to 10 % are found. In contrast, for the DRF model the results are still good, with errors in the B and D configurations of less than 1 % . In the A and C configurations the errors are slightly larger.

TABLE 5.2: *The DID and DRF models compared to the TDDFT results for dimers in the A configuration. The centre of mass distances r_{CM}, are given in Å and the dimer polarizabilities in Å^3. The horizontal line mark the shortest distance that is found in the simulations.*

A	1st axis (a)			2nd+3rd axes (b+c)			Abs. errors	
r_{CM}	DID	DRF	TDDFT	DID	DRF	TDDFT	DID	DRF
5	41.76	60.09	71.23	10.72	9.91	10.06	18.16%	6.21%
6	36.61	42.65	48.84	10.92	10.57	10.62	10.23%	4.54%
7	34.44	36.74	36.44	11.02	10.87	10.87	2.75%	0.27%
8	33.34	34.35	33.88	11.08	11.01	11.01	0.96%	0.46%
9	32.70	33.21	32.97	11.11	11.08	11.07	0.51%	0.30%
10	32.31	32.58	32.49	11.14	11.12	11.12	0.30%	0.09%
14	31.68	31.70	31.73	11.17	11.17	11.17	0.05%	0.03%
Av. Abs. error							4.7%	1.7%

5.2 Multipole contributions

The DRF model includes both the multipole and electron overlap contributions in an approximate way. From the results it is not immediately clear what the relative importance is of these two contributions. To get an idea about this aspect, one can set the screening functions to one for interactions between atoms in different molecules, leaving only the effect of the multipole contribution between the dimers, as described in chapter 4. In Table 5.6 this multipole model (POL) is compared with the DRF model for the A configuration as a representative example. The lack of intermolecular screening functions has a vanishing

TABLE 5.3: *The DID and DRF models compared to the TDDFT results for dimers in the B configuration. The centre of mass distances r_{CM}, are given in Å and the dimer polarizabilities in Å³. The horizontal line mark the shortest distance that is found in the simulations.*

B r_{CM}	1st axis (a)			2nd axis (b)			3rd axis (c)			Abs. errors	
	DID	DRF	TDDFT	DID	DRF	TDDFT	DID	DRF	TDDFT	DID	DRF
3	19.81	26.10	25.58	19.14	13.44	13.37	9.28	9.92	9.99	24.27%	1.09%
4	25.15	27.94	27.56	13.58	12.38	12.38	10.30	10.52	10.56	6.97%	0.75%
5	27.82	29.09	28.86	12.30	11.92	11.87	10.72	10.81	10.81	2.69%	0.41%
6	29.19	29.80	29.67	11.81	11.65	11.60	10.92	10.96	10.95	1.23%	0.32%
7	29.93	30.26	30.30	11.58	11.50	11.48	11.02	11.04	11.07	0.85%	0.19%
8	30.37	30.55	30.54	11.45	11.41	11.38	11.08	11.09	11.09	0.42%	0.10%
9	30.64	30.75	30.74	11.37	11.35	11.34	11.11	11.12	11.12	0.23%	0.04%
Av. Abs. error										5.2%	0.4%

TABLE 5.4: *The DID and DRF models compared to the TDDFT results for dimers in the C configuration. The centre of mass distances r_{CM}, are given in Å and the dimer polarizabilities in Å³. The horizontal line mark the shortest distance that is found in the simulations.*

C	1st axis (a)			2nd axis (b)			3rd axis (c)			Abs. errors	
r_{CM}	DID	DRF	TDDFT	DID	DRF	TDDFT	DID	DRF	TDDFT	DID	DRF
4	29.23	27.31	31.44	18.92	19.35	21.69	10.30	10.08	10.24	6.80%	8.50%
5	24.61	24.48	25.58	19.96	20.01	19.90	10.72	10.59	10.62	1.68%	1.71%
6	23.05	23.10	23.07	20.48	20.46	20.40	10.92	10.85	10.85	0.37%	0.14%
7	22.34	22.38	22.28	20.75	20.73	20.75	11.02	10.99	11.00	0.15%	0.21%
8	21.96	22.99	21.95	20.91	20.90	20.90	11.08	11.07	11.07	0.06%	0.06%
9	21.75	21.76	21.74	21.01	21.00	21.00	11.11	11.10	11.10	0.06%	0.03%
10	21.61	21.62	21.61	21.08	21.07	21.07	11.14	11.13	11.12	0.08%	0.05%
Av. Abs. error										1.3%	1.5%

TABLE 5.5: *The DID and DRF models compared to the TDDFT results for dimers in the D configuration. The centre of mass distances r_{CM}, are given in Å and the dimer polarizabilities in Å^3. The horizontal line mark the shortest distance that is found in the simulations.*

D	1st axis (a)			2nd+3rd axes (b+c)			Abs. errors	
r_{CM}	DID	DRF	TDDFT	DID	DRF	TDDFT	DID	DRF
3	16.77	19.16	19.02	19.14	12.61	12.50	25.59%	0.78%
4	18.92	19.89	19.79	13.58	12.18	12.14	6.88%	0.45%
5	19.96	20.37	20.31	12.30	11.84	11.80	2.56%	0.31%
6	20.48	20.67	20.65	11.81	11.62	11.66	0.98%	0.18%
7	20.75	20.85	20.86	11.58	11.49	11.50	0.58%	0.06%
8	20.91	20.97	20.96	11.45	11.40	11.40	0.31%	0.03%
9	21.01	21.04	21.04	11.37	11.35	11.34	0.18%	0.03%
Av. Abs. error							5.3%	0.3%

effect at separations larger than those found in the first solvation shell. Inside the first solvation shell of the A configuration the effect of the electron overlap is still rather small compared to the multipole effect. At very short distances where the distance between the sulfur atoms is much smaller than twice the van der Waals radius this multipole model breaks down and even gives unphysical negative polarizabilities. However, this only happens at distances shorter than those found in the MD simulations, which indicates that the major part of the DRF correction is due to the multipole effects and not to the electron overlap effect.

The local field generated at a point r around a monomer in a macroscopic field can be expressed in a molecular representation with a dipole-dipole polarizability α_1^1 and dipole-multipole polarizabilities α_1^n on the centre of mass of this monomer.

$$E^{\text{loc}}(r) = T_{11}(r)\alpha_1^1 E^{\text{mac}} + \sum_{n=2}^{\infty} T_{1n}(r)\alpha_1^n E^{\text{mac}} \tag{5.1}$$

Here $T_{11}(r)$ is the dipole tensor and $T_{1n}(r)$ is a dipole-multipole tensor. [156] In the case of carbon disulfide all dipole-multipole polarizabilities with even n vanish because of inversion symmetry. This leaves the dipole-octupole polarizability as the lowest order multipole polarizability. For carbon disulfide two independent components α_z^{30} and α_x^{31c} exist [156].

TABLE 5.6: *The importance of the multipole effects and the electron overlap effects (E.O.) in the A configuration estimated from the DID, POL and DRF models discussed in the text. The multipole contribution (M.Pol) is given by the difference between the POL model including multipole contributions and the DID models that does not include these. The electron overlap contribution (E.O.) is determined by the difference between the DRF model including both multipole effects and electron overlap and the POL model that includes multipole effect but not electron overlap. At centre of mass distances r_{CM} around 6.5 Å the sulfur atoms of the CS_2 molecules start touching each other. The polarizabilities are given in units of Å³.*

A	1st axis (a)						2nd+3rd axes (b+c)					
r_{CM}	DID	POL	DRF	TDDFT	M.Pol	E.O.	DID	POL	DRF	TDDFT	M.Pol	E.O.
5	41.76	-68.75	60.09	71.23	-110.51	128.84	10.72	9.57	9.91	10.06	-1.15	0.34
6	36.61	47.36	42.65	48.84	10.75	-4.71	10.92	10.52	10.57	10.62	-0.40	0.05
7	34.44	37.15	36.74	36.44	2.71	-0.41	11.02	10.86	10.87	10.87	-0.16	0.01
8	33.34	34.40	34.35	33.88	1.06	-0.05	11.08	11.01	11.01	11.01	-0.07	0.00
9	32.70	33.21	33.21	32.97	0.51	0.00	11.11	11.08	11.08	11.07	-0.03	0.00
10	32.31	32.59	32.58	32.49	0.28	-0.01	11.14	11.12	11.12	11.12	-0.02	0.00
14	31.68	31.70	31.70	31.73	0.02	0.00	11.17	11.17	11.17	11.17	0.00	0.00

In the DRF model the local field generated at a point r is determined by the effective atomic polarizabilities Π_i at the atomic centra r_i.

$$E^{\text{loc}}(r) = \sum_i \mathcal{T}(r - r_i)\Pi_i E^{\text{mac}} \tag{5.2}$$

Here $\mathcal{T}(r - r_i)$ is the modified dipole tensor, which at longer distances can be substituted with the dipole tensor $T_{11}(r)$. In the carbon disulfide molecule i is a summation over the two sulfur atoms and the carbon atom. This model can be expanded in powers of the distance r and comparison with the molecular model in Eq. (5.1) will provide expressions for the multipoles generated in the DRF model.

When a macroscopic electric field is applied *along* the molecular axis of the linear CS_2 molecules, the local field in a point on the axis displaced r from the center of mass in the molecular representation (Eq. (5.1)) is [156]

$$E^{\text{loc}}(r) = \frac{2}{r^3}\alpha_{zz}E^{\text{mac}} + \frac{4}{r^5}\alpha_z^{30}E^{\text{mac}} + \cdots . \tag{5.3}$$

In the long distance limit, where r is much longer than the C-S bondlength d that characterizes the molecular scale, the modified dipole tensor can be replaced by the dipole tensor in the DRF expression (Eq. (5.2)), which gives:

$$E^{\text{loc}}(r) = \left(\frac{2}{r^3}\Pi_{zz}^c + \frac{2}{(r+d)^3}\Pi_{zz}^s + \frac{2}{(r-d)^3}\Pi_{zz}^s\right) E^{\text{mac}}. \tag{5.4}$$

Expanding this DRF expression in powers of r gives

$$E^{\text{loc}}(r) = \frac{2}{r^3}(\Pi_{zz}^c + 2\Pi_{zz}^s)E^{\text{mac}} + \frac{4}{r^5}(6d^2\Pi_{zz}^s)E^{\text{mac}} + \cdots . \tag{5.5}$$

Comparing this with Eq. (5.3) the polarizability component α_{zz} and the dipole-octupole polarizability component α_z^{30} are identified in terms of the carbon and sulfur atom polarizabilities:

$$\alpha_{zz} = \Pi_{zz}^c + 2\Pi_{zz}^s \tag{5.6}$$
$$\alpha_z^{30} = 6d^2\Pi_{zz}^s \tag{5.7}$$

Similarly when a macroscopic electric field is applied *perpendicular to* the molecular axis, the local field in a point on the axis displaced r from the centre of mass in the molecular representation will be given by

$$E^{\text{loc}}(r) = \frac{-1}{r^3}\alpha_{xx}E^{\text{mac}} + \frac{-\sqrt{6}}{r^5}\alpha_x^{31c}E^{\text{mac}} + \cdots . \tag{5.8}$$

In the long distance limit, where the modified dipole tensor can be replaced by the dipole tensor the DRF expression is [156]

$$E^{\text{loc}}(r) = \left(\frac{-1}{r^3} \Pi_{xx}^c + \frac{-1}{(r+d)^3} \Pi_{xx}^s + \frac{-1}{(r-d)^3} \Pi_{xx}^s \right) E^{\text{mac}}. \tag{5.9}$$

Again d is the distance between a carbon and a sulfur atom. Expanding the DRF expression in powers of r gives

$$E^{\text{loc}}(r) = \frac{-1}{r^3} (\Pi_{xx}^c + 2\Pi_{xx}^s) E^{\text{mac}} + \frac{-\sqrt{6}}{r^5} (2\sqrt{6} d^2 \Pi_{xx}^s) E^{\text{mac}} + \cdots. \tag{5.10}$$

Comparing this result with Eq. (5.8) the polarizability compontent α_{xx} and the dipole-octupole polarizability component α_x^{31c} are identified as:

$$\alpha_{xx} = \Pi_{xx}^c + 2\Pi_{xx}^s \tag{5.11}$$

$$\alpha_x^{31c} = 2\sqrt{6} d^2 \Pi_{xx}^s \tag{5.12}$$

The expressions for the dipole polarizabilities as a sum of the effective atomic polarizabilities are identical to the expression given earlier in Eq. (4.15). The exact same relations could be derived considering the local field in a point perpendicular to the molecular axis or in an arbitrary point in space.

The dipole-octupole polarizability of carbon disulfide monomers can also be calculated using TDDFT. [142] In this way the two components α_z^{30} and α_x^{31c} were found to be 53.03 and 29.29 Å^5 respectively. From the expansion of the DRF expression for a single CS$_2$ molecule the dipole-octupole polarizability (Eqs. (5.7) and (5.12)) can also be estimated and values of 81.53 and 30.93 Å^5 are found. The discrepancy between the calculated and modeled α_z^{30} components explains some of the observed deviations between the DRF model and the TDDFT calculations.

The screening factor used was chosen by optimizing to the B and D dimer configurations in the second solvation shell. For this purpose the POLAR program by van Duijnen and Swart [61] was used. The DRF model employed here does not allow optimization to both the α_z^{30} and the α_x^{31c} component since it only contains three free variables in the case of CS$_2$ and two of these are used to give the correct single molecule polarizability components.

In principle the static electric fields can also influence the polarizability through the hyper-polarizabilities. In the case of CS$_2$ the most relevant contribution is a combination of the second hyper-polarizability γ and the electric field generated by the permanent quadrupole on CS$_2$. Such effects are neglected here but the good agreement between the TDDFT calculations and the DRF model indicates that this is a safe approximation. In a

recent study effects involving the permanent dipole moments and the hyper-polarizability β were investigated in formamide and N-methyl-formamide. [157]

5.3   Conclusion

The DRF model was used to improve the dipole-induced dipole description of the dimer polarizabilities of carbon disulfide by including induced multipole and electron overlap effects. This improved the quality of the theoretical description considerably as determined by comparing to the results of dimer calculations with TDDFT. The fact that the DRF model did not model the dipole-octupole interactions correctly leaves some room for improvement. The difference between the DID and DRF polarizabilities indicates that both the induced multipole and electron overlap effects are important for the third- and fifth-order Raman response. The induced multipole effects are probably the most important of the two. Further discussion will be found in chapter 9, where the investigation of liquid xenon is presented.

Chapter 6

Molecular dynamics

To follow the propagation of the nuclear dynamics, classical molecular dynamics simulations were applied. This limits the types of dynamics that can be treated accurately. If the number of available states is much larger than the number of particles, Boltzmann statistics applies and it is no problem to treat the dynamics classically. If the energy difference between the available states is not much smaller than $k_B T$ this is not the case any more and classical mechanics cannot be applied safely. Vibrational motion involving light atoms as hydrogen often have energies above $k_B T$ or of comparable magnitude. It will not be possible to describe this motion in the used approach and at room temperature also vibrational motion involving heavier atoms is problematic. [105, 158]

The finite field approach, described in chapter 3, was implemented in the molecular dynamics program GROMACS [159] and time-correlation functions were calculated from GROMACS trajectories. All simulations were done in the framework of this program making use of many of the algorithms already implemented in the program package. This in some cases also limited the choices of the simulation methods.

6.1 Simulation conditions

The GROMACS program uses a leap-frog algorithm [25, 160] to integrate the equations of motion. This modified Verlet scheme [161] ensures time reversibility and furthermore the loss of numerical precision is smaller than in the original Verlet scheme. [25] Given the position vector $\mathbf{r}$ and the acceleration vector $\mathbf{a}$ at time t and the velocity vector $\mathbf{v}$ at time $t - \delta t/2$ the new positions and velocities can be found at a short time interval δt later

applying Newtons equations on motion. [25]

$$\mathbf{v}(t + \delta t/2) = \mathbf{v}(t - \delta t/2) + \mathbf{a}(t)\delta t \tag{6.1}$$

$$\mathbf{r}(t + \delta t) = \mathbf{r}(t) + \mathbf{v}(t + \delta t/2)\delta t \tag{6.2}$$

The velocity vector at time t is

$$\mathbf{v}(t) = \frac{1}{2}(\mathbf{v}(t + \delta t/2) + \mathbf{v}(t - \delta t/2)). \tag{6.3}$$

In the simulations the isothermal-isobaric (constant NPT [number of particles, pressure and temperature]) ensemble is used. To keep the temperature constant the temperature coupling scheme suggested by Berendsen *et al.* [162] was used. In this scheme the velocities are scaled to keep the temperature fluctuating close to the desired mean value. A similar scheme [162] was also used to keep the pressure fluctuating around the desired mean value, scaling the box volume.

The simulations on carbon disulfide were done keeping the carbon disulfide molecules rigid. When calculating the response from the low frequency reorientational and inter-molecular motions, the vibrations with higher frequencies can be safely excluded. The coupling with the intramolecular vibration is expected to be small as long as the frequency of these vibrations are much larger than the reorientational and intermolecular frequencies. In Table 6.1 the calculated vibrational frequencies in carbon disulfide are shown together with those experimentally reported. [163] The lowest wavenumber found is 388 cm^{-1}, which is far above the reorientational and intermolecular wavenumbers that are all smaller than 200 cm^{-1}. Furthermore this vibration is not Raman active in the gas phase [163] where the lowest Raman active vibration has a wavenumber of 655 cm^{-1}. The molecules are treated as diatomic linear molecules in the simulation, distributing the forces on the centers of the real atoms on two simulation atoms. The real atoms are not carrying any mass but the mass and position of the simulation atoms ensures that the moment of inertia and total mass of the molecules are correctly reproduced. The distance between the atoms in the simulated diatomic molecule is kept constrained using the SHAKE algorithm. [164] The mass of the simulated atoms is half the mass of the carbon disulfide molecule, 38.0715 g/mol, and the distance between the two atoms is 2.882 Å, preserving a moment of inertia of 79.0395 Å^{2}g/mol.

The simulations were performed using periodic boundary conditions and the intermolec-ular forces are excluded if they exceed distances of approximately half a box length to avoid artifacts by restricting interactions to the nearest image. Simulations were performed with boxes containing 256 or 64 molecules.

TABLE 6.1: *Wavenumbers for the vibrations in carbon disulfide calculated with ADF using basisset V and the PW91 functional compared to experimental data. [163] Infrared active modes are indicated with (IR) while Raman active modes are indicated with (R).*

Mode	Bending (IR)	Symmetric stretch (R)	Asymmetric stretch (IR,R)
Calculation	388.0 cm^{-1}	655.2 cm^{-1}	1528.1 cm^{-1}
Experiment	396.7 cm^{-1}	656.5 cm^{-1}	1523 cm^{-1}

The force field utilized in the carbon disulfide calculations is a Lennard-Jones potential taken from literature, [165] which is widely used.

$$V_{LJ}(r_{ij}) = 4\epsilon_{ij} \left(\left(\frac{\sigma_{ij}}{r_{ij}} \right)^{12} - \left(\frac{\sigma_{ij}}{r_{ij}} \right)^{6} \right) \tag{6.4}$$

The potential is a three center potential with the centers placed on the real atoms, with the parameters given in Table 6.2. This potential was shown to give a fair description of properties such as density, diffusion constant and neutron and x-ray scattering data. [165]

TABLE 6.2: *Lennard-Jones potential parameters for the used potential originally suggested by Tildesley and Madden. [165] In their paper it was called potential A.*

Atom pair (ij)	σ_{ij}/nm	ϵ_{ij}/K
CC	0.335	51.20
CS	0.344	96.80
SS	0.352	183.00

At short distances this potential will be anisotropic because of the distance between the atomic centers, but in the limit of large molecular separations the potential will become isotropic because it is a sum of isotropic atomic potentials. The real intermolecular potential is anisotropic also in the limit of large separations. The used potential therefore cannot give a correct description of the molecular interactions on large distances. Fortunately, the interaction vanishes fast with distance and the discrepancy is likely to be of minor importance.

A sophisticated potential was developed by Burgos and Righini [166] taking the anisotropy of the force field correctly into account. Using a force field based on the DRF model described in chapter 4 is also a possibility for improvement. [167,168] Including patrial charges on the atoms would also improve the force field taking the quatropole interactions between the molecules into account.

6.2   Calculated properties

Under the given conditions (256 molecules, 100000 timesteps, 298 K, 1 bar) the density of liquid carbon disulfide was found to be 1.253 g/cm^3, which is slightly lower than earlier reported values of 1.26 g/cm^3 [96,165] The self diffusion coefficient, 3.85 $\times 10^{-5}$cm^{2}s^{-1}, was obtained using the Einstein relation [25]. It is slightly lower than the experimental value of 4.20 $\times 10^{-5}$cm^{2}s^{-1}. [169]

In Figure 5.2 the total radial distribution (C-C) function was presented together with the radial distribution functions for the four different configurations A-D given in Figure 5.1. In Figure 6.1 the parameters, Θ_A, Θ_B and φ, characterizing the configuration in a dimer, are given. All molecule pairs in the simulated liquid were distributed over four groups A, B, C or D, depending on which configuration they resemble most closely. The conditions for this assignment are listed in Table 6.3.

TABLE 6.3: *Conditions for assigning a molecular pair to one of the four groups A, B, C or D, when calculating the radial distribution functions. The angles are given in degrees.*

Orientation	Θ_A	Θ_B	φ
A	≤45	≤45	all
B	>45	>45	≤45
C	>45	≤45	all
	≤45	>45	all
D	>45	>45	>45

The first peak in the radial distribution function (Figure (5.2)) is dominated by B and D like configurations, where the molecular axes are perpendicular to the vector between the center of masses. The next peak in the radial distribution function is dominated by the C like configurations, where one molecular axis is perpendicular to the distance vector and the other is parallel. The A like configurations are more rare than the B, C

FIGURE 6.1: *The angles Θ_A, Θ_B and φ determining the geometry of the carbon disulfide dimers.*
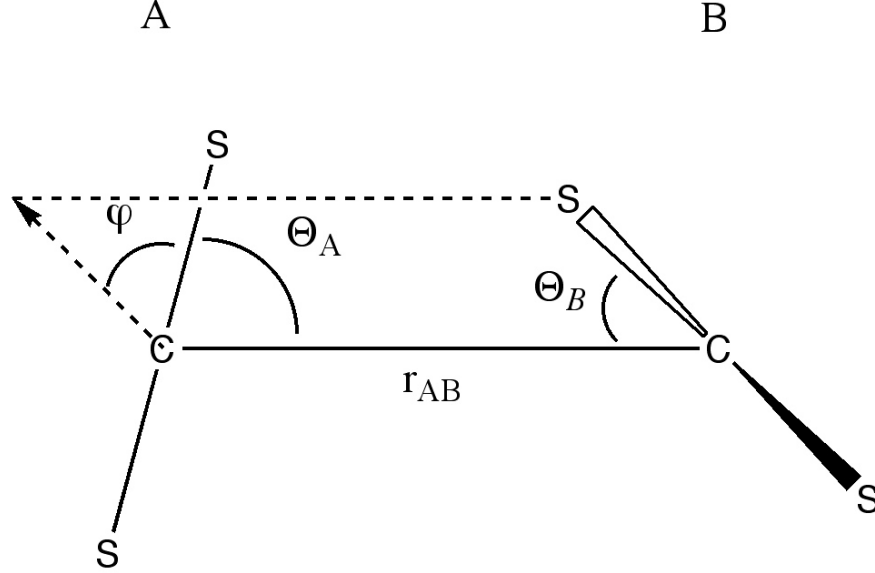
and D configurations and they are only found at distances above 5.5 Å. The total radial distribution function is in good agreement with radial distribution functions obtained by others, [165] even though the first peak in our calculation seems slightly more pronounced.

From 100 ps simulations the refractive index n (Eq. (4.16)) was calculated using the different susceptibility models described in chapter (4). In Table 6.4 the calculated numbers are compared with the experiment. [90] All calculations underestimates the true refractive index, but including local field effects improves the accuracy a lot. The slight deviation is probably due to a minor underestimation of the density in the simulations.

TABLE 6.4*: The refractive index of liquid CS_2 calculated with different polarizability models defined in chapter 4. The MOL model approximates the polarizability by the sum of the independent molecules, the DID model includes the dipole-induced dipole effect and the DRF model includes induced multipole effects and electron overlap.*

Model	n	dev. from Exp.
MOL	1.456	10.6 %
DID	1.615	0.8 %
DRF	1.596	2.0 %
Exp. [90]	1.628	-

Chapter 7

Raman spectra of liquid carbon disulfide

Carbon disulfide (CS_2) is the liquid studied most intensively by nonlinear Raman spectroscopy both experimentally [36, 37, 39–41, 45, 69, 74, 75, 81, 170–176] and theoretically. [55, 56, 58, 70, 77, 95, 96, 104, 105, 126, 133, 177–183] This is mainly due to the large polarizability and especially the large anisotropy in the polarizability of the carbon disulfide molecule. This results in a strong response, both for intermolecular modes and molecular reorientational motions, which makes carbon disulfide a favorable liquid to study.

In this chapter calculations on carbon disulfide are presented. These calculations were used to test the new finite field method described in chapter 3. This was done by comparing the third-order finite field results to results obtained with the time correlation function method. Furthermore the importance of the local field effects, discussed in chapter 4 and examined for dimers in chapter 5, were investigated in particular for the third-order response.

The fifth-order response was calculated using the finite field method. First, as will be described in section 7.3, this was done with the molecular polarizability model (MOL), described in chapter 4 and 5, giving a first estimate of the intensity of the true fifth-order signal. This absolute intensity of the response was compared with that expected for the competing third-order cascades as described in section 2.4, allowing us to give the first estimate of the ratio between the true and the cascaded fifth-order response. Then, the more accurate dipole-induced dipole model (DID) that includes a large part of the intermolecular response was used to give a more precise estimate of the intensity. This also allows investigating the difference between the various polarization directions. These

calculations are presented in section 7.4. Finally the direct reaction field model (DRF) that was optimized to the time-dependent density functional theory calculations as described in chapter 5, was used to give the best possible calculation of the fifth-order response allowing a first comparison with the most recent experiments in section 7.5.

7.1   The finite field method

In the first calculations with the finite field method [55] the molecular model for the first-order susceptibility (MOL) described in section 4.2 was used. This model had the advantages that the calculations were fairly rapid to perform and the computer code was rather simple. The model also implies that there is only one component of the response to consider, since independent molecules do not give rise to an isotropic response. Including only the single molecule (reorientational) motion is reasonable as a first approximation, since this motion is known to dominate the long diffusive tail observed in the third-order spectrum. The finite field response was obtained from 8000 simulations of 2 ps duration. The strength of the applied laser field was 0.383 V/Å. At this magnitude the response was found to be stong enough to separate from numerical noise and the higher order response weak enough to be neglected. This field stength was chosen after investigations on a wide range of field strengths. The correlation function response was obtained from a single simulation of 100 ps duration. The simulation box contained 256 molecules and the further simulation conditions were as described in chapter 6. In Figure 7.1 the calculated third-order response functions are compared with each other and with the experimental response function. [82]

In the comparison between the third-order responses, calculated using the equilibrium MD correlation function approach and the non-equilibrium finite field approach, almost perfect agreement is observed (Figure 7.1). The long diffusive tail of the experimentally observed signal is reproduced very well by both calculated response functions. The discrepancy with the experiment at short times is due to the neglect of local field effects. Previous correlation function calculations of the same third-order response function by Geiger and Ladanyi [96] have also shown that the long diffusive tail is well reproduced, even when one omits the local field effects. However, the peak at 200 fs is underestimated by a factor of 2 by not taking these effects into account. The comparison of our results with those of Geiger and Ladanyi [96] indicate that inclusion of local field effects in our calculations will give results in much better agreement with the experiment at short times.

FIGURE 7.1: *Third-order Raman response $\chi^{(3)}_{zzzz}$ of CS_2, calculated using the finite field method and the correlation function method employing the molecular approximation (MOL) of the first-order susceptibility. The experimental response [82] is also shown, scaled such that the tail overlaps the calculated tails.*
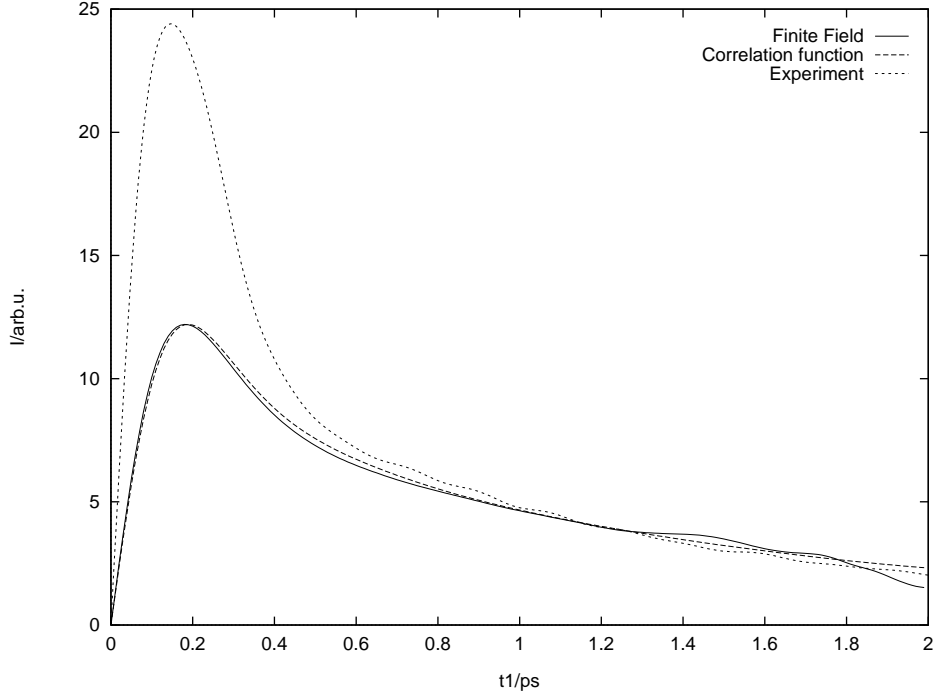
The finite field method used in the above calculations was proven to be reliable. This conclusion is based on the agreement between the third-order response functions calculated with the finite field method and the correlation function method. The finite field method can therefore also be applied with confidence for calculations that include local field effects and for the fifth-order calculations. This new method is a bit more time consuming in the present third-order calculations, but this is mainly due to the fact the correlation function can be simplified when local field effects are ignored.

7.2   Local field effects

Calculations on the third-order Raman response of CS_2 were also performed [62] using the DRF method, described in chapter 4, to include the local field effects. The cut-off distance beyond which the local field interactions are not taken into account was set to 20 Å and the interaction was softly reduced over a 0.2 Å thick region, using the method described in section 4.4. The simulated box contained 64 molecules and the simulations were repeated 10000 times to ensure high accuracy. The strength of the applied laser fields was 1.149 V/Å.

Calculations containing only the DID effect (DID), the pure multipole model (POL) and the DRF model including multipole and electron overlap effects (DRF) were performed. The anisotropic responses are shown in Figure 7.2. Comparing the single molecule result (MOL) of the previous section with the other responses makes clear that the subpicosecond peak is dominated by interaction induced effects and that these effects cannot be neglected as stated in the last section. The difference between the response calculated using the DID model with that of the POL model shows that the multipole effects are also quite important. The difference between the POL and DRF results is limited, showing the smaller influence of the close collision electron overlap effects. This is also what could be expected from the comparisons made in chapter 5.

In Figure 7.3 the same responses are shown but now normalized to peak height and together with the experimental response obtained by Steffen *et al.* [82] When plotted in this way the DID, POL and DRF models all look very similar to the experimental response in the subpicosecond peak area. In the long tail the DID response is somewhat lower than the experimental response whereas the POL and DRF are higher. This means that the DID model overestimates the ratio between the interaction induced effects and the single molecule response, and the POL and DRF models underestimate this ratio to a much lesser

FIGURE 7.2: *The anisotropic third-order Raman response of liquid CS_2 in units of 10^{-20} C^4m/J^3s.*
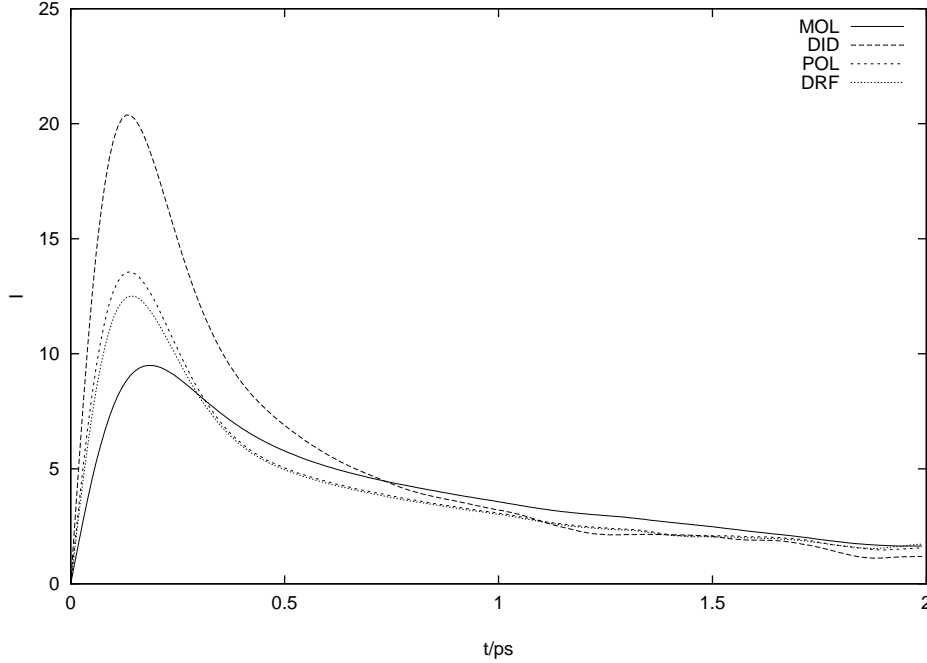

extent.

In Figure 7.4 the isotropic responses are shown. The single molecule contribution to this component is zero, so all response is originating from the interaction induced many-body effects. Note that these signals are about an order of magnitude or more weaker than the anisotropic response shown in Figure 7.2. A large difference is observed between the DID model and the models including multipole effects. Again the DID model is overestimating the interaction induced response. From this substantial difference it must be concluded that the induced multipole effects should be included when one calculates especially the isotropic third-order response. Unfortunately there are no reliable experimental results to compare with since the intensity is much smaller than the anisotropic response. Measurements by Blank *et al.* [74] just showed a very weak shoulder on the electronic response, but more recent measurements [64, 175, 184, 185] show promise for a more accurate measurement of the isotropic response.

To give a quantitative comparison between the different calculations the responses have been fitted to the functions given in Eqs. (3.30) and (3.31). In these fits it is assumed that the shape of the single molecule response is not dependent on the model used to describe

FIGURE 7.3: *The anisotropic third-order Raman response of liquid CS_2 normalized to one at the peak position.*
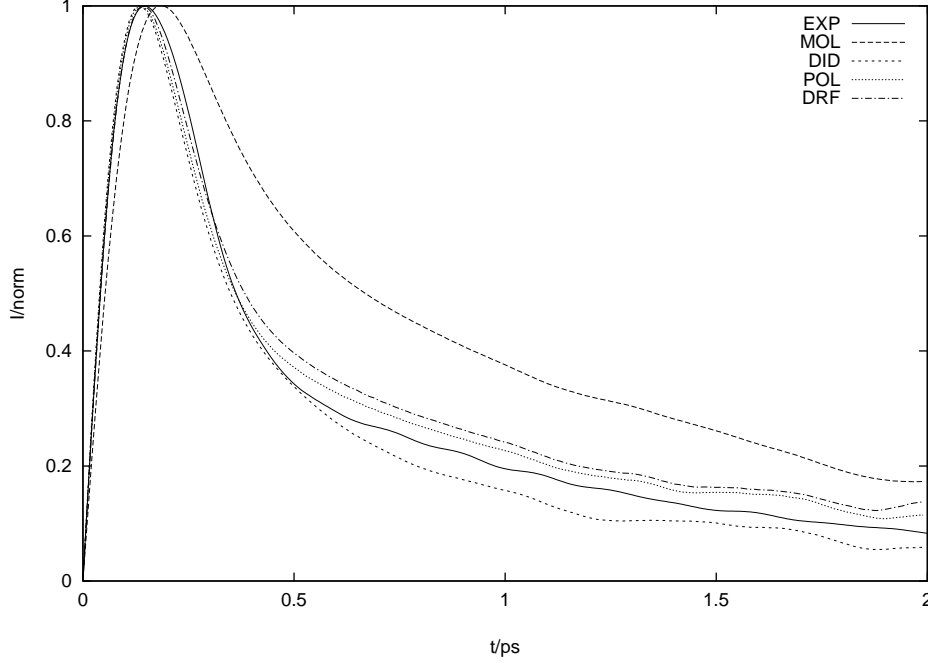

the interaction induced effects. The results are shown in Table 7.1. The single molecule (MOL) response has been fitted to Eq. (3.30) and the fit constants τ_D, τ_R, A_R, Ω_R and w_R that determine the shape of the single molecule response are kept fixed for the fits to the DID, POL and DRF results, while the constant I_D that determine the intensity is allowed to vary. No single molecule response is present in the isotropic response. From these fits it is clear that for the anisotropic response there is a big difference between the DID model and the models including the multipole effect. This is seen both in the I_C parameter characterizing the intensity and the τ_C and n parameters characterizing the shape of the interaction induced response. For the isotropic response the main difference is in the parameter characterizing the intensity. The ratio between the peak intensity of the anisotropic and the isotropic response changes dramatically from 7.57 in the DID model to 21.0 in the DRF model. These ratios provide a sensitive test of these models that can be determined experimentally.

For the single molecule response the librational part is found to be close to critically damped while the A_R and Ω_R parameters can be varied quite a bit without changing the function too much, as long as the product of these two constants is kept fixed. The

TABLE 7.1: *The fit constants for the calculated single molecule (Eq. 3.30) and interaction induced (Eq. 3.31) response, with I_D and I_C giving the intensities. No single molecule response is present in the isotropic response which is therefore fitted to the interaction induced expression (Eq. 3.31) with I_C as intensity.*

| | Anisotropic | | | | | | | | | Isotropic | | |
| | Single Molecule | | | | | | Inter. Ind. | | | Inter. Ind. | | |
	I_D	τ_D	τ_R	A_R	Ω_R	w_R	I_C	τ_C	n	I_C	τ_C	n
MOL	8.32	1.20	0.117	6.19	0.803	31.7	-	-	-	-	-	-
DID	5.88	-||-	-||-	-||-	-||-	-||-	22.26	0.183	1.83	4.506	0.156	1.53
POL	7.39	-||-	-||-	-||-	-||-	-||-	8.09	0.306	3.06	1.312	0.137	1.50
DRF	7.26	-||-	-||-	-||-	-||-	-||-	6.66	0.309	3.09	0.985	0.165	1.63

FIGURE 7.4: *The isotropic third-order Raman response of liquid CS_2 in units of 10^{-20} C^4m/J^3s. The response in molecular polarization model (MOL) is zero.*
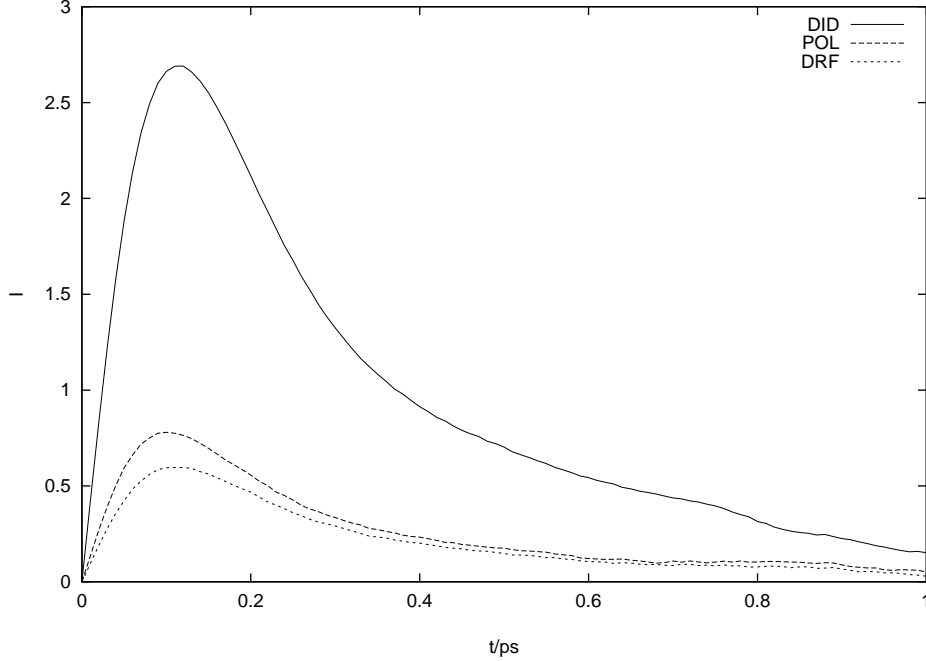
diffusional constant τ_D is found to be 1.20 ps, which is somewhat lower than the value 1.6 ps typically reported. [69, 117, 120, 121, 174] This is probably an artifact due to the truncation of the calculated response at 2 ps. The long tail domain is not really included in the simulation. This gives an uncertainty in the diffusional constant τ_D that may be partly due to compensation of the errors in the librational part of the response. The calculated third-order response was found to resemble the experimental result very well.

The observed rather small deviation between the response calculated using the DRF method and the experimental response does not need to originate only from the small remaining differences between the modeled and calculated polarizabilities. The fact that the force field used in the MD simulations is rather simple (as described in chapter 6) can also give rise to deviations. A molecular force field consisting of isotropic atomic Lennard-Jones potentials cannot give rise to the anisotropic asymptotical behavior that is present in anisotropic molecules as CS_2, but only mimics the anisotropy in the force field at short distances [165]. Furthermore, in the force field used the relatively large quadrupole moment in CS_2 is not taken into account. Test calculations showed that omitting the partial charges has little effect and the partial charges have not been included in order to allow comparison

with earlier studies where charges were also discarded.

The interaction induced effects observed for the third-order response will surely also have implications on the calculated higher (fifth) order Raman response, which is known to be even more sensitive to many-body effects in the optical response [56, 87, 103].

7.3 Molecular fifth-order response

The fifth-order response was first calculated [55] using the molecular model for the polarizability (MOL). This is done by averaging over 8000 finite field simulations with a duration of 0.75 ps. The strength of the applied laser fields was 0.383 V/Å. The result is shown in Figure 7.5. To give an indication of the noise introduced by the perturbation of the system, the spread on the mean value of the response function at each time t_2 is also plotted in Figure 7.5 for the calculation with t_1=0.2 ps. The peak intensity was found to be 0.98 $\times 10^{-25}$ C^{6}m^3/J^{5}s^2 which occurs for t_1=0.2 ps and t_2=0.2 ps.

FIGURE 7.5: *Fifth-order response* $\chi^{(5)}_{zzzzzz}$, *calculated using the finite field method. The different lines correspond to different values of* t_1, *with* t_1 *increasing from 0.1* ps *in the left trace to 0.7* ps *in the right trace in steps of 0.1* ps. *The positively inclined line at the bottom signifies the noise level in the calculation with* t_1=0.2 ps.
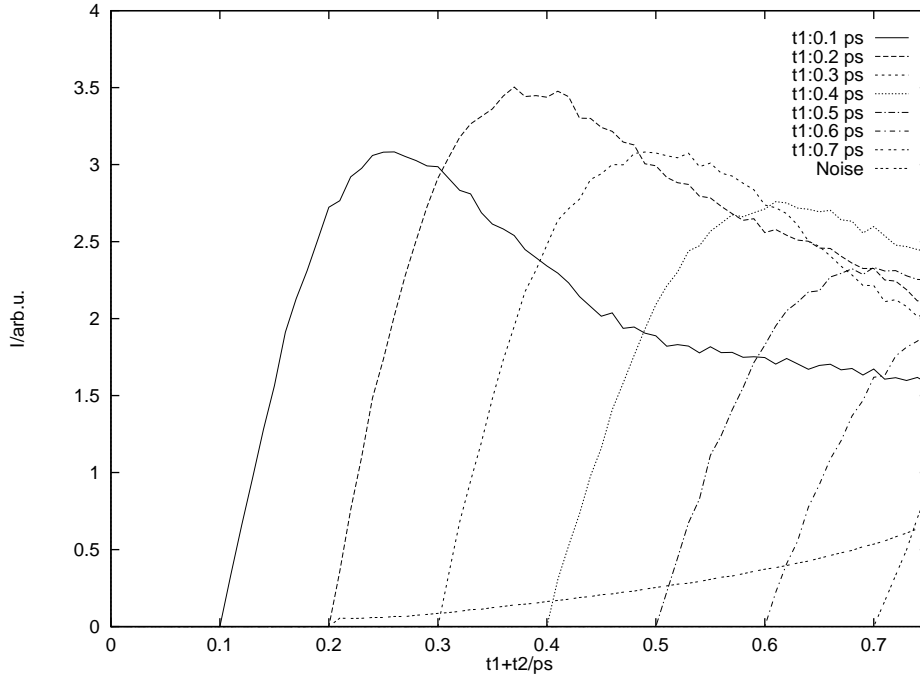
The intensity ratio of the cascaded and fifth-order response can be estimated from the peak values of the third- and fifth-order response functions in the sample. Using the calculated response function peak intensities, the experiment independent ratio (Eq. (2.34)) is found to be 0.0104 in the MOL model. With this information Eq. (2.33) gives an approximate intensity ratio of the two types of response of 4×10^6 in favour of the third-order cascade processes when a wavelength of 620 nm, a sample size of 1 mm and perfect phase matching, $f(\Delta kl) = 1$ is taken. This indicates that the cascade process should be very severely mismatched in phase under experimental conditions, in order to be able to observe the two-dimensional fifth-order Raman signal. Such mismatch was not present in most experiments reported so far [38–41], but recent multi-color experiments have increased the phase mismatch considerably. Possibly the discrimination against cascaded processes is then sufficiently to isolate the true fitfh-order response. [43–45]

The estimated intensity ratio of 4 million between the 3rd-order cascading processes and the true fifth-order response, in favour of the cascading processes before taking phase matching into account, supports the conclusions of Blank *et al.* [41] that all earlier reported experimental results of two-dimensional Raman scattering actually dealt with cascading processes, instead.

7.4   Fifth-order DID response

The time dependence and intensity ratio against the cascaded processes was calculated in the previous section for a sample of independent molecules. Interaction induced effects may modify these results considerably. Therefore, the fifth-order response including the dipole induced-dipole (DID) contribution was calculated. This was done by applying the finite field method with 1000 simulations for each of the four combinations of applied laser fields shown in Eq. (3.2) and for t_1 values from 20 fs to 200 fs in 20 fs steps and t_2 values from 0 to 200 fs in 10 fs steps. The strength of the applied laser fields was 1.149 V/Å. All calculated tensor components were obtained from two sets of trajectories that differ in the polarization directions of the laser fields: one that has the polarization direction of the first laser pulse pair along the z-axis and one that has the polarization direction of the first laser pulse pair along the y-axis. The laser pulse pair applied after the delay t_1 is always applied with the polarization direction along the z-axis. The zz component and the yy component of the first-order susceptibility are calculated after the delay t_2. This provides the $\chi^{(5)}_{zzzzzz}$, $\chi^{(5)}_{zzzzyy}$, and $\chi^{(5)}_{zzyyzz}$ components, from which the desired $\chi^{(5)}_{zzzzzz}$, $\chi^{(5)}_{mmzzzz}$, $\chi^{(5)}_{zzmmzz}$, $\chi^{(5)}_{zzzzmm}$ and

$\chi^{(5)}_{llzzl'l'}$ tensor elements can be calculated as also mentioned in chapter 3. These calculated components are shown in Figure 7.6. Cuts through the surfaces along the diagonal and for t_2 fixed at 120 fs are shown for the different components in Figure 7.7 and Figure 7.8. In Table 7.2 the peak intensities are given and in Table 7.3 the peak positions of the cascading processes and the calculated fifth-order response are listed together with the experimental positions given by Blank *et al.* [74] Table 7.4 contains the experiment-independent intensity ratios as defined in Eq. (2.34). Assuming an experimental wavelength of 620 nm, a sample length of 1 mm and perfect phase matching conditions, Δkl , the experimental factor is 3.9×10^8 (Eq. (2.35)). In the experiments performed by Blank *et al.* [74] a wavelength of 800 nm is used, which favours the true response with a factor of 1.6 in comparison with the conditions considered here.

TABLE 7.2: *Peak values for the calculated response functions using the finite field method (FF) and the time correlation function method (TCF) when possible. Third-order values are given in units of 10^{-20} C^{4}m/J^{3}s and the fifth-order values in units of 10^{-25} C^{6}m^3/J^{5}s^2. (For comparison with data in c.g.s. units: 1* e.s.u. *(or* cm^3)= 1.11264$\times 10^{-16}$C^{2}m^{2}J^{-1}, 1 erg = 10^{-7} J and 1 C^{4}m/J^{3}s = 8.07761$\times 10^6$cm^{3}erg^{-1}ps^{-1})*

$\chi^{(n)}_{a\cdots b}$	FF	TCF	Deviation
$\chi^{(3)}_{zzzz}$	28.59	28.28	1.1 %
$\chi^{(3)}_{zzmm}$	2.37	2.40	-1.2 %
$\chi^{(3)}_{zyzy}$	19.73	19.21	2.7 %
$\chi^{(3)}_{zzll}$	-1.12	-1.10	-.18 %
$\chi^{(5)}_{zzzzzz}$	0.107	-	-
$\chi^{(5)}_{mmzzzz}$	0.0327	-	-
$\chi^{(5)}_{zzmmzz}$	0.0481	-	-
$\chi^{(5)}_{zzzzmm}$	0.0346	-	-
$\chi^{(5)}_{llzzl'l'}$	-0.0252	-	-

The case least discriminating against cascaded processes is the $\chi^{(5)}_{zzzzzz}$ response, where the intensity ratio between the most intense cascaded signal and the true fifth-order response becomes 2.8×10^6 in favor of the cascading processes, when the experimental factor above is used. In the last section, where the local field effects were not included, this ratio was found to be 4×10^6. For the magic angle component $\chi^{(5)}_{zzmmzz}$ the intensity ratio for the parallel cascaded response is found to be 9.8×10^4. For the $\chi^{(5)}_{llzzl'l'}$ response this ratio

FIGURE 7.6*: Five polarization components of the fifth-order response of carbon disulfide calculated using the finite field method. The plots are made with ten equidistant contour lines.*
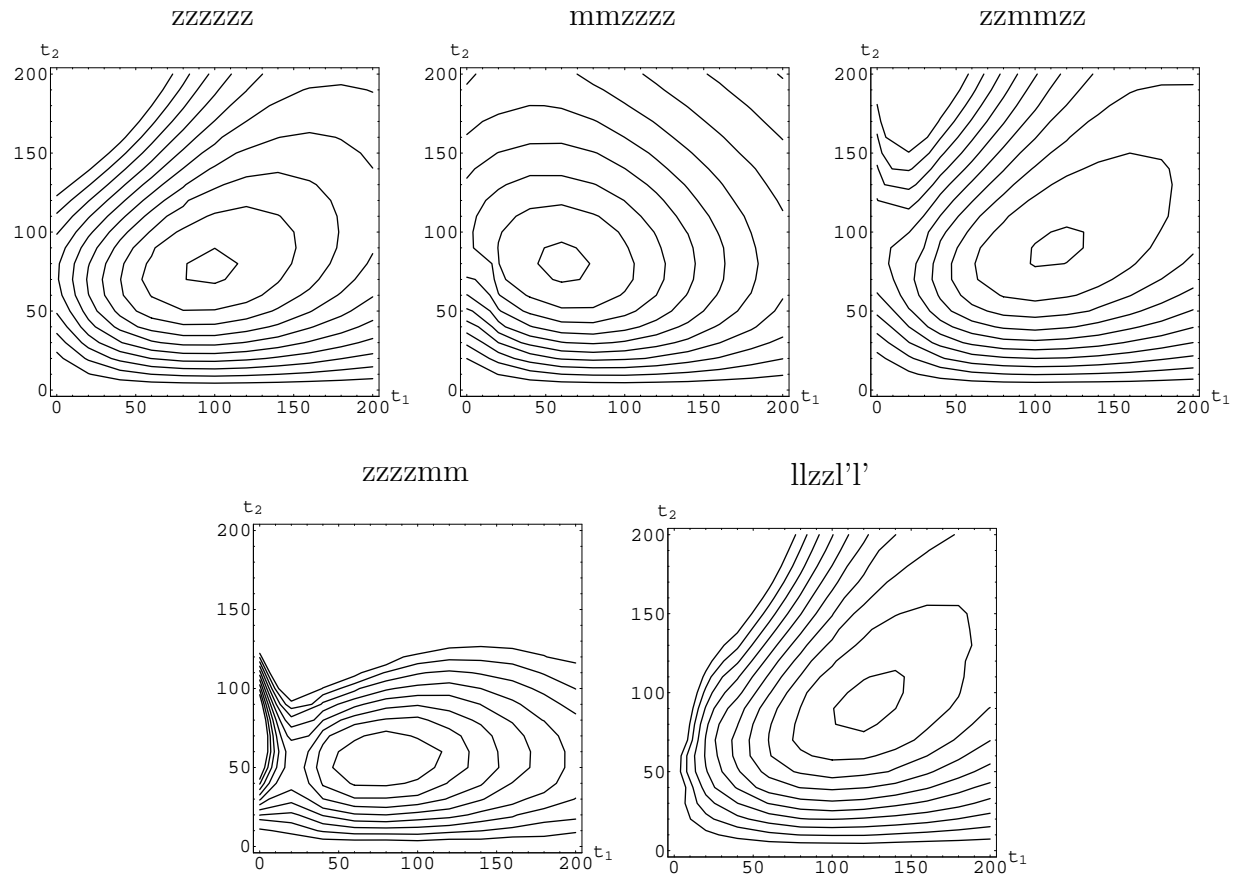
FIGURE 7.7: *Diagonal cut through the two-dimensional fifth-order response surfaces. The full line is the $\chi^{(5)}_{zzzzzz}$ component, the dotted line is the $\chi^{(5)}_{mmzzzz}$ component, the dashed line is the $\chi^{(5)}_{zzmmzz}$ component, the long dashed line is the $\chi^{(5)}_{zzzzmm}$ component, and the dashed-dotted line is the $\chi^{(5)}_{llzzl'l'}$ component. The response is given in units of $10^{-25}\mathrm{C}^6\mathrm{m}^3/\mathrm{J}^5\mathrm{s}^2$.*
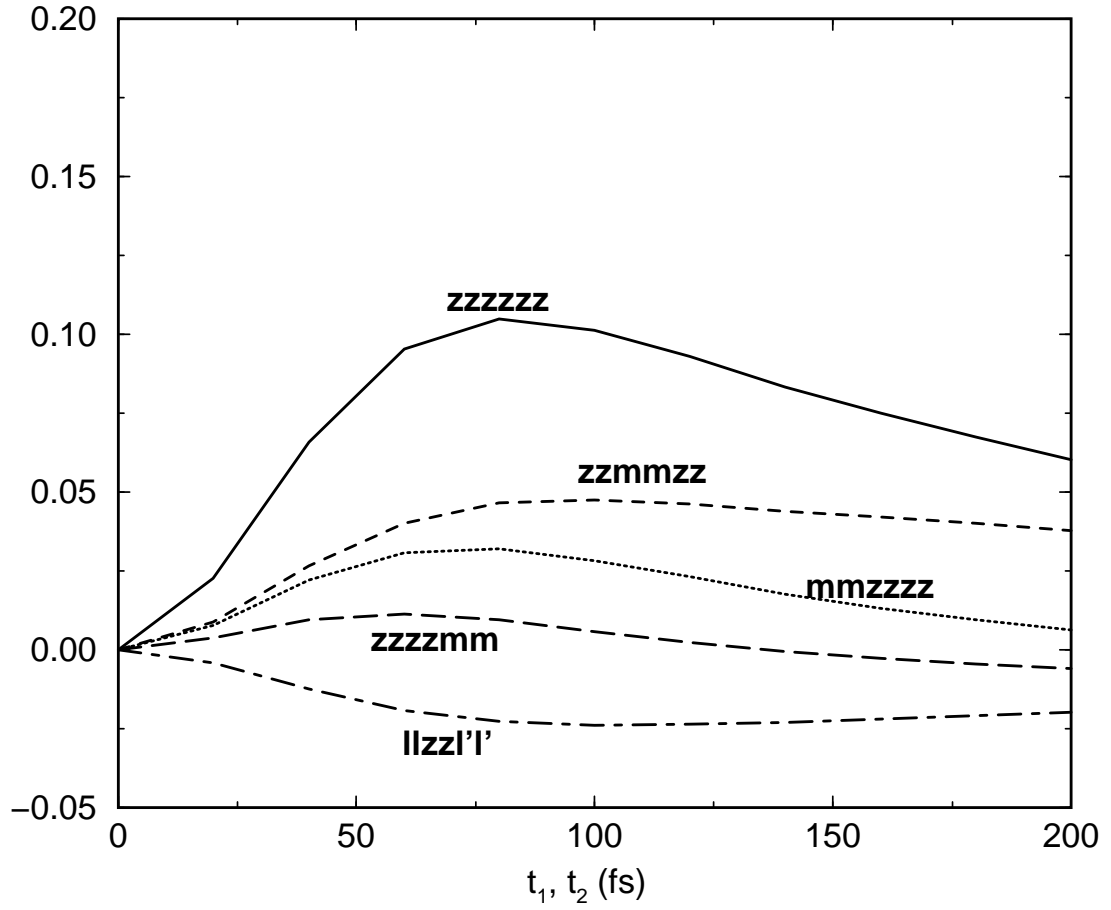
FIGURE 7.8: *Cut through the two-dimensional fifth-order response surfaces with t_2 fixed at 120 fs. The full line is the $\chi^{(5)}_{zzzzzz}$ component, the dotted line is the $\chi^{(5)}_{mmzzzz}$ component, the dashed line is the $\chi^{(5)}_{zzmmzz}$ component, the long dashed line is the $\chi^{(5)}_{zzzzmm}$ component, and the dashed-dotted line is the $\chi^{(5)}_{llzzl'l'}$ component. The response is given in units of $10^{-25}C^6m^3/J^5s^2$.*
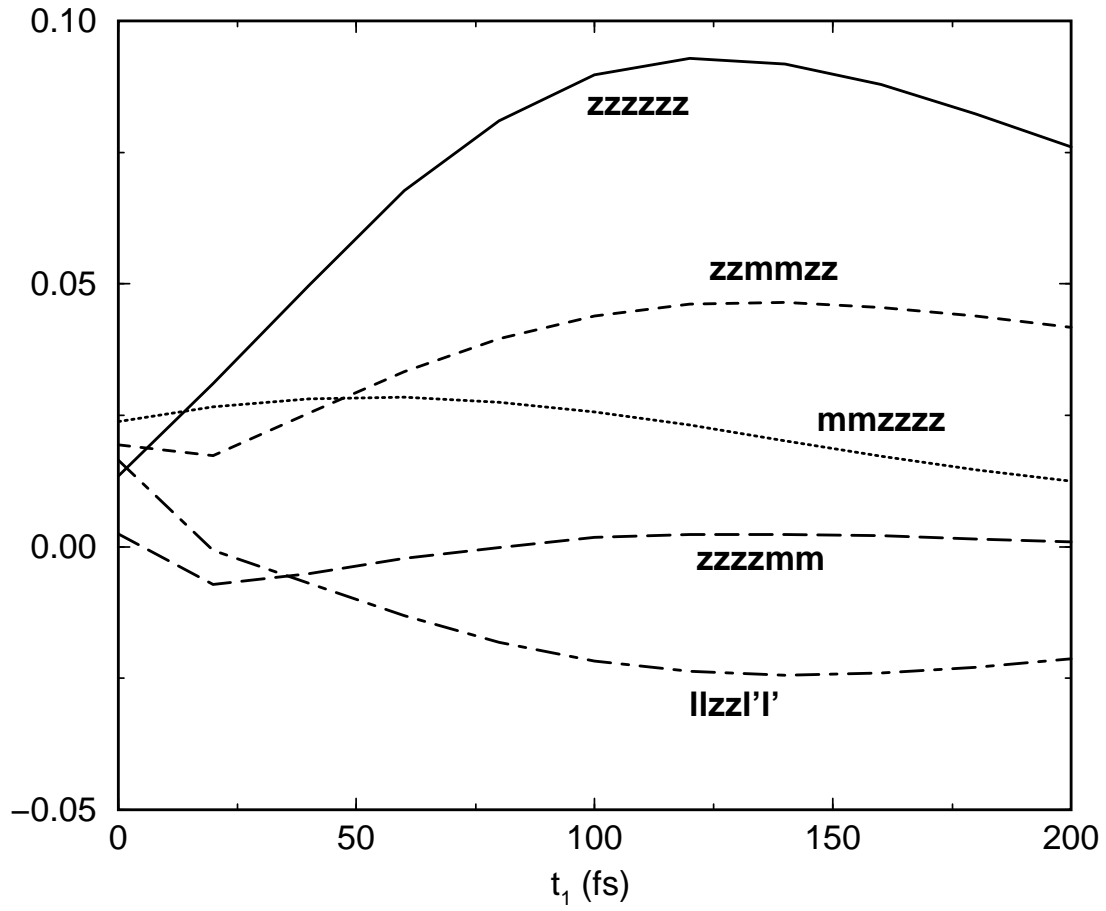
TABLE 7.3: *Peak positions for the direct fifth-order response and the cascading response compared with the experimental results of Blank et al. [74] The peak positions are given as (t_1, t_2) in units of* fs.

$\chi^{(5)}_{abcdef}$	$\chi^{(5)}_{abcdef}$	$\chi^{(5)}_{\text{seq}}$	$\chi^{(5)}_{\text{par}}$	Exp.
$\chi^{(5)}_{zzzzzz}$	(100,80)	(140,140)	(0,140)	(60,110)
$\chi^{(5)}_{mmzzzz}$	(60,80)	(140,110)	(0,110)	-
$\chi^{(5)}_{zzmmzz}$	(100,90)	(110,110)	(-30,110)	-
$\chi^{(5)}_{zzzzmm}$	(80,50)	(110,140)	(30,140)	(0,120)
$\chi^{(5)}_{llzzl'l'}$	(120,90)	(200,200)	(0,200)	-

TABLE 7.4: *Experimental independent intensity ratios between the peaks of the cascaded response and the fifth-order response for the different polarization components.*

$\chi^{(5)}_{abcdef}$	R_{seq}	R_{par}
$\chi^{(5)}_{zzzzzz}$	7.2×10^{-3}	7.2×10^{-3}
$\chi^{(5)}_{mmzzzz}$	5.3×10^{-4}	3.7×10^{-6}
$\chi^{(5)}_{zzmmzz}$	1.7×10^{-6}	2.5×10^{-4}
$\chi^{(5)}_{zzzzmm}$	4.7×10^{-4}	4.7×10^{-4}
$\chi^{(5)}_{llzzl'l'}$	3.1×10^{-7}	3.1×10^{-7}

is only 1.2×10^2, which allows to discriminate against the cascaded response, when the intermediate phase matching factor is better than 1×10^3. This is the order of magnitude reported experimentally [74].

The fifth-order magic tensor elements $\chi^{(5)}_{mmzzzz}$, $\chi^{(5)}_{zzmmzz}$ and $\chi^{(5)}_{zzzzmm}$ are all approximately three times smaller than the $\chi^{(5)}_{zzzzzz}$ component. The ratio between the polarized and magic angle components in the third-order experiment is approximately 12 in favor of the polarized component. This implies that the isotropic part of the response, which cannot be explained without interaction induced effects, is much stronger in the fifth-order response than in the third-order response. The sensitivity of the fifth-order response to many-body effects, found here, was recently also inferred from INM calculations by Murry *et al.* [87] This probably also means that the fifth-order signal is more sensitive to other interaction induced effects than the DID effect accounted for here. The induced multipoles, described in chapter 2, are very likely to give a significant contribution to the fifth-order response. This will be treated in the following section.

The differences between the nuclear part of the experimental signal [74] and the calculated response are pronounced. Both the $\chi^{(5)}_{zzzzzz}$ and the $\chi^{(5)}_{zzzzmm}$ component of the experimental response have sharp peaks closer to the t_2-axis than shown in the rather flat calculated two-dimensional surfaces of Figure 7.6. This probably indicates that the signals are contaminated with parallel cascaded response that peaks on or close to the axis.

Comparing the calculated and experimental response is complicated by the fact that the experimental signals may include contributions from combined electronic/nuclear response along the time axes and pure electronic response for both time delays equal to zero. [72] These responses depend on the higher order non-linear electronic responses γ and ζ (or the macroscopic electronic counterparts $\chi^{(3)}$ and $\chi^{(5)}$) respectively as shown in section 2.2. Since they are confined to the origin and the time axes, problems with separating nuclear and electronic response are limited to these areas. In addition the experimental spectra are broadened by the width of the applied laser pulses. This experimental artifact is best corrected for by deconvoluting the experimental response before comparing it with the calculated ideal response using delta function pulses. Recently a method for doing this with the fifth-order homodyne detected response has been published. [83]

The estimated ratios between the cascaded processes and the direct fifth-order response are in favor of the cascaded processes, even when the experimental factor in Eq. (2.35) with a realistic phase matching factor is taken into account. However, the ratio is smaller than in studies not taking the local field effects into account [55] and for the $\chi^{(5)}_{llzzl'l'}$ component

the ratio is close to one. This again indicates the importance of interaction induced effects in the fifth-order response. The calculations still support the conclusion by Blank *et al.* [41] that all experiments performed earlier are dominated by the cascaded processes.

In the light of the recent experiments, that were claimed to contain direct fifth-order response, [74] it seems that the theory overestimates the intensity ratios or that the experiment overestimates the mismatch in the intermediate phase matching factors. The experimental factor might be connected with uncertainties concerning, for instance, the beam divergence or the sample length, which is not only determined by the sample thickness, but also by the overlap of the laser beams. [41] The estimated intermediate phase matching conditions, discriminating the fifth-order signals against the third-order cascaded response, is also not fully determined due to uncertainty in the orientation of the laser beams. On the other hand, the interaction induced effects might be calculated more accurately by including higher order terms in the multipole expansion and/or collision induced contributions [62] as will be done in the following section.

7.5   Fifth-order DRF response

In the third-order Raman response the inclusion of induced multipole effects and electron overlap were found to be important. The fifth-order response is more sensitive to the detailed coordinate dependence of the first-order susceptibility and therefore the induced multipole effects and the electron overlap can be expected to be even more important in the fifth-order response than in the third-order response.

To obtain the highest accuracy in the calculations, the inverted force variant of the finite field method described in chapter 3 was applied in the calculation of the fifth-order response with the DRF model. This allowed using a laser strength of 1.915 V/^{TM} without introducing higher order artifacts. The calculations were performed on a simulation box with 64 molecules and repeated for 4000 different starting configurations. The response was calculated for times t_1 and t_2 between 0 and 600 fs, with a 20 fs resolution. For comparison the MOL, DID and POL model responses were also calculated under the same conditions, but with a slightly lower laser strength of 1.724 V/^{TM} for the MOL and DID models. In the DID calculations only 2000 starting configurations were needed. The calculated responses for the $\chi^{(5)}_{zzzzzz}$ and $\chi^{(5)}_{mmzzzz}$ polarization directions are shown in Figure 7.9 and Figure 7.10.

For the $\chi^{(5)}_{zzzzzz}$ component the molecular response is somewhat elongated along the t_2

axis. The response found with the DID model including intermolecular interactions is more symmetric, while the POL and DRF model responses are even more stretched out along the t_2 axis than the pure molecular response. In the third-order response the induced multipoles were seen to damp the effect of the dipole-induced dipoles. This also seems to be the case in the fifth-order response, but in fifth-order the POL model stretches the response even more along the t_2 axis than the molecular model does. Furthermore, slight differences are also observed between the POL and DRF model responses showing that electron cloud overlap is of some importance.

In the $\chi^{(5)}_{mmzzzz}$ response the signal is independent of the individual molecular orientations and the molecular polarizability model does not give rise to optical response. The differences between the DID, POL and DRF models along the t_2 axis are even more pronounced for this component, as shown in Figure 7.10. The DID model response is rather symmetrical, while the POL and DRF model responses shows a ridge along the t_2 axis. This clearly shows that the multipole effect is also of crucial importance in the fifth-order response. The effect of electron cloud overlap is clearly visible in the area where t_1 and t_2 are 100 fs. A clear peak is seen in the DID and POL models, while this is not observable in the DRF model response where the electron overlap is taken into account.

At the present moment we can only speculate on the interpretation of the spectrum. The long ridges along the t_2-axis can possibly be explained by a model suggested by Steffen and Duppen [186] involving population relaxation during the second time delay. However, the response is more complicated than that. It is essential to understand why the DID response is rather symmetric while the DRF response is highly assymetric. The only difference between these two models is the distance and orientation dependence of the polarizability, as reported in chapter 5. There it was shown that the polarizability at short intermolecular distances was damped in the DRF model. This means that the contribution to the response from molecules at short separations is smaller in the DRF model than in the DID model. This could indicate that dimers at short separations are responsible for the rather symmetric part of the response, while dimers at larger separations give rise to the response along the axis. It is reasonable that the shape and nature of the response depends on the distance between the molecules, since the intermolecular forces they experience will be much different. More investigations will be needed to give an exact interpretation of the spectral features.

The multi-color experiments published recently [45, 187, 188] were claimed to be in good qualitative agreement with the results reported in last section. Some of these experimental

FIGURE 7.9: *The calculated fifth-order response $\chi^{(5)}_{zzzzzz}$ with the MOL, DID, POL and DRF models for the first-order susceptibility. The plots are made with ten equidistant contour lines.*
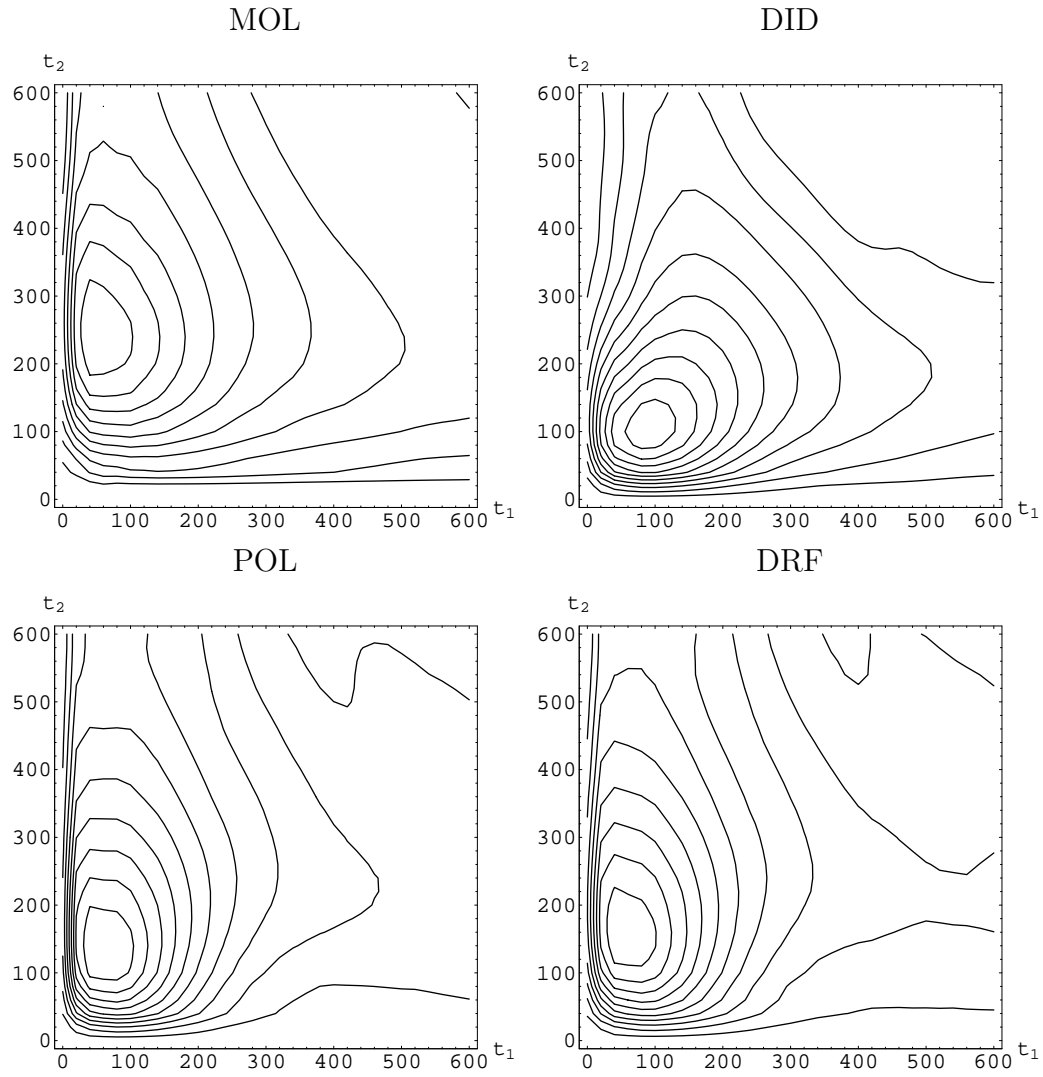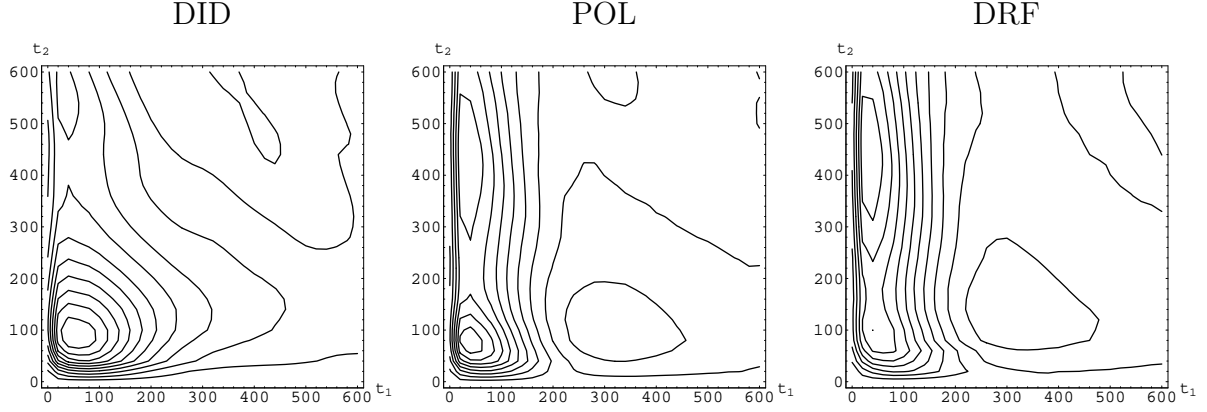
FIGURE 7.10: *The calculated fifth-order response* $\chi^{(5)}_{mmzzzz}$ *with the DID, POL and DRF models for the first-order susceptibility. In the MOL model this response vanishes. The plots are made with ten equidistant contour lines.*


results can be seen in Figure 7.11. In these experiments the cascaded processes are severely suppressed by the phase mismatch. For the $\chi^{(5)}_{zzzzzz}$ component shown in Figure 7.11 a long tail along the t_2 (τ_4) axis is observed in agreement with the response calculated with the DRF model. Since only cuts through the two-dimensional surface have been presented with this experimental method, a more detailed comparison is impossible.

In recent theoretical [101] and experimental studies [189] nodal lines in the $\chi^{(5)}_{zzzzzz}$ response of CS_2 were reported. Such features are not observed in the multi-color experiments by Kubarych [45, 187, 188] nor in the present simulations. In the DID response reported in section 7.4 the response indeed becomes slightly negative along the t_2-axis for the $\chi^{(5)}_{zzzzzz}$ component, when t_2 is large, but this has been identified as an artifact due to higher-order response. This artifact was eliminated in the later simulations by applying the inverted force approach.

7.6   Conclusion

Since the instantaneous normal mode calculations [58, 87, 103, 106] lack the ability to describe diffusive motion, and the time correlation function response can in fifth-order only be done on very small systems, [59, 101] the finite field approach is the most promising method for further applications. The finite field method was shown to give the same third-order response as the time correlation function method, giving confidence that the method

FIGURE 7.11: *The experimental response reported by Kubarych et al. [45]. The full lines are the in-phase signal (dominated by true response), while the dotted lines are the in-quadrature signal (dominated by cascades). Cuts through the two-dimensional surface are shown along the t_2 (τ_4) axis, along the t_1 (τ_2) axis and along the diagonal (shown from top to bottom). The $\chi^{(5)}_{zzzzzz}$, $\chi^{(5)}_{zyzzzy}$ and $\chi^{(5)}_{zzmmzz}$ components are shown from left to right.*
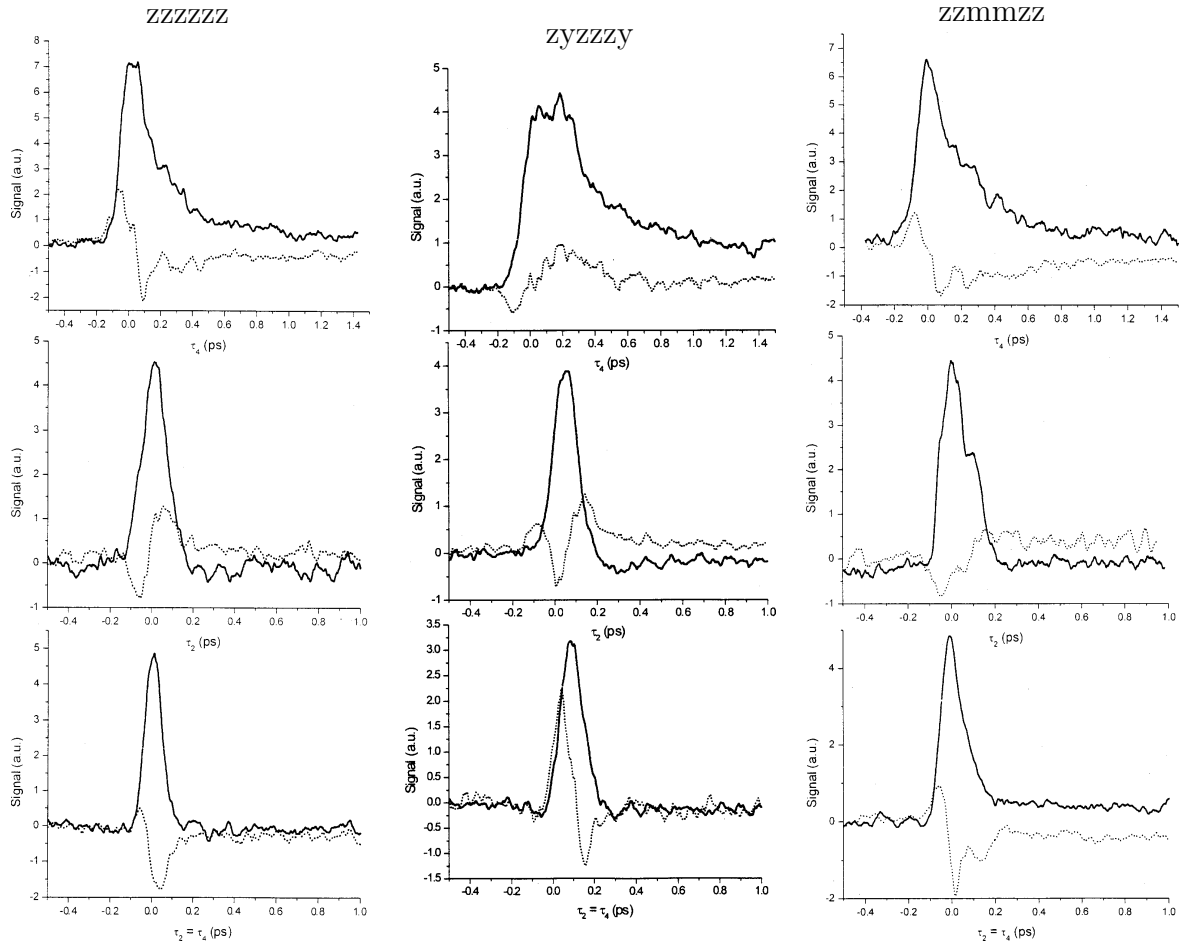
is reliable. This method makes it possible to provide reasonable estimates of the relative intensity of the true fifth-order response and the competing third-order cascades.

This study showed that close collision effects caused by induced multipoles and electron cloud overlap are crucial for giving a correct description of both the third- and fifth-order response. The close collision effects are most important in the isotropic third-order and fifth-order responses, where the difference between the results calculated with the different polarizability models are most pronounced. This proves that fifth-order response is a strong tool for investigating these close collision effects as well as the intermolecular motion giving rise to the many-body response.

Still further research is required in order to give a clear interpretation of the spectra and in order to establish a clear consensus between the experimental and theoretical results. This will allow fifth-order Raman spectroscopy to become a useful method for studying the complicated motion of liquids.

Chapter 8

Many-body effects in the stimulated Raman response of binary mixtures: A comparison between Theory and Experiment

The subpicosecond dynamics of binary mixtures of carbon disulfide and alkane were studied using third-order time-resolved Raman techniques. Both the anisotropic and the isotropic responses were investigated. These depend differently on many-body contributions to the first-order susceptibility and probe different modes in the liquid. The anisotropic response is dominated by single molecule effects, whereas the isotropic response is completely determined by many-body contributions since the single molecule response vanishes. To interpret the experimental results, molecular dynamics simulations were performed on model mixtures. The effect of dilution on the subpicosecond response cannot be explained by many-body effects in the first-order susceptibility alone. Aggregation due to permanent quadrupole moments on the carbon disulfide molecules and density changes upon dilution are also inadequate explanations for the observed effect. Apparently the character of the many-body dynamics itself is modified by the change of the molecular force fields, when carbon disulfide molecules are replaced by alkanes.

8.1   Introduction

Femtosecond laser spectroscopy techniques are powerful methods to study the ultrafast dynamics in liquids. Experiments such as the (heterodyned) optical Kerr effect [68,69,174] and transient grating scattering [70,71] allow the observation of induced motions in real time rather than as resonances. For a molecule to be Raman active the polarizability has to be coordinate dependent. In anisotropic molecules the polarizability depends on the orientational coordinate of the molecules and hence a rotational Raman response is observed. In the liquid phase this response will be highly-influenced by the many-body interaction between the individual rotating molecule and the surrounding molecules. The many-body interactions result in line broadening of the response in the frequency domain, corresponding to an, often exponentially, decaying tail in the time domain.

The molecular polarizability itself is also affected by the presence of other polarizable molecules in the neighbourhood, due to local field effects. In liquids, the Raman response is therefore also determined by the coordinate dependence of the many-body (macroscopic) counterpart to the polarizability, i.e. the first-order susceptibility. Now, not only the individual single molecule coordinates but also the intermolecular coordinates become important. The many-body effects in the first-order susceptibility give rise to response due to dynamics in the local structure, allowing observations of collisions, collective movements and structural effects.

The influence of many-body interactions on the first-order susceptibility can be investigated through dilution studies. Such studies provide information not only on the many-body dynamics and the local field effects in the liquid, but also on the structure of the diluted liquid. The formation of clusters of molecules in the mixture will tend to preserve the response from many-body effects in the first-order susceptibility, whereas a solvent effectively isolating the polarizable molecules from each other will suppress this part of the response to some extent.

Various liquid mixtures have been investigated experimentally using third-order nonlinear Raman response techniques to probe the ultrafast dynamics. [68,69,117,118,120,121, 174,190–192] Diluted carbon disulfide belongs to one of the most studied systems because of the intense anisotropic response of this molecule. Studies of carbon disulfide have been done in mixtures with alkanes, [68,69,117,118] chlorine substituted methane [120,121,174] and various alcohols. [120] Also Molecular Dynamics (MD) simulations were performed previously on mixtures of carbon disulfide and carbon tetrachloride, [193,194] but to our

knowledge no calculations have been reported of the third-order nonlinear Raman response of liquid mixtures.

The *anisotropic* third-order nonlinear Raman response can be roughly separated into three main features, i.e. the diffusive, the interaction-induced and the librational response. The diffusive response is caused by the diffusive realignment of single molecules. Only this contribution can be clearly recognized because of its distinct and slow exponential decay. The interaction-induced response is originating from intermolecular motions getting intensity from the dipole-induced dipole effects (local field effects) and higher multipole and collision effects. [62] The librational response comes from single molecules moving in the local potential of neighboring molecules.

The *isotropic* third-order nonlinear Raman response is in general much weaker than the anisotropic response. It is solely due to the interaction induced effects. Very few investigations have been done on the isotropic response, [74, 175, 184, 185] despite of the fact that it provides an opportunity to investigate many-body effects without the disturbing influence of the single molecule response. The obvious reason for avoiding the isotropic response has been its very low intensity.

All investigations on mixtures till now have been interpreted in terms of analytical models at a macroscopic level of theory, assigning the non-diffusional response either to librational degrees of freedom [69, 117, 174] or interaction induced response. [120] These approaches were based on an interpretation in phenomenological terms, such as homogeneous or inhomogeneous broadening of the Raman response or an atomic collision model, originally proposed for low density media. [119] Recently a macroscopic model was presented [122] that describes the diffusional and non-diffusional response in terms of abstract oscillators in which the microscopic many-body dynamics is summarized.

Getting an understanding of the optical response on a microscopic (molecular) scale in terms of molecular properties such as force fields, atomic masses and polarizabilities would be preferable. Using Molecular Dynamics (MD) simulations one can perform studies on real systems to get insight into the effects of dilution on a microscopic scale. This is particularly valuable when these results are compared to experimental investigations of how changes in the local environment of molecules affect the many-body part of the Raman signals.

In this paper the effect of dilution is investigated for binary mixtures of carbon disulfide with various alkanes. The anisotropic and the isotropic responses are examined both experimentally and theoretically. In section 8.2 the theory used to analyze the data is developed and in section 8.3 the experiments are described. The experimental results

are compared with theory and molecular dynamics simulations of an idealized mixture in section 8.4, together with a discussion of possible explanations of the deviations. The conclusions are presented in section 8.5.

8.2   Theory

The change of the non-linear Raman spectrum upon dilution will be considered for the simple case, where the dynamics of the system does not change upon dilution. Furthermore, it will be assumed that only one of the two components in the mixture contributes to the Raman response. The interaction induced contribution to the susceptibility will be treated within the first-order approximation to the dipole-induced dipole model. In this model the effective molecular polarizabilities, when local fields are present, are given by: [56, 95–97]

$$\mathbf{\Pi}_i^{(1)} = \alpha_i + \alpha_i \sum_{j \neq i} \mathbf{T}_{ij} \alpha_j + \frac{4\pi \langle \chi^{(1)} \rangle}{3} \alpha_i. \tag{8.1}$$

Here α_i is the single molecule polarizability tensor, $\mathbf{T}_{ij}$ is the dipole tensor and $\langle \chi^{(1)} \rangle$ is the constant average susceptibility. The first-order (linear) approximation is used here to provide insight into the physics of interaction-induced optical response. When performing actual calculations of the response (see section 8.4), the full DID effect will be taken into account.

The first-order dipole-induced dipole polarizability is the response to the macroscopic electric field inside a dielectric medium and not to the external electric field, eliminating sample shape dependent effects. This means that the molecules feel the local field generated by a dielectric medium in the total space around them. This is the first term of Eq. (8.1). The dipole-induced dipole coupling in the local surrounding of a molecule will be taken into account explicitly through the second term of Eq. (8.1). The volume in which this is done we will call the cavity. Since the coupling is calculated explicitly in this volume, a term has to be subtracted that contains the effect of the dielectric medium inside the cavity. This is the third term in Eq. (8.1).

The full dipole-induced dipole effect is accounted for if in the second term of Eq. (8.1) the polarizability α_j of the molecules generating the local fields on the considered molecule i is replaced by the effective polarizability Π_j. This takes into account that the dipole on molecule j is also induced by a local field. The set of equations will then have to be solved self-consistently. [56, 95–97] As mentioned above, in the MD-calculations that will be reported in section 8.4, this self-consistency was fully taken into account.

To shorten the notation, the induced polarizability $\alpha_i \mathbf{T}_{ij} \alpha_j$ will be abbreviated with $\mathbf{D}_{ij}$. The instantaneous susceptibility in an ensemble is given by the ensemble average of the effective polarizabilities

$$\chi^{(1)} = \frac{1}{V} \sum_i \left(\alpha_i + \sum_{j \neq i} \mathbf{D}_{ij} + \frac{4\pi \langle \chi^{(1)} \rangle}{3} \alpha_i \right) \tag{8.2}$$

where V is the ensemble volume.

The third-order Raman response is given by the time correlation function [50, 55, 77, 97]

$$\chi^{(3)}_{abcd}(t) = -\frac{V}{2k_B T} \langle \dot{\chi}^{(1)}_{ab}(t) \chi^{(1)}_{cd}(0) \rangle. \tag{8.3}$$

Substituting the instantaneous susceptibility Eq. (8.2) into this equation reveals six types of terms, which will be denoted RA, DI, CA, C1, C2, and C3 respectively. These we will now describe one at a time, omitting the proportionality factor $-\frac{1}{2k_B T V}$ and the indices for the polarization directions.

The single molecule realignment term (RA) is proportional to:

$$\begin{aligned}
R^{RA}(t) &= \sum_{i,j} \langle \dot{\alpha}_i(t) \alpha_j(0) \rangle \\
&= \sum_i \langle \dot{\alpha}_i(t) \alpha_i(0) \rangle + \sum_i \sum_{j \neq i} \langle \dot{\alpha}_i(t) \alpha_j(0) \rangle \\
&= \sum_i \langle \dot{\alpha}_i(t) \alpha_i(0) \rangle
\end{aligned} \tag{8.4}$$

This term only depends on the rotational motion of single molecules, since the derivative of the correlation between the molecular polarizabilities of two randomly chosen different molecules, in the second term on the second line, vanishes. Furthermore, this term is zero for the isotropic response, since the time derivative of the molecular polarizability is zero.

The dipole interaction terms (DI) are proportional to:

$$\begin{aligned}
R^{DI}(t) &= \sum_{i,k} \sum_{\substack{j \neq i \\ l \neq k}} \left\langle \dot{D}_{ij}(t) D_{kl}(0) \right\rangle \\
&= \sum_i \sum_{j \neq i} \left(\left\langle \dot{D}_{ij}(t) D_{ij}(0) \right\rangle + \left\langle \dot{D}_{ij}(t) D_{ji}(0) \right\rangle \right) \\
&+ \sum_i \sum_{j \neq i} \sum_{k \neq i,j} \left(\begin{array}{c} \left\langle \dot{D}_{ij}(t) D_{ik}(0) \right\rangle + \left\langle \dot{D}_{ij}(t) D_{ki}(0) \right\rangle \\ + \left\langle \dot{D}_{ij}(t) D_{kj}(0) \right\rangle + \left\langle \dot{D}_{ij}(t) D_{jk}(0) \right\rangle \end{array} \right) \\
&+ \sum_i \sum_{j \neq i} \sum_{k \neq i,j} \sum_{l \neq i,j,k} \left\langle \dot{D}_{ij}(t) D_{kl}(0) \right\rangle
\end{aligned} \tag{8.5}$$

The last term vanishes, because the correlation between the dipole interaction on two independent pairs of molecules does not vary in time.

The cross terms between the single molecule realignment and the dipole interaction (C1) are proportional to:

$$
\begin{aligned}
R^{C1}(t) &= \sum_{i,k}\sum_{j\neq i}\left(\langle\dot\alpha_k(t)D_{ij}(0)\rangle + \left\langle\dot D_{ij}(t)\alpha_k(0)\right\rangle\right)\\
&= \sum_{i}\sum_{j\neq i}\left(\langle\dot\alpha_i(t)D_{ij}(0)\rangle + \langle\dot\alpha_i(t)D_{ji}(0)\rangle + \left\langle\dot D_{ij}(t)\alpha_i(0)\right\rangle + \left\langle\dot D_{ji}(t)\alpha_i(0)\right\rangle\right)\\
&+ \sum_{i}\sum_{j\neq i}\sum_{k\neq i,j}\left(\langle\dot\alpha_i(t)D_{jk}(0)\rangle + \left\langle\dot D_{jk}(t)\alpha_i(0)\right\rangle\right)\\
&= \sum_{i}\sum_{j\neq i}\left(\langle\dot\alpha_i(t)D_{ij}(0)\rangle + \langle\dot\alpha_i(t)D_{ji}(0)\rangle + \left\langle\dot D_{ij}(t)\alpha_i(0)\right\rangle + \left\langle\dot D_{ji}(t)\alpha_i(0)\right\rangle\right)
\end{aligned}
\tag{8.6}
$$

Here the last equality is based on the fact that the correlation between the polarizability (α_i) on one molecule and the polarizability on a second one induced by yet another molecule (D_{jk}) is constant in time.

The remaining contributions to the third-order Raman response arise from correlations with the last term of Eq. (8.2). This term eliminates the effect from a dielectric medium inside the cavity since the dipole-induced dipole coupling is explicitly taken into account in that volume. All of these contributions can be expressed in terms of the single molecule polarizabilities in Eq. (8.4) and (8.6), scaled with a factor $\frac{4\pi\langle\chi^{(1)}\rangle}{3}$ or $\left(\frac{4\pi\langle\chi^{(1)}\rangle}{3}\right)^2$. The cavity correction term (CA) is given by

$$
R^{CA}(t) = \left(\frac{4\pi\langle\chi^{(1)}\rangle}{3}\right)^2\sum_i\langle\dot\alpha_i(t)\alpha_i(0)\rangle.
\tag{8.7}
$$

The single molecule realignment - cavity correction cross term (C2) is given by

$$
R^{C2}(t) = 2\frac{4\pi\langle\chi^{(1)}\rangle}{3}\sum_i\langle\dot\alpha_i(t)\alpha_i(0)\rangle.
\tag{8.8}
$$

And finally the cross term between the dipole interaction and the cavity correction terms (C3) is given by

$$
R^{C3}(t) = \frac{4\pi\langle\chi^{(1)}\rangle}{3}\sum_i\sum_{j\neq i}\left(\begin{array}{c}\langle\dot\alpha_i(t)D_{ij}(0)\rangle + \langle\dot\alpha_i(t)D_{ji}(0)\rangle\\ +\left\langle\dot D_{ij}(t)\alpha_i(0)\right\rangle + \left\langle\dot D_{ji}(t)\alpha_i(0)\right\rangle\end{array}\right).
\tag{8.9}
$$

Dilution can be looked upon as replacing Raman active molecules with molecules that do not contribute to the Raman response. Removing active chromophores from the solution

is equivalent to reducing the summations in Eqs. (8.4) to (8.9). From the single summation in the last line of Eq. (8.4) it can be seen that the single molecule realignment part of the response scales linearly with the concentration. The C1 cross term that depends on the correlation between the rotational motion of a molecule and a dipole interaction involving the same molecule consist of a double summation and is growing quadratic with the concentration. The dipole interaction term (DI) involves both a double and a triple summation, giving rise to quadratic and cubic growth respectively.

In the terms involving the cavity correction (CA, C2 and C3), as a first approximation the constant average susceptibility $\langle \chi^{(1)} \rangle$ can be taken to be proportional to the concentration. Consequently these terms scale quadratically (C2) and cubically (C3 and CA), with the concentration respectively. These three last contributions should be seen as corrections to the terms involving the dipole interaction, since the cavity correction ensures that the dielectric medium inside the cavity, where the interactions are taken explicitly into account through the dipole interaction scheme, is not counted twice.

This analysis suggests that, in general, terms scaling in a linear, quadratic or cubic fashion with the concentration upon dilution can be found. It should be mentioned that by the use of the first-order DID model instead of the full self-consistent DID model terms are omitted that also scale with quadratic and higher powers, but only the single molecule realignment term scales linearly.

Some of the terms found can sometimes be excluded by using symmetry arguments. For instance, the terms including single molecule polarizabilities are vanishing in the isotropic response since the trace of the single molecule polarizability is constant as long as intramolecular vibrational motion can be neglected. The isotropic response is then dominated by the terms in Eq. (8.5), scaling quadratic and cubic in the concentration.

In a real mixture, the ideal conditions considered till now will never be found. Structural, dynamical and chemical changes of the liquid can take place upon dilution. Differences in molecular shapes and sizes of the two components will change the structure and dynamics of the liquid. Furthermore, the differences in the weak forces, binding the molecules together in the liquid, might change the structure and dynamics as well. For instance, in mixtures of water and ethanol the structural changes due to redistribution of hydrogen bonds result in a considerably decrease of the molar volume. In liquids with weaker bonding types, similar effects will take place but on a smaller scale. In some cases, specific intermolecular forces can also have drastic effects. Dimers, clusters, micelles and molecular aggregates are examples of systems, where individual molecules associate with

each other. Such molecular structures can be expected to be relatively stable upon dilution and they will often give rise to distinctively different optical responses than unassociated single molecules. Chemical reactions in the mixture, giving rise to breaking or formation of covalent bonds, will of course also change the response considerably.

In general the optical signals are strongly dependent on the concentration of Raman active molecules. The growth rate depends on how many individual molecules are needed to produce the response. Only one Raman active molecule is needed in the single molecule reorientational response (RA), while at least two molecules are involved in the interaction induced parts of the response leading to quadratic or higher order dependence in the concentration.

To get a picture of the terms that are determining the Raman response, molecular dynamics simulations on diluted systems using the full DID model, [56,95–97] were performed. Thus, the information content of the experiments concerning the structural dynamics of liquids can be evaluated. In such simulations a fraction of the molecules can be made invisible and excluded from the susceptibility calculations. This is identical to reducing the sums in Eqs. (8.4) to (8.9). In this way an ideal solution is obtained, where the structure and dynamics of the system is maintained during the process of dilution.

The ideal mixture will thus be a mixture of two almost identical molecules. Experimental deviation from ideal behavior will provide valuable information on the different properties of the two types of molecules and about their respective interactions. Investigations on a wider range of mixtures can provide valuable information on molecular interactions in general.

8.3 Experiment

Kerr effect and transient grating scattering experiments were employed to study the third-order time resolved Raman response of carbon disulfide and carbon disulfide / alkane binary mixtures. These experiments were performed by A. Pugzlys and G. D. Crînguş from the Ultrafast Laser Laboratory, Materials Science Centre at Rijksuniversiteit Groningen.

The OHD-Kerr experiments were performed as proposed by McMorrow *et al.* [174] Briefly, we used a Ti:sapphire oscillator (Mai Tai, Spectra-Physics) delivering ∼70 fs pulses centered around 800 nm at an 82 MHz repetition rate. After pre-compression in a fused silica prism pair, the pulses with an energy of 7 nJ/pulse were split into pump and probe beams with a ratio 10:1, respectively. The probe pulse was variably delayed by a computer

controlled delay stage. The pump and probe beams, polarized at 45° with respect to each other, were focused into a sample by using a spherical mirror of $r = 25$ cm. The necessary pump and probe polarization orientations were set by 3 mm thick Glan-Taylor polarizers and a $\lambda/2$ plate in the pump beam. A 90° out-of-phase local oscillator field for the signal was generated by insertion of a $\lambda/4$ plate in the probe beam and detuning of the probe polarizer by ∼1.5 degrees. By measuring the cross-correlation function of the pump and probe beams in a 20 μm BBO crystal and applying a deconvolution procedure in frequency domain, [195,196] the distortions introduced by the instantaneous electronic response were separated from the (delayed) response due to the induced nuclear dynamics in the liquid.

The transient grating experiments in BOXCAR geometry were performed by using a 1 kHz Ti:sapphire laser system (Hurricane, Spectra-Physics) and optical parametric amplifier (OPA). The laser system produces 120 fs, 800 μJ pulses at 1 kHz centered at 800 nm. About ∼300 μJ pulses were split off to pump a traveling wave optical parametric amplifier (TOPAS, Light Conversion LTD). The sample was excited with pulses centered at a wavelength of 700 nm (second harmonics of the signal wave of the TOPAS at 1400 nm). Before splitting into two pump and a probe beam, the output was compressed to ∼50 fs in a double-pass compressor based on two fused silica prisms. In addition to pulse shortening, the compressor allows spatial separation of the different spectral components of the parametric light (signal and idler beams). The pulse shape was determined by frequency resolved optical gating (FROG). [197, 198] The experiments were performed with pulses, attenuated to an energy of less than 15 nJ per pulse. After setting the polarization of the beams by $\lambda/2$ plates and 3 mm thick Glan-Taylor polarizers, they were focused into the sample with a spherical mirror of $r = 25$ cm. Different tensor elements of the third-order nonlinear optical response function $\chi_{ijkl}^{(3)}$ can be determined by varying the polarizations of the interacting beams as well as selecting a polarization direction in the detection. The signal was filtered by a Glan-Taylor polarizer, detected by a silicon photodiode, processed by lock-in amplifier, digitized and stored in a computer for further analysis.

The samples consisted of binary mixtures of CS_2 and alkane solvents (pentane, heptane and decane) placed in a 1 mm standing quartz cell. To avoid heating effects the sample was stirred with a glass-coated metal stirrer placed inside the cell and a rotating magnet. CS_2 as well as pentane, heptane and decane (all spectroscopic grade) were obtained from Merck and Lab-Scan and used without further purification. In order to remove dust particles the solvents were filtered by using 0.2 μm pore size filters directly before injection into the cell.

8.4   Results and discussion

The third-order Raman response was calculated using MD for idealized diluted carbon
disulfide. These mixtures, as already described in section 8.2, consist of chromophore
carbon disulfide molecules that contribute to the optical response, and so-called ghost
carbon disulfide molecules. These later ones do not contribute to the Raman response
but fill out the void between the chromophores and preserve the dynamic behavior of the
liquid. We choose to calculate such an idealized diluted sample rather than a specific
mixture in order to obtain general information on the effects of dilution upon many-body
effects. The deviations from this model, that are observed in experimental results, can then
be directly related to specific physical effects that provide information on the microscopic
structure and dynamics of the liquid. Furthermore, changing the properties of the ghost
molecules slightly allows the investigation of the effect of changing the properties of the
solvent. Therefore, more general information about dilution effects can be obtained then
if one particular mixture was studied.

The time correlation function method [50, 97] was employed to calculate the response
function from the dynamics, which was simulated using the conditions described in chapter
6 of this thesis. A common literature force field [165] of atomic Lennard-Jones type was
used:

$$V_{LJ} = 4\epsilon \left[\left(\frac{\sigma}{r} \right)^{12} - \left(\frac{\sigma}{r} \right)^{6} \right] \tag{8.10}$$

Here ϵ is the depth of the potential well and σ a characteristic distance. The simulations
were done with 64 and 256 molecule simulation boxes in 5 ns trajectories. The degree of
dilution was set by varying the relative number of chromophores with polarizabilities and
ghost molecules without polarizabilities.

The experiments were performed on mixtures of carbon disulfide and the alkanes pen-
tane, heptane and decane. Some of the important physical properties of the pure liquids
are listed in Table 8.1. The mixtures have been prepared with volume fractions of carbon
disulfide of 30 %, 50 %, 70 % and 100 % for the anisotropic OHD-Kerr experiments and
from 0 to 100 % with 10 % intervals for the isotropic transient grating experiments.

In the OHD-Kerr experiment, used to measure the anisotropic response, the sample is
excited by two pump fields originating from the same laser pulse. After a time delay the
signal is measured as the induced rotation of the polarization. The observed signal for pure
CS_2 is shown in Figure 8.1. At zero time delay an instantaneous response of electronic
origin is observed, followed by a rising nuclear signal. After reaching its maximum, the

TABLE 8.1: *Density, viscosity and refractive index of the pure liquids at 20 °C. [90]*

| liquid	ρ (g/ml)	η (cP)	n_D
pentane	0.6262	0.240	1.3575
heptane	0.6837	0.409	1.3878
decane	0.7300	0.92	1.4102
CS_2	1.2632	0.363	1.6319

signal starts to decay, first non-exponentially and later in an exponential way. The electronic part of the response can be eliminated together with the pulse shape dependence by deconvolution of the signal, [195, 196] so that the pure impulsive nuclear anisotropic response is obtained.

In the transient grating experiments, two different pump beams are used to induce a grating in the sample from which a delayed prope pulse is Bragg scattered. For parallel polarized pump pulses and prope and detection polarizations at magic angle, the isotropic response is measured. The signal measured for pure CS_2 is shown in Figure 8.1. An instant electronic response is observed as well as a weak isotropic nuclear response with finite rise time. In principle the electronic response can be removed using a deconvolution procedure, [83] but if the nuclear signal is very weak, noise introduced by this procedure will severely contaminate the signal. Therefore the deconvolution procedure has not been applied. Instead, the isotropic response was only examined at long time delays, where the electronic response vanishes.

In the anisotropic OHD-Kerr experiment, the relaxation time in pure CS_2 is found to be 1.72 ps. Others have reported values of 1.70 ps, [120,121] 1.65 ps [69] and 1.61 ps [117,174], which are all comparable to the decay rate measured here. The MD simulation yielded a decay rate of 1.44 ps. The difference between the experimental and calculated realignment relaxation times is due to a slightly lower diffusion rate in the modeled liquid [169] than in the experiment, and to some extent to the noise in the tail of the calculated response.

The observed diffusional decay times at delays larger than 2 ps are listed in Table 8.2. It is seen that the reorientational relaxation time of the carbon disulfide molecules is decreasing upon dilution with pentane, relatively constant upon dilution with heptane and increasing when carbon disulfide is diluted with decane. This behavior correlates well with the relative values of the viscosity, listed in Table 8.1. According to the Stokes-Einstein-

FIGURE 8.1: *The measured response of pure CS_2. The OHD-Kerr signal (a) is shown in full line together with the nuclear response (long-dashed) and the pure electronic response (dashed line). This is the anisotropic part of the stimulated Raman response. The transient grating signal (b) was measured employing a probe pulse and analyser polarization both with polarization at magic angle compared to the pump pulses. The electronic response dominates the weak nuclear response that is also shown with a magnification of a factor of 100. This is the isotropic part of the stimulated Raman response.*
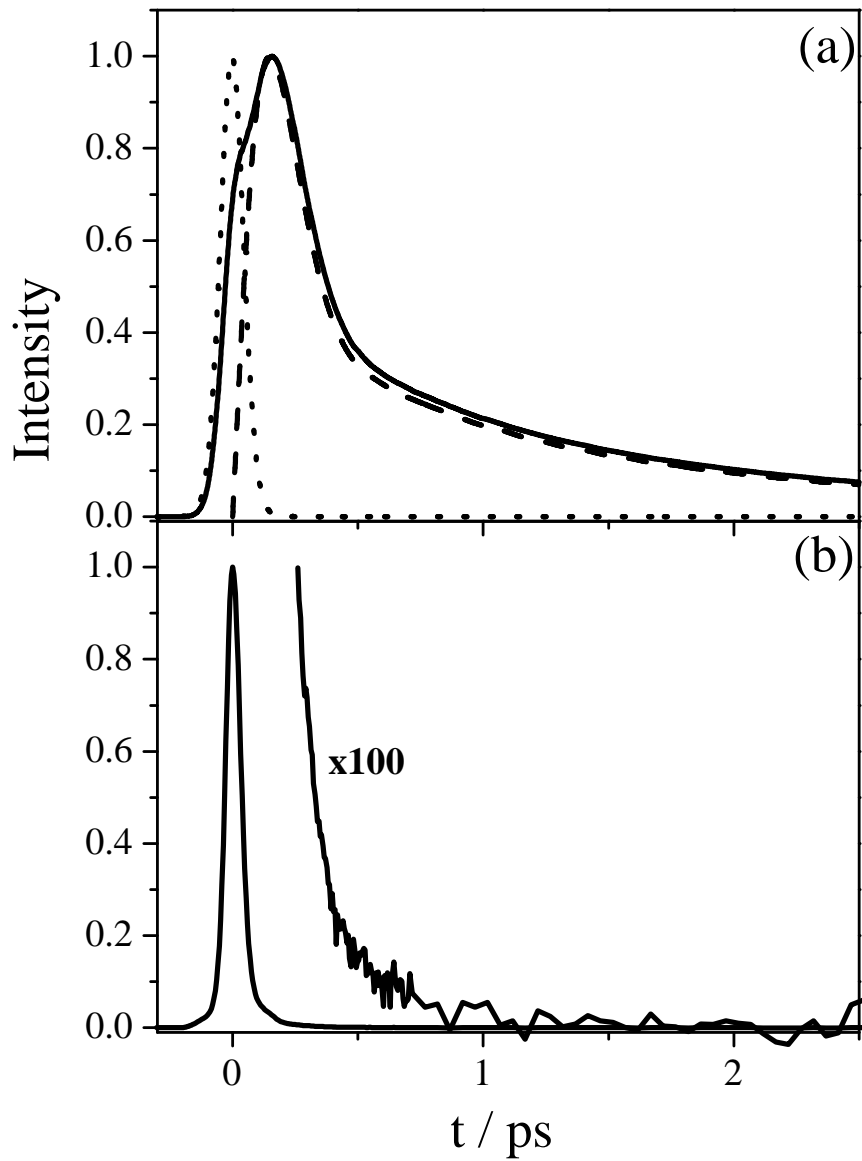
Debye relation [191] the reorientational relaxation time is:

$$\tau_D = c\frac{\eta}{kT} + \tau_0 \tag{8.11}$$

where c is a positive constant. In the MD simulations of the ideal mixtures the relaxation time should be constant. Values between 1.41 and 1.53 ps are found when only considering the data after 1.5 ps. The relative large spread is an indication of the uncertainty due to the fact that the Raman signal intensity in the tail rapidly becomes small.

TABLE 8.2: *The time constant in* ps *for the diffusive decay extracted from data after 2* ps. *(1.5* ps *for the MD) The concentration of* CS_2 *molecules in the mixture with alkanes is given as the volume percentage.*

solvent	100 %	70 %	50 %	30 %
pentane	1.72	1.56	1.48	1.40
heptane	1.72	1.67	1.68	1.78
decane	1.72	1.74	1.85	2.03
MD	1.44	1.53	1.41	1.48

Many authors have chosen to fit the observed response to phenomenological models of the dynamics. For instance, a sum of diffusional and librational response [68, 69, 117] was considered, and also a sum of diffusional and interaction induced response. [120] Theoretical investigations [77] show that both librational and interaction induced response are of importance and any model based fit should include both effects to be able to give a correct description of the generation of the Raman signals. Since the same response can be fitted to models ignoring either the librational or the interaction induced response, the physical interpretation of such fits is questionable. When interpreted in terms of the correlation functions given in Eqs. (8.4) to (8.9), the diffusional decay and the librational response both belong to the single molecule term Eq. (8.4), while the interaction induced response is covered by Eqs. (8.5)-(8.9).

Experimentally, the relative importance of the single molecule and many-body contributions can, in principle, be inferred from the concentration dependence of the intensity of the Raman response. When the structural, dynamic and chemical effects upon dilution are sufficiently small, only the single molecule term depends linearly on the concentration (see section 8.2). So, fitting the response to a third-order polynomial in the concentration at every delay gives the relative importance of the various terms. In the MD simulations the

single molecule term can be found in the same way, but also by simply excluding the DID terms. Comparing the calculated single molecule term found in both ways gives a check on the fitting procedure. In Figure 8.2 the linear scaling parts of the third-order responses are shown for the dilution with the three alkanes, together with the linear scaling part of the ideal dilution calculation and the calculated third-order response excluding interaction induced effects.

FIGURE 8.2: *The linearly scaling part of the anisotropic response found in the three alkanes, from the ideal mixture calculation and from a calculation excluding multi-body effects in the polarizability.*
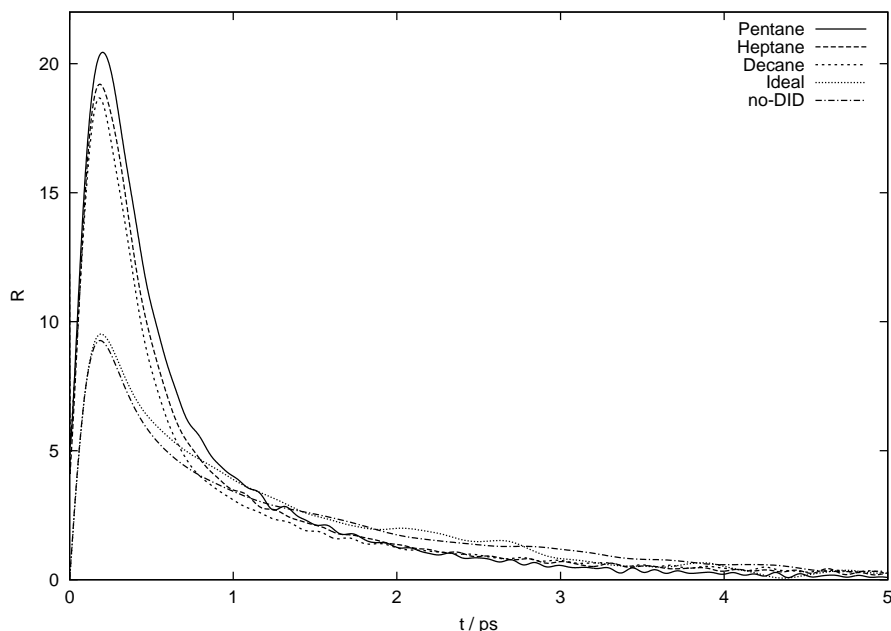
The linear scaling responses of the experimental solutions are all very similar to each other. The linearly scaling response of the ideal dilution calculations resembles the single molecule response calculated excluding interaction induced effects. However, there is a striking difference between the experimental and the theoretical linear scaling curves of Figure 8.2. Examining the normalized Raman responses at various concentrations of CS_2 in Figure 8.3 shows little difference between the experiments, whereas the intensity of the peak decreases rapidly compared to the tail upon dilution in the simulated response.

Steffen *et al.* [69] suggested that the almost constant ratio between the initial and the diffusive response upon dilution might be due to the formation of CS_2 aggregates bound together by the big quadrupole moments in CS_2. Larger domains of CS_2 would indeed

FIGURE 8.3: *The normalized CS_2-alkane anisotropic Raman response, measured by OHD Kerr experiments at CS_2 volume fractions of 30, 50, 70 and 100%. (a) pentane, (b) heptane, (c) decane and (d) ideal mixture simulation.*
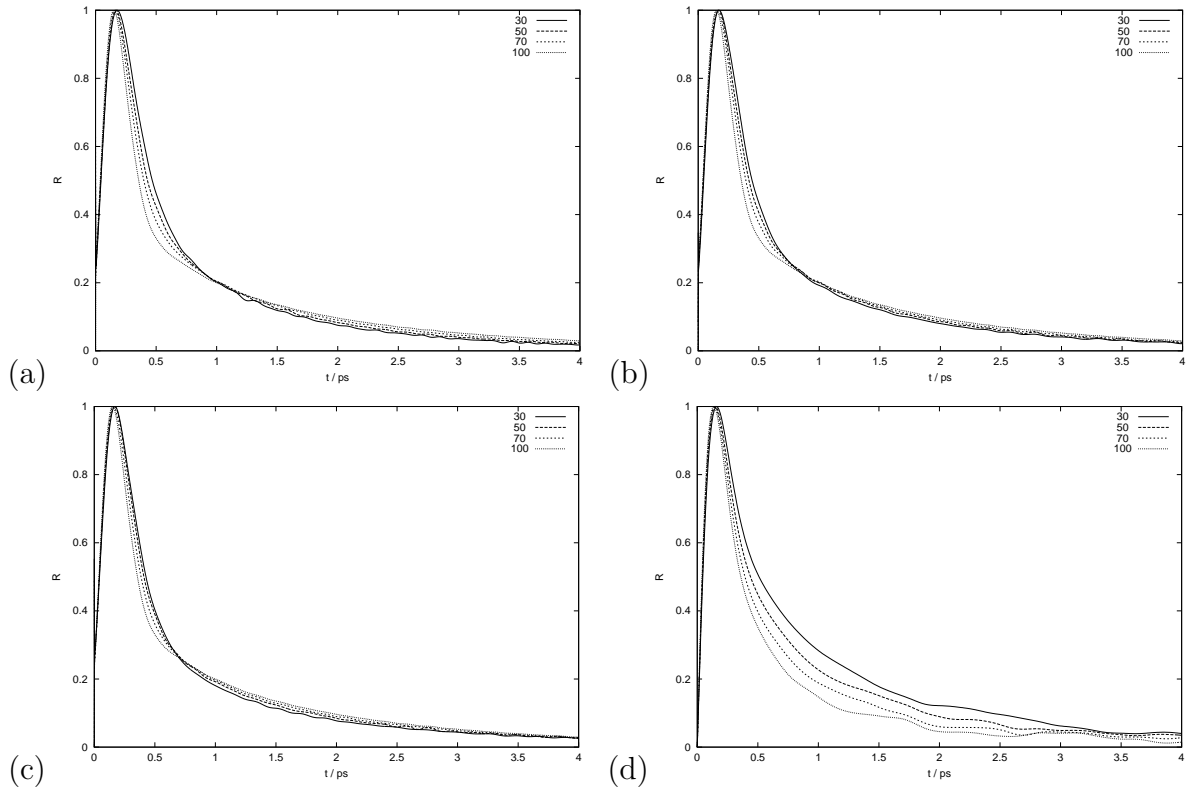
explain the observed discrepancy between experiment and calculations. This theory can be tested by adding charges on the chromophore molecules and not on the ghost molecules in order to simulate a mixture of molecules with large quadrupole moments that might tend to stick together, and molecules with no quadrupole moments.

Charges of -0.308 e on the carbon atoms and 0.154 e on the sulfur atoms were placed on the chromophores in a calculation with 32 chromophore molecules and 32 ghost molecules. The resulting carbon-carbon radial distribution functions are shown in Figure 8.4. Only small differences are observed between the chromophore-chromophore, chromophore-ghost and ghost-ghost radial distribution functions, so aggregation apparently does not occur. The stimulated anisotropic Raman response of this mixture is shown in Figure 8.5, showing no difference compared to the result without quadrupole moments.

FIGURE 8.4: *Radial distribution functions (centre of mass) for calculations with chromophores (C) with quadrupole moments and ghost molecules (X) without quadrupole moments.*
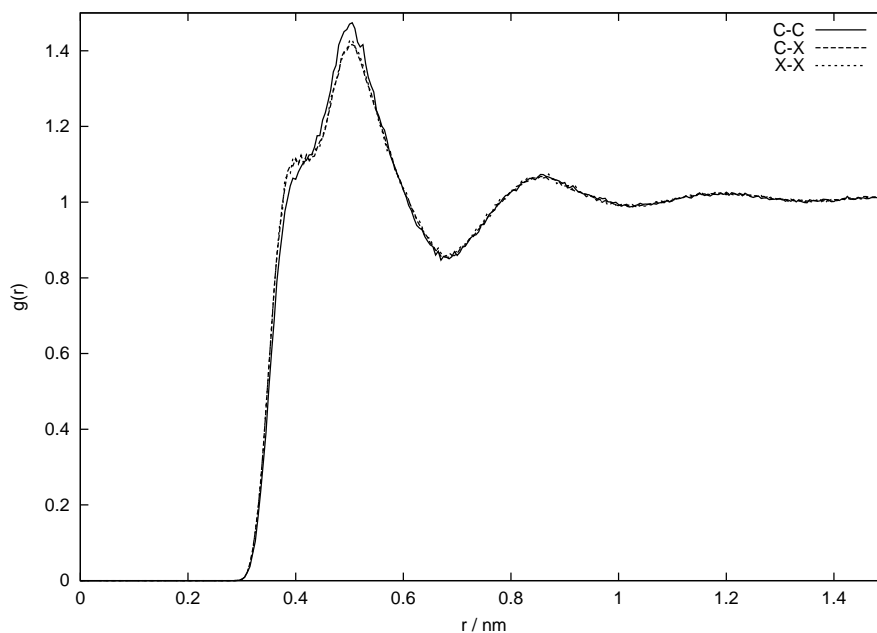
Another possible explanation for the discrepancy between the simulation of the idealized mixture and the experiment may be found in the fact that all alkanes have densities half the size of the CS_2 density (see Table 8.1). If fluctuations of the density play a role in the initial response, one could imagine that surrounding the chromophores with molecules with lower density enhances the initial response. This could then explain why the initial

FIGURE 8.5: *The calculated anisotropic response of mixtures of 32 chromophores and 32 ghost molecules. The response of an ideal mixture is compared with calculations, where the chromophores have quadrupole moments (Q-pol), where the molecular weight of the ghost molecules is lowered (Low Density) and where the depth of the LJ potential is reduced from 183* K *to 120* K *on the ghost molecule sulfur atoms.*
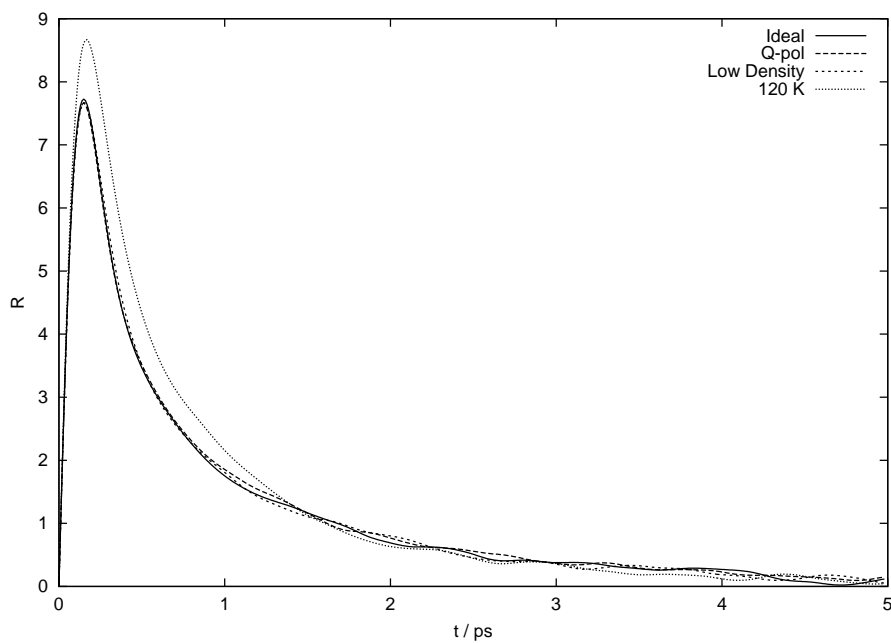
response is not suppressed experimentally, while it is in the simulation of the idealized mixture, where the density is constant. This idea can be investigated by lowering the mass of the ghost molecules.

Reducing the mass of the ghost molecules from 76.143 g/mol to 58.0716 g/mol and thereby the density of the liquid from 1.26 to 1.09 g/ml when an equal number of chromophore and ghost molecules are present, shows only minor changes in the Raman response as can be seen in Figure 8.5. So, the change of the density upon dilution apparently also cannot explain the observed discrepancy between simulation and experiment.

The van der Waals interactions between alkane molecules are in general weaker than the intermolecular interactions found in highly polarizable molecules as CS_2. In the CS_2-alkane mixtures the CS_2 molecules can be expected to experience more shallow potentials than in the pure liquid. It is possible that this enhances the librational and interaction induced responses at early times. Varying the depth of the LJ-potential on the ghost molecules, can give a clue on the importance of such effects. The presence of more shallow potentials was used previously as an argument to explain the decrease of the maximum in the frequency domain (Fourier transformed) spectrum of the Raman response upon dilution. [68, 69, 117, 118]

Examining the dependence on the force field is rather difficult, since changing the force field will most likely also change the volume of the liquid considerably and hence the volume fraction of CS_2. Furthermore, properties such as the viscosity and the density will also be affected, as is of course also the case in the real experiment. A simulation was performed with a potential depth ϵ of 120 K instead of 183 K on the sulfur atoms in the ghost molecules. The combination rule $\epsilon_{ij} = (\epsilon_{ii}\epsilon_{jj})^{1/2}$ for interactions of these sulfur atoms with the other types of atoms was applied. This mimics the more shallow potentials expected in alkane mixtures. The volume grows with approximately 10 % giving a decrease of the effective volume fraction of CS_2 from 0.5 to 0.457. The simulated response is shown in Figure 8.5, where it has been scaled to give approximately the same diffusive tail as the other responses. Now a clear difference is observed compared to the idealized solution calculation. The initial response is stronger even though the volume fraction of CS_2 is lower. This clearly shows that the solvent force field is crucial for the Raman response. Typical potential depths used to describe interactions of CH_3 and CH_2 groups in liquid alkanes are well below 100 K, [159, 199] but these could not be applied in the simulations since the ghost molecules would then be similar to the small alkanes ethane and propane. These are both gaseous at room temperature because of their small size.

A general explanation for the deviations between the simulations on the idealized solutions and the experiments could be that the model potentials are not good enough to describe the response. The force field is an atomic LJ model, [165] which has been used for virtually all studies on carbon disulfide. In the present study the molecules are kept rigid and no charges are distributed on the atoms. Other studies [104, 126] have included intra-molecular motion and charges, but that does not cause any significant change of the low frequency spectrum considered here. Carbon disulfide is a very anisotropic molecule and a high anisotropy can therefore be expected in the van der Waals forces. As also stated in the paper where the LJ model, used here, was first described, [165] a model with isotropic atomic forces cannot describe the anisotropic interactions of a molecule properly at all distances. It will have an isotropic asymptotic behavior in the long distance limit instead of the correct anisotropic asymptotic behavior. However the substantial differences observed between theory and experiment at low concentrations are unlikely to arise from small errors in a model that gives a good description of the pure liquid.

So far, we discussed the concentration dependence of the anisotropic Raman response, i.e. $\chi^{(3)}_{xzxz}$. The isotropic response is about one order of magnitude weaker than the anisotropic one. Since the isotropic response was measured using transient grating scattering, i.e. a homodyne detection technique, the square of the response function is measured and the isotropic signal therefore is considerably weaker than the anisotropic signal measured with the same technique. This unfortunately leads to far bigger uncertainties in the experimental results.

The isotropic response contains no contributions from single molecule effects. So, if the mixture is behaving as in the idealized simulations, the isotropic response contains quadratic and cubic scaling terms due to interaction induced contributions, but no linearly scaling terms. The power dependence in the volume fraction of the measured signal is shown in Figure 8.6 together with the measured signal for pure CS_2. At short delay times, where the electronic response dominates, the intensity is growing with the second power in the volume fraction. Since this is a homodyne experiment, in which the square of the response function is measured, this indicates that the electronic response is predominantly a single molecule property, depending on the number of CS_2 molecules present in the mixture. At longer delay times (>200 fs), where the nuclear response is expected to dominate the response, the power dependence of the measured signal is clearly larger than 2; it reaches a value of 3 or more. In the theory section it was shown that the interaction-induced nuclear response is expected to grow at least quadratically in the volume fraction and the

measured intensity therefore has to show at least 4th and higher-order power dependence. The fact that this is not seen here shows that a mixture of different power dependences on the concentration is present. This means that not only two-body interactions in the first-order susceptibility are important but also other many-body interactions. Fitting to one power is therefore too simple.

FIGURE 8.6: *The power dependence (dots) of the isotropic signal intensity in a mixture of CS_2 and pentane. The electronic signal scales quadratically. Higher power dependence is found in the nuclear part of the response. The response for pure CS_2 is shown as the dashed line, with the nuclear tail also displayed 20 times amplified as the solid line.*
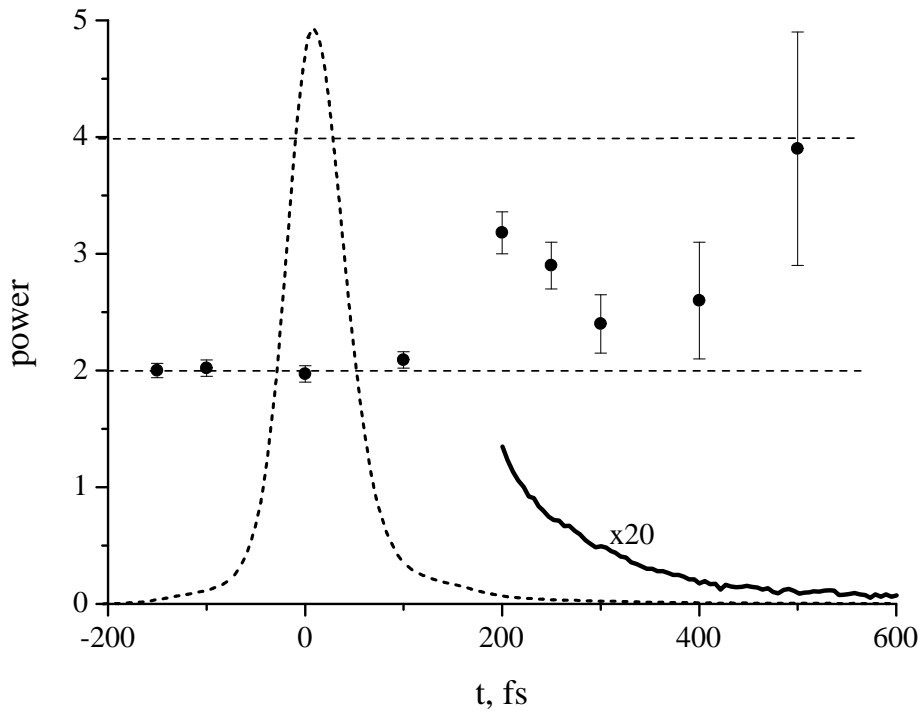
In Figure 8.7 the concentration dependence of the nuclear isotropic response (square root of the signal intensity) is shown at 300 fs, where the electronic response is expected to have vanished completely. Within the precision of the experiment the behavior of the different CS_2 alkane mixtures are the same. The behavior of the simulated response seems to overestimate the response at high CS_2 fractions. If CS_2 aggregates were formed in the liquid one would expect the opposite effect, i.e. slower disappearance of the multi-body

isotropic response than predicted by simulations on the ideal mixture.

FIGURE 8.7: *The concentration dependence of the isotropic response at 300* fs *in the three* CS_2*-alkane mixtures and in the simulation of an ideal mixture. The concentration of* CS_2 *molecules in the mixture with alkanes is given at the volume percentage.*
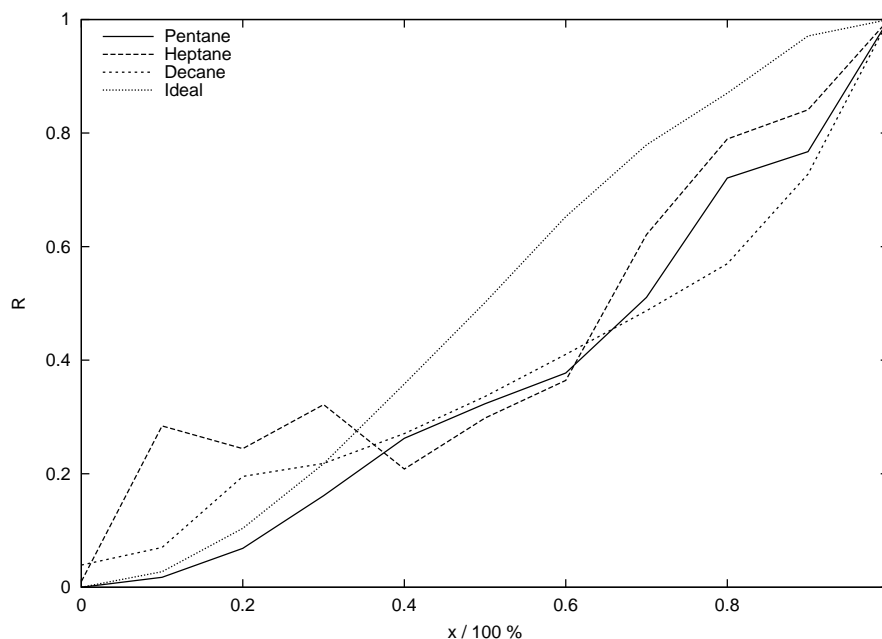
8.5   Conclusions

In this study the anisotropic and isotropic third-order Raman responses have been measured for mixtures of carbon disulfide with a series of alkanes. The experimental results were compared with molecular dynamics simulations of different model mixtures. Significant differences were found between the simplest model and the experiments in the subpicosecond regime. The initial response does not disappear as fast with concentration as predicted by the theoretical calculations. Using molecular dynamics we examined some of the possible microscopic explanations for the peculiar deviations. We succeeded in ruling out both aggregation due to large quadrupole moments on carbon disulfide and density fluctuations in the inhomogenious medium as sources of the discrepancies. In contrast, the shallowness of the potentials found in alkanes could provide a convincing explanation, as shown by the model calculations. The shallow potentials are probably leading to an increase of the librational response at a rate that compensates for the decrease of the

interaction-induced response, when diluting. Intramolecular solvent vibrations and the lack of a true anisotropic potential for carbon disulfide cannot be ruled out completely as partial explanations of the differences, since only rigid molecules have been used in the simulations. Further investigations with systematic variations of solvent potentials and vibrational degrees of freedom will be needed to get a more detailed microscopic picture of the optical response.

We showed that the isotropic response is measurable and reveals important information about the interaction induced response. Also in the isotropic response deviations were observed between the theory and experiments. In contrast to the initial anisotropic response, the isotropic response seems to disappear faster upon dilution in the high concentration limit than predicted by the simulations, which again provides strong evidence against the formation of aggregates. Further studies of the isotropic response should provide more information about the nature of the intermolecular motion and interaction-induced effects in the third-order Raman response.

Chapter 9

Liquid xenon as an ideal probe for many-body effects in impulsive Raman scattering

The collision induced effects in the third-order Raman response of liquid xenon have been studied both experimentally and theoretically. The effect of electron cloud overlap on the polarizability of xenon dimers was studied using accurate time-dependent density functional theory calculations. The dimer polarizabilities were used to fit parameters in a direct reaction field model that can be generalized to condensed phase systems. This model was employed in molecular dynamics simulations in order to calculate the impulsive Raman response of liquid xenon. Excellent agreement is found between the shape of the calculated and the measured anisotropic part of the response. The shape of this response is little affected by the electron overlap effects, but the intensity is strongly influenced by it. The shape of the isotropic response is predicted to be strongly dependent on electron overlap effects.

9.1 Introduction

Atomic liquids are special because no intramolecular nuclear degrees of freedom are found in these systems. Therefore they provide a unique possibility of studying intermolecular interactions and motions, avoiding any contribution from or coupling to intramolecular degrees of freedom. Xenon is a noble gas that forms an atomic liquid at a relatively high temperature due to its large atomic mass and high polarizability. The later effect not only

gives rise to substantial interatomic coupling, but also to efficient interactions with optical fields.

Dynamic (inelastic) light scattering was employed by a number of groups to study the properties of liquid xenon. [200–202] In these experiments the information is obtained in the form of a (Raman) spectrum of interatomic motion. More recently, these frequency-domain spontaneous light scattering methods were complemented with a variety of time-domain techniques, based on stimulated light scattering of short (femtosecond) laser pulses. [68–71, 117, 118, 120, 121, 174, 190–192] Examples of these techniques are the (heterodyned) optical Kerr effect [68, 69] and transient grating scattering. [70, 71] These experiments probe the evolution of the first-order susceptibility (the macroscopic polarizability) after impulsive excitation of the system, allowing observation of the liquid motion in real time. The time-domain data of these third-order nonlinear optical experiments are related to the frequency-domain spectra from spontaneous light scattering by Fourier transformation.

Isolated xenon atoms have constant isotropic polarizabilities and therefore will not give rise to any Raman response. However, in the condensed phase many-body interactions lead to fluctuations in the susceptibility and hence a measurable Raman response. This makes atomic liquids such as liquid xenon excellent probes for studies of intermolecular interactions and motions. Some fifteen years ago, Greene *et al.* [203] reported experimental results on the third-order Raman response of liquid xenon. Their limited time resolution allowed them to measure only the tail of the signal, which was found to be well described by exponential decay. This does not agree with the results of the earlier light scattering measurement by Gornall *et al.* [200], which Bucaro and Litovitz [119] fitted to an analytical expression that shows t^{-n} decay in the long time limit. This expression was derived [119] using a model based on gas phase collisions.

Dipole-induced dipole interactions arise from the fact that two molecules in a macroscopic electric field do not only feel this macroscopic field, but also the local field generated by the dipoles induced on other molecules. The electron overlap effect arises when molecules come so close to each other that their electron clouds overlap, which will then also affect their polarizability. In most calculations of the third-order response till now, only the dipole-induced dipole effect has been taken into account. [56, 77, 95–98, 133, 181] A few studies have used an atomic dipole-induced dipole (DID) model, [103, 104] placing polarizabilities not only on the centre of mass, but on all atoms, thereby including induced multipoles in an approximate manner. Recently a study including both induced multipoles and electron overlap in the calculation of the third-order response of CS_2 was reported. [62]

In that case it was shown that the effects of induced multipoles are more important than electron overlap. For xenon there are no induced multipole effects, since this is a spherical symmetric atom, so that only many-body interactions caused by the electron overlap effect and DID remains.

In this chapter the many-body aspects of the third-order Raman response of liquid xenon are studied experimentally and by simulation. In section 9.2 the theory behind the calculations is outlined. In section 9.3 the experiments are presented. The simulations are described and compared to the experimental results in section 9.4. Finally the conclusions are presented in section 9.5.

9.2 Theory

The stimulated Raman response is governed by the third-order response function $\chi^{(3)}_{abcd}(t_1)$, where c and d denote the polarization directions of two initial laser fields that interact with the sample. After a delay t_1 the time evolution of the system is probed by a laser field with polarization direction b. This results in the emission of a signal field that is detected with polarization direction a. In the isotropic liquid phase two linear independent components of the third-order response exist. [53] These can be chosen to be the isotropic ($\chi^{(3)}_{zzmm}$) and anisotropic ($\chi^{(3)}_{zxzx}$) components, where m denotes an axis forming an angle, often denoted the magic angle, of 54.74° with the z-axis.

In the finite field method (FF), [55,56,62] the third-order response function is calculated by simulating the conditions of the experiment. The forces, due to the optical fields E_c and E_d are actually applied in the simulation. The response is measured by calculating the susceptibility $\chi^{(1)}_{ab;cd}(t)$, at later time steps. The procedure is repeated for numerous trajectories with different starting configurations producing sufficient statistical material. The background noise $\chi^{(1)}_{ab;00}(t)$, from calculations without the applied forces is subtracted to improve accuracy. For laser fields with duration Δt and a number density N in the sample the response function is given by:

$$\chi^{(3)}_{abcd}(t) = \frac{\chi^{(1)}_{ab;cd}(t) - \chi^{(1)}_{ab;00}(t)}{4\pi\epsilon_0 N E_c E_d \Delta t}. \tag{9.1}$$

The FF method has been shown to be equally good as the more conventional time-correlation function method, when the third-order response function is calculated. [55] In terms of calculating costs and possibilities it is superior to this method, when higher order response functions such as $\chi^{(5)}_{abcdef}(t_1, t_2)$ are evaluated as seen in chapter 7. [55,56]

Bucaro and Litovitz derived an expression for the spontaneous Raman scattering (frequency domain) due to interaction induced effects, based on an atomic collision model. [119] This is related by a Fourier transform to the stimulated third-order Raman response (time domain). [119]

$$\chi^{(3)}(t) \propto \frac{\tau_C^n \sin(n \tan^{-1}(t/\tau_C))}{\left(t^2 + \tau_C^2\right)^{n/2}}, \tag{9.2}$$

where τ_C is the collision time and n is related to the character of the interaction. The expression has been used by several authors to fit experimental spectra. [62, 119, 120] One should be very careful doing this, since it was derived for collisions of isolated dimers with zero impact parameter. [119] The frequency domain response was originally given as

$$\chi^{(3)}(\omega) \propto \omega^{2[(m-7)/7]} \exp(-\omega/\omega_0), \tag{9.3}$$

where ω_0 is the inverse of τ_C and $2[(m-7)/7]$ is equal to $n-1$ ($m = [7n+7]/2$). In the paper by Bucaro and Litovitz [119] the time constant τ_C was related to the interaction parameters in an approximate way.

$$\tau_C \approx \frac{1}{6}\pi r_0(\mu/kT)^{1/2}\left[1 - (2/\pi)\tan^{-1}(2\epsilon/kT)^{1/2}\right] \tag{9.4}$$

Here ϵ and r_0 are the potential depth and distance in a supposed Lennard-Jones potential and μ is the reduced mass. The constant m was related to the polarizability dependence on the interatomic distance r.

$$\alpha(r) - \alpha(\infty) \propto r^{-m} \tag{9.5}$$

We will use time-dependent density functional theory (TDDFT) [136] to calculate the microscopic counterpart of the susceptibility, i.e. the polarizability. Since this method is far too time consuming to be used to calculate the polarizability of large numbers of molecules, the more efficient but approximated direct reaction field (DRF) model [60, 61, 127, 128, 156] is employed for this purpose. The parameters of this model are optimized to reproduce the TDDFT results for dimers. The DRF model is then generalized to calculate the first-order susceptibility of MD simulation boxes containing hundreds of atoms. See also chapter 5.

In the DRF model [60, 61, 127, 128, 156], the conventional dipole field tensor that describes the dipole induced-dipole interaction, is replaced by a modified one that also takes the effect of overlapping electron clouds into account. The first-order susceptibilities $\chi^{(1)}$

in Eq.(9.1) can be found by solving a linear set of equations [56, 60, 95, 96, 127, 128]

$$\chi^{(1)} = \frac{1}{V} \sum_p \Pi_p \tag{9.6}$$

$$\sum_p B_{qp} \Pi_p = L \tag{9.7}$$

$$B_{qp} \equiv \alpha_q^{-1} \delta_{qp} - \mathcal{T}_{qp}(1 - \delta_{qp}) \tag{9.8}$$

where Π_p is an effective polarizability on atom p, α_p is the isolated atom polarizability, V the volume and L the Lorentz factor. The modified dipole field tensor $\mathcal{T}_{pq}$ is given by:

$$\mathcal{T}_{pq} = \frac{3 f_{pq}^T (\hat{r}_{pq} : \hat{r}_{pq}) - f_{pq}^E}{r_{pq}^3}. \tag{9.9}$$

Here $\mathbf{r}_{pq}$ is the distance vector between the interacting dipoles. The screening functions f_{pq}^T and f_{pq}^E take the effect of overlapping charge densities into account. In the DID limit these factors are one. In the exponential density model they are [60, 128]

$$f_{pq}^E = 1 - \left(\frac{1}{2} \nu_{pq}^2 + \nu_{pq} + 1 \right) \exp(-\nu_{pq}) \tag{9.10}$$

$$f_{pq}^T = f_{pq}^E - \frac{\nu_{pq}^3}{6} \exp(-\nu_{pq}) \tag{9.11}$$

$$\nu_{pq} = \frac{\mathbf{a} r_{pq}}{(\alpha_p \alpha_q)^{1/6}}. \tag{9.12}$$

The empiric screening factor $\mathbf{a}$, and the atomic polarizability α are usually optimized to give as good a description of the molecular polarizability as possible for a wide variety of molecules. [128] In this work on liquid xenon the model will be optimized to reproduce the TDDFT result for the polarizability of a xenon dimer. Subsequently, the DRF approach was used to calculate the first-order susceptibility, in the same manner as described in our paper on CS_2. [62]

In Figure 9.1 the two possible interatomic motions in a dimer are sketched, i.e. a dimer rotation and a dimer collision with zero impact parameter. The dimer rotation will not change the isotropic polarizability of the dimer and hence will only contribute to the anisotropic response. The head on collisions will change both the anisotropic and the isotropic polarizability and will therefore give a contribution to both components of the optical response.

FIGURE 9.1*: Dimer rotation and dimer collision. Rotation only changes the anisotropic polarizability. Collision changes both the isotropic and the anisotropic polarizability.*

9.3   Experiments

The anisotropic Raman response of xenon was measured in an OHD-Kerr experiment, as proposed by McMorrow and Lotshaw. [174] These experiments were performed by A. Pug-zlys and G. D. Crînguş from the Ultrafast Laser Laboratory, Materials Science Centre at Rijksuniversiteit Groningen.

Briefly, we used a Ti:sapphire oscillator (Mai Tai, Spectra- Physics) delivering $\sim$70 fs pulses centered around 800 nm at an 82 MHz repetition rate. The output of the laser after pre-compression in a doublepass compressor based on two fused silica prisms, was ca. 7 nJ per pulse. This output was split into pump and probe beams with a ratio of 10:1 respectively. The probe pulse was variably delayed by a computer controlled delay stage. The pump and probe beams were polarized at 45° with respect to each other and were focussed into a sample by using a spherical mirror of r=25 cm. The necessary pump and probe polarization orientations were set by 3 mm thick Glan-Taylor polarizers and a $\lambda/2$ plate in the pump beam. The energy of the excitation pulses in the sample place did not exceed 2 nJ per pulse. The 90° out-of-phase local oscillator field was generated by insertion of a $\lambda/4$ plate in the probe beam and detuning of the probe polarizer by $\sim$1.5°. By measuring the crosscorrelation function of the pump and probe beams in a 20 μm BBO crystal and applying a deconvolution procedure in frequency domain [195, 196] the inertial nuclear contributions to the transients were separated from distortions introduced by the instantaneous electronic response.

Liquid xenon was condensed into the 2 cm path length sample space of a liquid nitrogen flow cryostat (Oxford DN1714) from 99.997 % purity xenon gas. Experiments were performed at a temperature of 164±0.5 K. The temperature of the liquid xenon was controlled by employing an active feedback device and monitored during the experiments. At

1 bar the melting point of xenon is 161.25 K and the boiling point is 166.15 K. [90] The dependence of the OHD Kerr response on temperature was investigated over this range, but was found to be almost negligible.

The experimental result of an OHD Kerr effect experiment at 164 K is shown in Figure (9.2). It is clear that the nuclear contribution to this signal is rather small compared to the electronic one. When the later is removed by Fourier deconvolution, [195, 196] the dashed trace is obtained. It is proportional to the anisotropic component $\chi_{zxzx}^{(3)}$ of the third-order Raman response of liquid xenon. This result will be compared to simulations below.

FIGURE 9.2: *The measured anisotropic third-order Raman response (solid line), together with the anisotropic deconvoluted nuclear response (dashed line), obtained by deconvoluting the electronic response.*
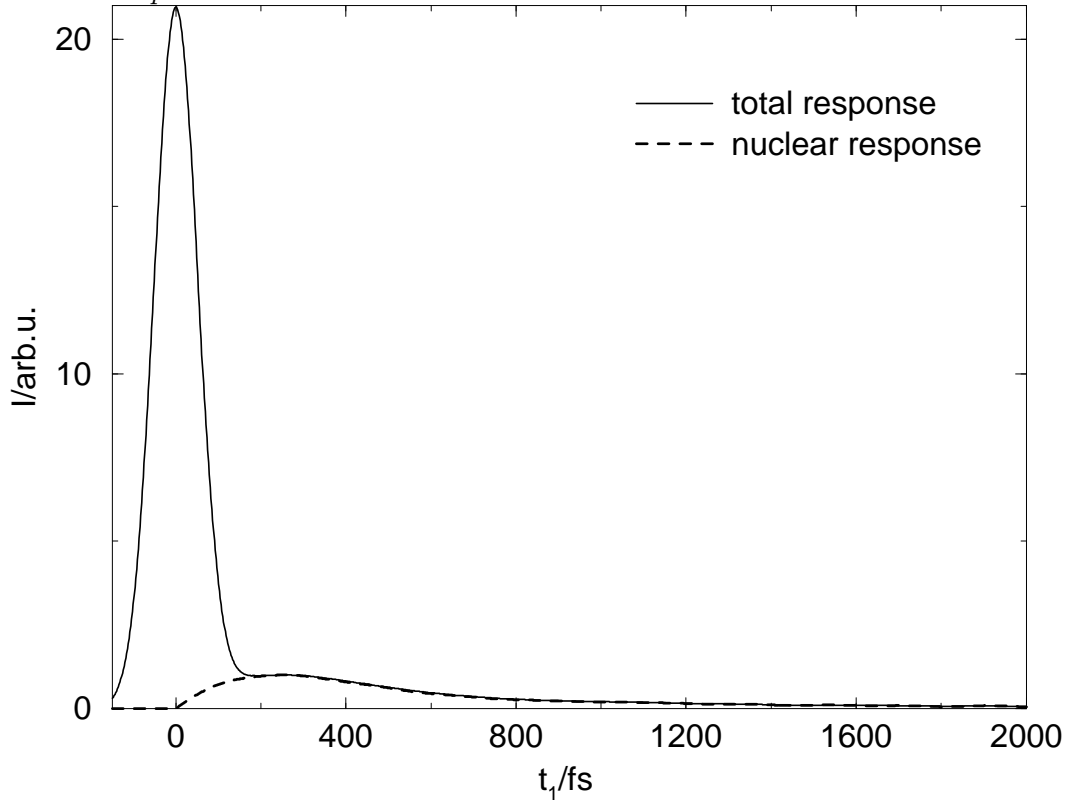
9.4   Simulations

The frequency dependent polarizability of the xenon atom and dimer were calculated with Time Dependent Density Functional Theory (TDDFT), using the Amsterdam Density Functional (ADF) [136, 148, 149, 151, 152] package. The basis set used is a standard ADF ZORA all electron triple zeta basis set with polarization (called "ZORA V all electron") to which diffuse functions have been added (Table 9.1). This is required for calculations of the polarizability, where displacement of weakly bound electrons in the diffuse region gives a significant contribution. The set of fit-functions was also expanded (Table 9.2) and new coefficients were found with the program GENFIT, which is part of the ADF distribution. The LB94 [153] potential with proper asymptotic behavior in the diffuse region was used in these calculations. This potential was shown to give good results for the polarizability of a large series of molecules. [137] Relativistic effects are expected to be of some importance since xenon is a rather heavy element. [204–206] The scaled ZORA approach, [207–210] implemented in ADF, was used to take the scalar relativistic effects into account. The value for the atomic polarizability of xenon at a frequency of 0.0934 a.u. was found to be 4.177 Å, deviating only 1% from experiment. [201] Typical absolute deviations in such polarizability calculations, using the same method, are 3.6% [137].

TABLE 9.1: *Exponents of the diffuse functions added to the ADF Xe V ZORA basis set with specific n power dependence in the radial part and spherical harmonic behavior.*

s-functions		p-functions		d-functions		f-functions	
n	exponent	n	exponent	n	exponent	n	exponent
5	1.2	4	3.2	3	6.2	4	1.3
	0.8		2.133	4	2.1		0.889
	0.533	5	0.81		1.4		0.0.593
	0.355		0.506		0.933		0.395
			0.316		0.622		
			0.198		0.415		
			0.123				

In order to compare the relative importance of the DID and collisional many-body effects on the optical response, simulations were performed where only the DID effect was incorporated, and simulations in which both effects were taken into account by the DRF

TABLE 9.2: *Number of fit functions added to the ADF Xe V ZORA basis set with specific n power dependence in the radial part and spherical harmonic behavior.*

s-functions		p-functions		d-functions		f-functions		d-functions	
n	no. fit f.	n	no. fit f.	n	no. fit f.	n	no. fit f.	n	no. fit f.
1	6	1		1		1		1	
2	2	2	1	2		2		2	
3	2	3	1	3	2	3		3	
4	2	4	3	4	3	4	3	4	
5	3	5	4	5	3	5	4	5	3
6	4	6	4	6	5	6	5	6	4
7	4	7	5	7	5	7	7	7	5
8	5	8	6	8	6	8	8	8	7
9	6	9	7	9	7				

method. In both the DID and DRF calculations the TDDFT single atom polarizability is taken as the starting point. All polarizabilities were calculated at a frequency of 0.076071 a.u. (598.96 nm), at which frequency the calculated atomic polarizability is 4.116 Å. The DRF model was optimized to the TDDFT calculations with the POLAR program [61]. In the optimization the xenon polarizabilities were kept fixed at the calculated single atom value of 4.116 Å. The screening factor **a**, which takes account of the electron cloud overlap, was optimized to dimer calculations with interatomic distances from 3 to 8 Å. It was found to be 2.58785, which is somewhat higher than the value of 1.9088 found in the optimization of a wide range of molecules. [61] The dimer polarizabilities, found with the DID and DRF models, as well as with TDDFT, are shown in Figure 9.3. At an interatomic distance of 4.3 Å, where the first solvation shell peaks, the value for the polarizability α_{zz} obtained with the DID model is 1.2% too high compared to the TDDFT result. At the closest interatomic distance found in the simulations, 3.55 Å, the DID polarizability α_{zz} is 5.5% too high. The slope of the DID polarizability versus interatomic distance is much steeper than the slope of the TDDFT curve. The optimized DRF model on the other hand shows excellent agreement with the TDDFT results.

MD simulations were performed with Gromacs 1.6 [159]. The temperature was set to 163 K and the pressure to 1 bar. The calculation box contains 256 atoms. The Lennard-Jones coefficients for the simulations were obtained by a fit to the xenon potential energy

FIGURE 9.3: *Dimer polarizabilities calculated parallel and perpendicular to the interatomic (x) axis.*
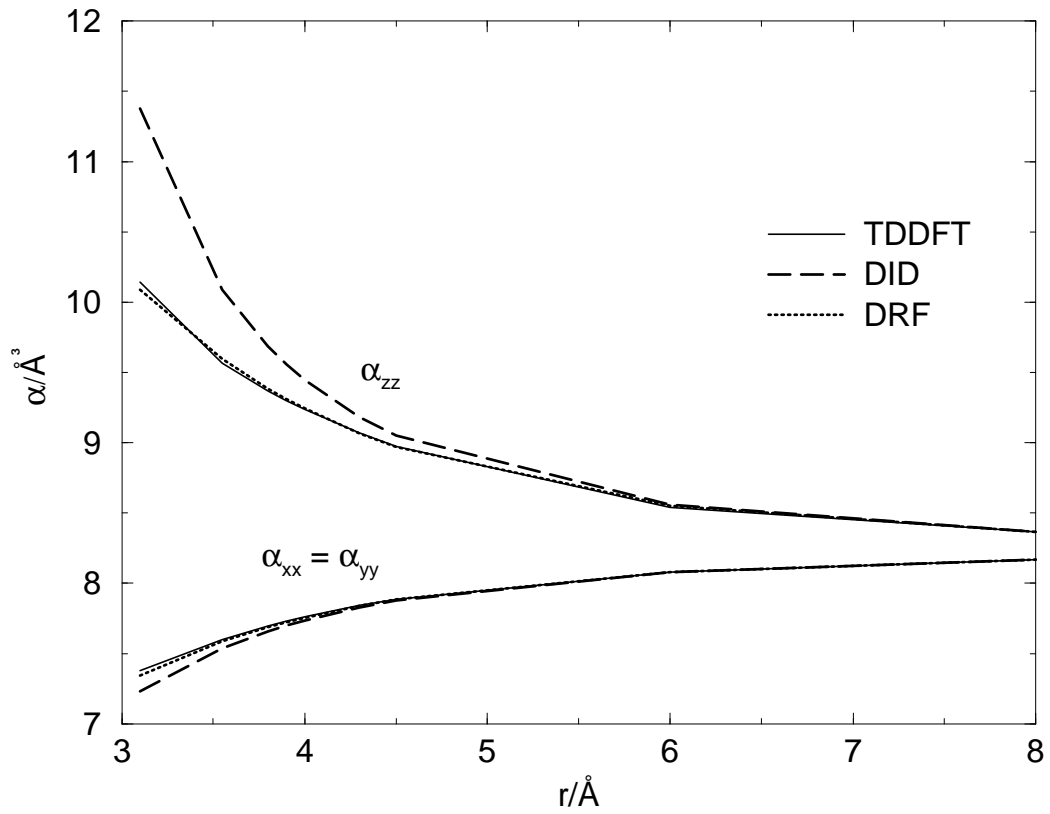
curve recently calculated by Faas *et al.* [205]. The coefficients are: $C_6 = 3.379 \times 10^{-2}$ kJ nm^6/mol and $C_{12} = 1.380 \times 10^{-4}$ kJ nm^{12}/mol. The calculated MD density of 2.9 kg/l shows good agreement with the literature value [211] of 2.969 kg/l, measured at 161.36 K and 0.8203 bar.

The third-order Raman response calculated with the DID model and the DRF model are compared in Figure 9.4. The first striking feature is that the isotropic response is very small compared to the anisotropic response, as was expected (see Sec. II). The isotropic response is almost fifty times smaller than the anisotropic response. The second noticable observation is the fact that the anisotropic responses, calculated with the DID and DRF models, have the same overall shape but very different intensities. Including electron overlap reduces the signal intensity by a factor of one and a half.

FIGURE 9.4: *The isotropic and anisotropic third-order responses calculated with the DID and DRF model.*
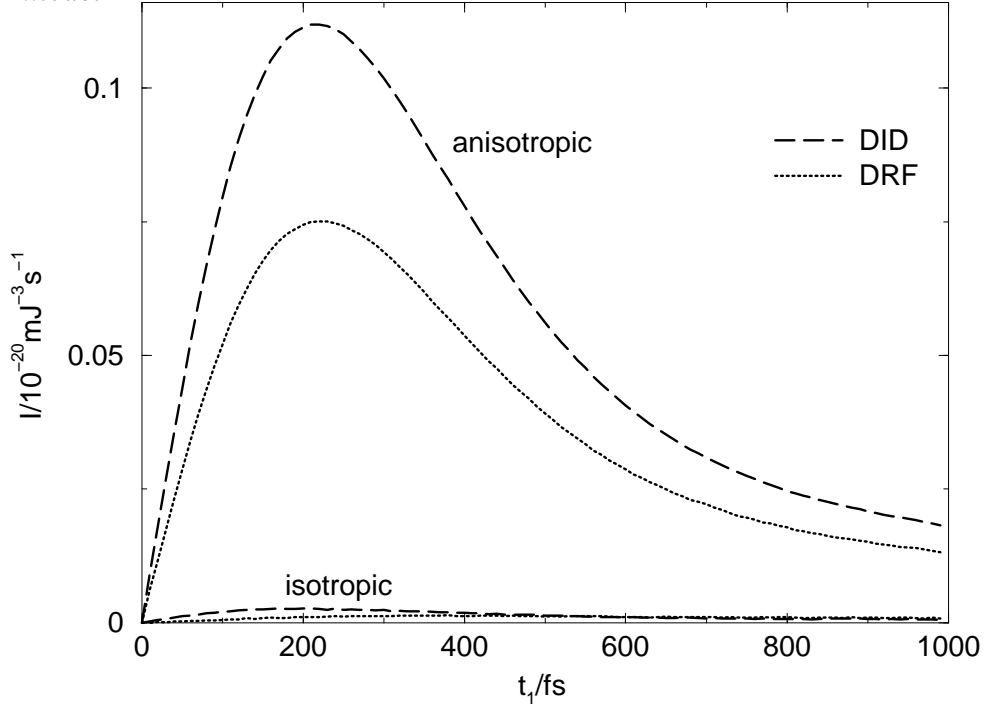
In Figure 9.5 the calculated isotropic responses are compared. Because of the small intensities of these signals, the signal-to-noise ratio is rather small. It is clear however that the shapes of the isotropic responses of the two models are not the same. Both the isotropic and anisotropic responses have been fitted to the atomic collision model expression

(Eq.(9.2)) given in Sec. II. The values for the respective constants are shown in Table 9.3. For comparison, the value for the time constant τ_c was also calculated to be 418 fs with the thermodynamic expression Eq.(9.4). The time constant τ_c of the isotropic DRF result comes closest to τ_c from expression (9.4). This is to be expected since the phenomenological model was derived for atomic collisions with zero impact parameter. The isotropic response indeed depends on these collisions but not on the dimer rotations.

FIGURE 9.5: *Comparison of the third-order isotropic responses calculated with the DID and DRF models.*
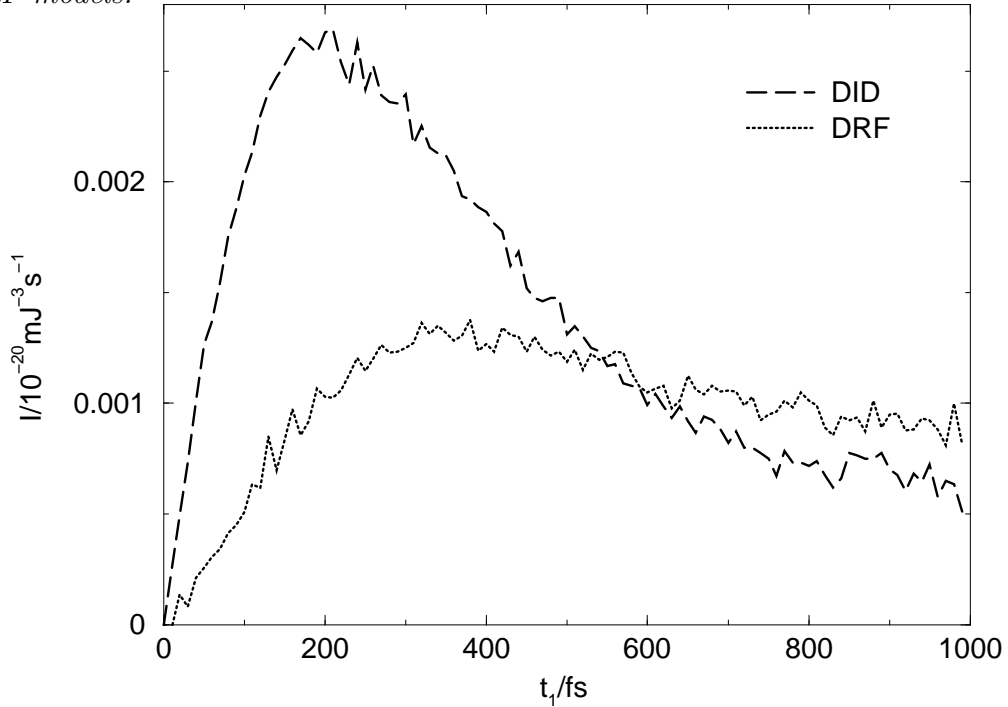
The absolute intensity can not be found experimentally, therefore only the shape of the response can be compared. The normalized anisotropic DRF and DID nuclear responses both show excellent agreement with the measured response (see Figure 9.6). However, the maximum occurs somewhat earlier in the calculated curves than in the experimental curve. The difference is very small, but the DRF result seems to be slightly closer to the experiment, especially in the tail.

TABLE 9.3*: Values for τ_c, n and m found from fits to calculations and experiment. I_C is the intensity.*

	Anisotropic			Isotropic	
	exp.	DID	DRF	DID	DRF
I_C	-	0.173	0.116	0.00442	0.00242
τ_c/fs	342	353	359	267	427
n	1.72	1.92	1.90	1.52	1.13
m	9.5	10	10	8.8	7.5

FIGURE 9.6*: Comparison of the normalized calculated anisotropic third-order Raman response with the deconvoluted anisotropic nuclear experimental response.*
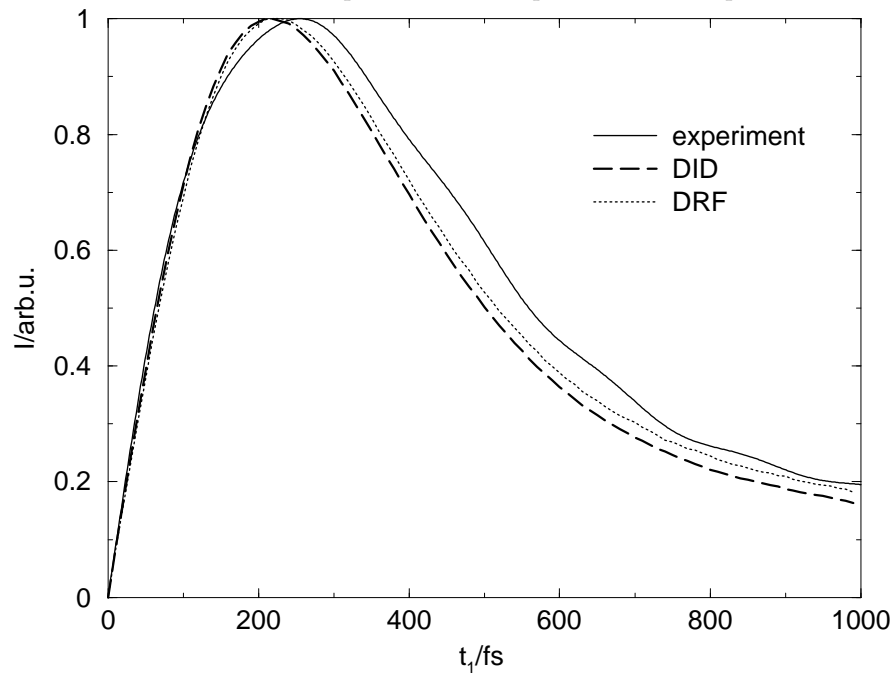
9.5   Conclusions

Liquid xenon was studied to investigate the effects of overlapping electron clouds and dipole induced-dipole interactions on the optical response. Xenon is eminently suited for this purpose, since the single atoms do not generate a Raman signal and all observed response is therefore due to many-body effects. Experimental results on impulsive anisotropic scattering were obtained by OHD-Kerr experiments. MD simulations were performed using the DRF model for the optical interactions, optimized against TDDFT calculations of the polarizability of dimers.

By comparing the DRF results to a model in which only DID effects are taken into account, it was shown that electron overlap effects are quite important, also at distances typically found in MD simulations. The electron overlap effect is seen to lower the intensity of the response. In the anisotropic case the shape of the response was only slightly affected by the electron overlap effect, whereas for the isotropic response the shape was found to be quite sensitive to the electron overlap effect.

Both the DID and DRF calculated responses agree excellently with the shape of the measured anisotropic response, even though the DRF result is slightly closer to the experimental one. The small deviations observed can originate both from experimental factors such as small errors introduced in the deconvolution procedure and from approximations done in the calculations such as the use of a Lennard-Jones potential. The fact that the maximum of the calculated signal occurs at a somewhat shorter timescale than the experimental one, might in that case be indicative of too high intermolecular frequencies, i.e. of too steep potentials.

It would be interesting if it was possible to detect the very weak isotropic response experimentally, since the shape was found to be very sensitive to the electron overlap effect in the calculations. Recent developments in the spectroscopical techniques [175] might make such measurements possible. Such attemps are now in progress.

Both the calculated and experimental response functions could be fitted quite well to the expression in Eq. (9.2). The fit constants agree reasonably well with the theory of Bucaro and Litovitz, [119] but we believe that one should be cautious interpreting the liquid response with a model based on collisions in vacuum with zero impact parameter.

The importance of electron overlap effects will probably also be observable in the fifth-order response of xenon that has been investigated theoretically by others. [59,86] Supposing that the difficulties of the experimental techniques, [41,74] used to detect the fifth-order

signals, can be overcome, the fifth-order response might provide other important clues to the importance of the electron overlap effects.

126

Summary

Many important chemical reactions take place in the liquid phase. Transition state models with one effective reaction coordinate are used to model such reactions, but in reality the reactions are affected by the complex dynamics of the liquid. For example, diffusion will determine the speed the reactive species are brought together to form a possibly reactive complex or transition state. The stability of such a complex and the time it takes to convert it into products is likely to be highly affected by the dynamics of the surrounding liquid. This make the low frequency modes in the liquid, that are connected with diffusional and intermolecular motion, an important subject to investigate.

In third-order Raman spectroscopy, that became available with pulsed lasers, the liquid motion is studied in real time rather than as resonances. This is done by applying a pair of pump pulses, exciting the low frequency modes of the liquid and after a delay probing the induced motion by a third laser field. This experiment reveals the low frequency modes of the liquid in time-domain, giving information about the diffusive reorientation of molecules and the intermolecular vibrations in the liquid. From this spectrum it is unfortunately impossible to distinguish between the different kinds of line broadening / relaxation mechanisms. Therefore Tanimura and Mukamel suggested the more complex fifth-order Raman experiment in 1993. [35] Here the sample is first pumped using a pair of laser pulses. After a delay t_1 a pair of mixing pulses are applied and finally after a second delay t_2 the response is measured with a fifth pulse, the probe pulse. In this way a two-dimensional spectrum in time is obtained, which not only contains information about the relaxation mechanisms of the liquid motion, but also information on mode coupling and anharmonicity.

Various groups have tried experimentally [38,39,81,84] to obtain the fifth-order Raman response of liquid carbon disulfide (CS_2), which is expected to have an especially strong response because of the high polarizability and polarizability anisotropy of the individual molecules. When this study took its beginning the observed response was poorly under-

stood and it did not seem possible to interpret the results with any of the known models developed for this purpose. The idea with the present study was to simulate the response using molecular dynamics to describe the liquid motion, which in all earlier theoretical approaches to the fifth-order response had been modeled using various kinds of harmonic oscillator models. [35, 58, 72] Full molecular dynamics simulations could possibly provide a better understanding of the observed spectrum.

All earlier approaches to obtain the (third- and) fifth-order Raman responses were based on time correlation functions. For the fifth-order response the time correlation function expression contains a two-time Poisson bracket, which is very time consuming to evaluate [55, 57] unless the motion can be described in an analytical way as in, for example, the harmonic oscillator models. The evaluation of the Poisson bracket involves calculating the effect of any distortion of the phase space coordinates at one time on all phase space coordinates at another time. [57, 58] In this study another approach, based on simply simulating the experiment directly, was developed. This approach is called the finite field method because the (pump) laser fields applied in the experiment are also applied directly in the (non-equilibrium) molecular dynamics simulations. The advantage of this approach lies in the fact that only the effect of the particular distortion of the phase space coordinates related to the Raman excitation on the phase space coordinates at later times is calculated. Thus, the problem is considerably reduced. [55]

The finite field approach was implemented in an existing molecular dynamics program and simulations were performed on carbon disulfide using simulation parameters developed earlier in time correlation function calculations on the third-order response. The third-order response was calculated using both the finite field method and the time correlation function method to test the reliability of the finite field method. The results of the two different methods were found to be in excellent agreement with each other and the finite field method was proven to be a reliable method to calculate the non-linear Raman response. [55]

The fifth-order response was also calculated using the new finite field method. In the meantime new experiments on carbon disulfide had been performed [41] and these suggested that the experimentally observed response was not the real fifth-order response, but a combination of two third-order processes taking place two different places in the liquid, called third-order cascades. The observed response did therefore not contain any information that could not be obtained from the third-order experiment. It is known that mismatching the phase of the laser fields in the experiment leads to discrimination against the cascade processes, but this mismatch did not seem big enough to eliminate the

cascade processes. From the third- and fifth-order responses calculated in this study the intensity ratio between the true fifth-order response and the contaminating cascades could be estimated. This was done and the experimental observation was confirmed. [55] It was found that the phase mismatch should suppress the cascaded response with more than a factor of a million to reduce them to the same level of intensity as that of the true response. The suppressing factor estimated to be present in the experiments was about three orders of magnitude smaller and considerable improvements of the experimental methods were found to be required if true fifth-order response should be obtained.

The Raman response is determined by the coordinate dependence of the polarizability or in a macroscopic system the coordinate dependency of the first-order susceptibility. This means that knowledge of the first-order susceptibility and its coordinate dependence in the simulated liquid is needed in order to calculate the Raman response. In the first simulations of the fifth-order response the susceptibility was approximated by assuming that no interaction between the molecular polarizability was present. [55] This is a rather crude approximation and excludes the intermolecular motion from the calculations. On the other hand it gives a correct description of the molecular reorientational motion and it was sufficient to give the first true estimate of the intensity ratio between the true fifth-order response and the competing cascaded processes. Furthermore it provided a test of the performance of the developed finite field method.

When a polarizable molecule is subjected to an electric field the molecule is polarized. This induced polarization again generates a local electric field around the molecule, which can be felt by other nearby molecules. A molecule in a liquid therefore does not only feel the applied electric field, but also the local fields generated by the induced polarization on molecules in its close neighborhood. This gives rise to a collective polarizability contributing to the susceptibility, which then depends on the intermolecular coordinates. Therefore the intermolecular motion will also contribute to the Raman spectrum. The local field effects can be modeled assuming that dipoles are induced on the molecular center of masses and that these induced-dipoles generate electric dipole fields. This model is called the dipole-induced dipole model (DID). It was implemented and applied in the calculation of the third- and fifth-order Raman responses. [56]

In the molecular polarizability model without lacal field effects the isotropic part of the susceptibility is unaffected by the motion in the simulated liquid and only response depending on the anisotropic part of the susceptibility is found. This also means that the reorientational single molecule motion does not contribute to the isotropic response and the

isotropic response is solely due to intermolecular dynamics. Experimentally the anisotropic and isotropic response can be separated by changing the polarization directions of the laser fields. This allows, for example, the observation of the intermolecular dynamics without any disturbing single molecule response. For carbon disulfide the third-order isotropic response is found to be about one order of magnitude weaker than the anisotropic response. [56,62,75]

This knowledge can be used to suppress the cascaded third-order processes by polarization selectivity, since these processes can be forced to go through the weak isotropic process reducing the intensity of the cascaded process by about one order of magnitude. In the experiments this is done by tilting the polarization direction of one of the applied pair of laser fields by the 'magic angle' (54.7°). [75] This can be done even more effectively by separating the polarization of the first pair of laser fields by 120°, and applying the polarization direction of the probe pulse in the middle. The special advantage of this configuration that goes under names as 'the pie configuration' and has been named by others 'the la Cour angle' and 'the Dutch cross' is that it discriminates against all possible third-order cascades in an equal way. [56] Using the dipole-induced dipole model the third- and fifth-order responses were calculated and the intensity rations between the true fifth-order response and the cascaded processes were estimated for different polarization directions of the laser fields. The 'magic angle' configurations of the response were found to discriminate better against the cascaded processes than the configuration, where all polarizations are parallel. The pie configuration was found to be even better, but none of them were found sufficient to solve the cascade problem without other improvements of the experimental techniques as well. [56]

Recent developments in experimental fifth-order techniques involving laser fields with different optical frequencies seem to reduce the contribution from the third-order cascades much more than the original experiments in which only one laser frequency was employed. A group in Toronto performed an extensive set of experimental measurements using this experimental technique. [45] They found their results to be in good qualitative agreement with the fifth-order response calculated in this study, [56] when the dipole-induced dipole model was employed. Deviations between these calculated spectra and the measurements might be due to the limitations of the dipole induced-dipole model.

The dipole induced-dipole model does not take all possible local field effects into account. Modeling the induced polarization in the molecules by dipoles on the center of mass is not sufficient, because of the extended structure of molecules also higher order (multipole) polarization will be induced. Furthermore, the polarizable electron clouds are smeared out

in the space around the nuclei allowing electron clouds from different molecules to overlap changing the overall polarizability. These effects, often denoted close collision effects, can be taken into account in an approximate way with, for example, the direct reaction field model (DRF) [60, 61, 128]. In this model, each atom is treated as a polarizable unit of an exponentially decaying electron cloud. The model contains a number of parameters that can be optimized to give the best description of the polarizability of an interacting set of molecules. To do that, time-dependent density functional theory calculations have been performed on the carbon disulfide monomer and on dimers. The DRF model was optimized to these calculations, which gave a quite different interaction than obtained with the simpler dipole induced-dipole model. The induced-multipole effect was found to be more important than the electron overlap effects in the calculation on the CS_2 dimers. [62]

The third-order Raman spectrum was calculated using the DRF model for the susceptibility, in order to examine the importance of the close collision effects. The induced-multipole effects were found to lower the intensity of the response due to intermolecular motion. This especially affects the isotropic spectrum where the intensity is overestimated considerably by the dipole induced-dipole model. Similar effects can be expected to be important in the fifth-order response. Since this response is more sensitive to local field effects it is expected to be even more sensitive to the close collision effects than the third-order response. [62] In connection with this study we performed an investigation on the influence of electron cloud overlap in liquid xenon. This investigation showed that the electron cloud overlap plays a crucial role for both the anisotropic and isotropic third-order response. In the case of xenon, both these responses are completely dominated by intermolecular motion. [65]

The local field effects have a strong influence on the spectrum when diluting the liquid. This comes about because the local field effects arise due to interactions between the molecules and these many-body effects depend on the probability of finding molecules at distances where the interaction is strong. The more molecules participate in a particular type of liquid motion, the faster the Raman response from this motion will vanish upon dilution with less interacting molecules. Simulations have been performed with an idealized mixture of carbon disulfide and 'ghost molecules' with the same dynamical properties as carbon disulfide but no molecular polarizability. This allows studying the effect of dilution in a very general way. The results were compared with experiments performed by the laser spectroscopy group on mixtures of carbon disulfide and alkanes. A clear discrepancy between the simulated and measured spectra was observed. In an earlier experimental

131

study, the peculiar behavior of the experimental response was speculated to be due to formation of carbon disulfide clusters kept together by the quadrupole moment of carbon disulfide. [69] Changing the properties of the ghost molecules in the simulation, such as the charges, molecular weights etc., all but one possible explanation was eliminated. The weaker van der Waals forces in the alkanes are the main reason for the spectral changes when diluting carbon disulfide with alkane molecules. [64]

Further calculations on the fifth-order spectra of CS_2 include the close collision effects. They were performed to investigate the implications on these spectra and to provide the best possible calculated response to compare with experiments and use fore their interpretation. From these calculations it is seen that the close collision effects give an important contribution to the spectra.

Resum/ (Summary in Danish)

Mange vigtige kemiske reaktioner foreg'r i v$\leq skefasen.Transitionstatemodellermed/neffektivreakti$
$skenskompleksedynamik.Diffusionbestemmerforeksempelhastigheden, hvormedreaktanterbringes$
$ngerafdenomgivendev \leq skesdynamik.Detteg > rdelavfrekventebev \leq gelseriv \leq$
$skenforbundetmeddiffusionogbev \leq gelsemellemmolekylertiletvigtigtemneatunders >$
$ge.$

I tredie-ordens Raman spektroskopi, som blev muligt med puls lasere, studeres v$\leq$
$skebev \leq gelsenitidsudviklingistedetforsomresonanser.Detteg > resvedatp'l \leq ggeetparpumpepulse$
$skebev \leq gelser, ogefterenpauseunders > gedeninduceredebev \leq gelsemedettredielaserfelt.Detteeks$
$ggerdelavfrekventev \leq skebev \leq gelseritidsdom \leq netoggiverinformationomdiffusivreorientering$
$rreumuligtatadskilleforskelligeslagslinieforbrednings/relaksationsmekanismeridettespektrum.De$
$ordenseksperiment.1001[35]Idettepumpespr > venf > rstvedhj \leq lpafetlaserpulspar.Etparblanding$
$ggesefterenventetidt_1$ og til sidst m'les responset efter endnu en ventetid t_2 ved hj$\leq$
$lpafenfemtepuls.P'dennem'deopn'settodimensionaltspektrumitid, derikkeblotindeholderinformatio$
$skebev \leq gelsensrelaksationsmekanismer, menogs'informationomkoblingafbev \leq gelseroganharmo$

Forskellige grupper har pr¿vet at m'le dette femte-ordens Raman spektrum af flydende
carbondisulfid (CS_2) eksperimentelt. [38, 39, 81, 84] Carbondisulfid forventes at have et
specielt st$\leq rktresponsp'grundafdetenkeltemolekylesstorepolariserbarhedogpolariserbarhedsanisotr$
$remuligtatforklaremednogenafdekendtemodellerudviklettildetteform'l.Ideenmedstudietvaratsimul$
$skebev \leq gelsen, derialletidligerestudieraffemte-ordensresponsblevmodelleretvedhj \leq$
$lpafforskelligeslagsharmoniskoscillatormodeller.1001[35, 58, 72]Enbedreforst'elseafdetobservered$
$lpaffuldst \leq ndigemolekyldynamiksimulationer.$

Alle tidligere fremgangsm'der til at beregne det (tredie- og) femte-ordens Raman re-
spons har v$\leq retbaseretp'klassisketidskorrelationsfunktioner.Tidskorrelationsfunktionsudtrykket$
$ordensresponsetindeholderenPoissonparentes, derermegettidskr \leq vendeatudregne1001[55, 57]medn$
$gelsenkanbeskrivesp'enanalytiskm'desomdetforeksempelkang > resiharmoniskoscillatormodellerne$
$1001[57, 58]Idettestudieblevennyfremgangsm'deudviklet, derbaseresp'simpelthenatsimulereeksperi$

ggesieksperimentetogs'p'l ≤ ggesdirektei(ikke−ligev ≤ gts)molekyldynamiksimulationer.Fordelenu
sentligt.1001[55]

Finite field metoden blev realiseret i et eksisterende molekyldynamik program og sim-
ulationer blev udf¿rt p' carbondisulfid ved anvendelse af simulations parametre udviklet i
tidligere tidskorrelationsfunktionsberegninger af tredie-ordens responset. Tredie-ordens re-
sponset blev beregnet ved hj≤ *lpafb'definitefieldmetodenogtidskorrelationsfunktionsmetodenforatt*
reiglimrendeoverensstemmelsemedhinandenogfinitefieldmetodenvistesigatv ≤ reenp'lideligmetode
line ≤ reRamanrespons.1001[55]

Femte-ordens responset blev ogs' beregnet ved hj≤ *lpafdennyefinitefieldmetode.Imellemtidenvar*
*rt*1001[41]*ogdisseantydede, atdeteksperimenteltobserveraderesponsikkevardetvirkeligefemte−*
ordensrespons, menenkombinationaftotredie−ordensprocesserkaldetkaskaderespons, derfindersted
sken.Detobserveraderesponsindeholdtderforingennyinformation, somikkekunnefindesitredie−
ordensresponset.Deterkendt, atkaskadeprocessernekanundertrykkeseksperimenteltvedatfejlmatche
restornoktilatkunneeliminerekaskadeprocesserne.V edhj ≤ lpaftredie−ogfemte−ordensrespons
ordensresponsogtredie−ordenskaskadeprocesserneestimeres.Detteblevgjortogdeneksperimentelleob
ordenskaskadeprocesserneerlangtst ≤ rkereenddetrigtigefemte−ordensrespons, blevbekr ≤
ftet.1001[55]*Detblevopdaget, atfasefejlmatchningenskulleundertrykkekaskaderesponsetmedmereen*
ordensrespons.Deneksperimentelleundertrykkendefaktorblevestimerettilatv ≤ reomkringtrest >
rrelsesordnermindreogenbetydeligforbedringafdeeksperimentellemetoderern > dvendig, hvisderigt
ordensresponsskalkunnem'les.

Raman responset bestemmes af polariserbarhedens koordinatafh≤ *ngighedelleretmakroskopisksys*
rste−ordenssusceptibilitetenskoordinatafh ≤ ngighed.Dettebetyderatvidenomf > rste−
ordenssusceptibilitetenogdenskoordinatafh ≤ ngighedidensimuleredev ≤ skeern > dvendigiberegnin
rstesimulationeraffemte−ordensresponsetblevsusceptibilitetenantagetatkunnebeskrivestiln ≤
rmelsesvistvedatantage, atderikkevarnogenvekselvirkningmellemdemolekyl ≤ repolariserbarheder.
1001[55]*Detteerentemmeliggrovantagelseogdenudelukkermedtagelsenafbev ≤ gelserderinvolvererfl*
kkeligtilatgivedenf > rsterigtigevurderingafintensitetsforholdetmellemdetrigtigefemte−
ordensresponsogdekonkurrerendekaskadeprocesser.Endvideregjordeantagelsendetmuligtatforetage
rstetestafdenudvikledefinitefieldmetode.

N'r et polariserbart molekyle uds≤ *ttesforetelektriskfeltpolariseresmolekylet.Deninduceredepola*
rkesafandremolekylert ≤ tp'.Derform ≤ rkeretmolekyleienv ≤ skeikkeblotdetp'trykteelektriskefel
rhed.Dettegiveranledningtilenkollektivpolariserbarhed, derbidragertilsusceptibiliteten, soms'afh ≤
ngerafdeintermolekyl ≤ rekoordinater.Derforvilintermolekyl ≤ rebev ≤ gelserogs'bidragetilRaman
remassecentreogatdisseinduceradedipolergenerererelektriskedipolfelter.Dennemodelkaldesdipol−

*induceretdipolmodellen(DID).Denblevrealiseretoganvendtiberegningenaftredie−ogfemte−ordensRamanresponserne.*1001[56]

I den molekyl≤ *repolariserbarhedsmodelerdenisotropedelafsusceptibilitetenuafh ≤ ngigafalbev ≤ gelseidensimuleredev ≤ skeogkunresponsderafh ≤ ngerafdenanisotropedelafsuscep rbev ≤ gelse.Detanisotropeogisotroperesponskanadskilleseksperimenteltvedat ≤ ndrelaserfelternes rebev ≤ gelserudenforstyrrenderesponsfraenkeltmolekyler.Detisotropetredie−ordensresponsafcar recirkaenst > rrelsesordensvagereenddeanisotroperespons.*1001[56, 62, 75]

Denne viden kan anvendes til at undertrykke tredie-ordens kaskadeprocesserne ved hj≤ *lpafpolarisationsselektivitet,idetdisseprocesserkantvingestilatforl > begennemdensvageisotropepro rrelsorden.Detteopn'sieksperimentetvedatdrejepolarisationsretningenforenafdep'tryktelaserfeltpa* [75] Dette kan g¿res mere effektivt ved at separere polarsationsretningen af de to f¿rste laserpulspar med 120° og lade polarisationsretningen af m'lepulsen v≤ *remidtimellem.Denspecielleforo rtekonfigurationen'ogafandreerblevetnavngivet'laCourvinklen'og'detHollandskekors',eratdenunde ordenskaskadeprocesserligeeffektivt.*1001[56]*Tredie−ogfemte−ordensresponsetblevberegnetvedhj lpafdipol−induceretdipolmodellenogintensitetsforholdetmellemdetrigtigefemte−ordensresponsogk rtekonfigurationenvarbetydeligbedre,meningenafdemvartilstr ≤ kkeligetilatl > sekaskadeproblem* 1001[56]

Nylig udvikling af den eksperimentelle femte-ordens teknik involverende laserfelter med forskellige optiske frekvenser ser ud til at reducere bidraget fra tredie-orden kaskade pro-cesser langt mere end i de oprindelige eksperimenter, der kun anvendte en laser frekvens. En gruppe i Toronto udf¿rte omfattende eksperimentelle m'linger ved hj≤ *lpafdenneeksperimentelleteknik* 1001[45]*Deresresultatervistesigatv ≤ reigodkvalitativoverensstemmelsemedfemte−ordensresponse* 1001[56]*n'rdipol−induceretdipolmodellenblevanvendt.Forskellemellemdisseberegnedespektreogm'lin induceretdipolmodellensbegr ≤ nsninger.*

Dipol-induceret dipol modellen tager ikke h¿jde for alle effekter af det lokale felt. At modellere den inducerede polarisation i molekylerne med dipoler p' massecentrene er utilstr≤ *kkeligt.P'grundafdenmolekyl ≤ restrukturvilh > jereordens(multipol)polarisationogs'opst roverlapmellemelektronskyerne,der ≤ ndrerdensamledepolariserbarhed.Derkantagesh > jdefordisseeffekter,oftekaldet'closecollision'effekter,p'entiln ≤ rmetvisvedanvendelseafforekser* 1001[60, 61, 128]*hvordetenkelteatombehandles,somenpolariserbarenhedmedeneksponentieltaftagend ngigt ≤ thedsfunktionalteori(TDDFT)beregningerafpolariserbarhedenblevudf > rtp'carbondisulfi induceretdipolmodel.Effektenafdeinduceredemultipolervistesigatv ≤ revigtigereendeffektenafde* 1001[62]

Tredie-ordens Raman spektret blev beregnet ved hj≤ *lpafDRFmodellenforf > rste−*

135

$ordenssusceptibiliteten for at unders > gebetydningen af 'closecollision' effekterne$
$nkeintensiteten af responset fra den mellem molekyl \leq rebev \leq gelse. Dettemanifesterersigspecieltide$
$induceretdipolemodellen. Lignendeeffekterkanforventesifemte-ordensspektretidetdetteresponsern$
$lsomtforlokalfelteffekterogderforogs`kanforventesatv \leq remeref > lsomtfor'closecollision'effe$
$ordensresponset.1001[62]Iforbindelsenmeddettestudieforetogvienunders > gelseafelektronskyoverl$
$gelseviste, atelektronskyoverlapeffekterneidettetilf \leq ldespillerenvigtigrolleb`deidenanisotropeogd$
$ordensspektret, sombeggedomineresfuldst \leq ndigafdenintermolekyl \leq rebev \leq gelse.$
1001[65]

Lokalfelteffekterne har en stor indflydelse p' spektret n'r $v\leq skenfortyndes. Detteerfordilokalfeltef$
$ngerafsandsynlighedenforatfindemolekylerneindenfordenafstand, hvorvekselvirkningenerst \leq$
$rk. Jofleremolekylerderdeltagerienbestemttypev \leq skebev \leq gelsejohurtigereforsvinderRamanresp$
$gelsevedfortyndingmedsvagerevekselvirkendemolekyler. Simulationerblevudf > rtp`enidealiseretv \leq$
$skeblandingafcarbondisulfidog'sp > gelsesmolekyler'meddesammedynamiskeegenskabersomcarbon$
$rpolariserbarhed. Dettemuliggjordestudietaffortyndingseffekterp`enmegetgenerelm`de. Resultateri$
$rtilaserspektroskopigruppenp`RijksuniversiteitGroningen. Enklarforskelmellemsimulationsresult$
$rselafdeteksperimentellerespronsforesl`etatkunneskyldesdannelsenafcarbondisulfidklumper, derho$
$1001[69]Vedat \leq ndresp > gelsesmolekylernesegenskaberisimulationen, s`somelektriskedeladninger$
$r/nelimineret. DesvagerevanderWaalskr \leq fterialkanmolekylerneerdenenestetingderkanforklaref$
1001[64]

Beregninger af femte-ordens spektre for carbondisulfid, der tager h¿jde for 'close collision' effekter er foretaget for at unders¿ge deres betydning for disse spektre og give det bedst mulige beregnede respons at sammenligne med eksperimentelle spektre og anvende til at tyde disse. Af beregningerne ses, at 'close collision' effekterne giver et vigtigt bidrag til spektrene.

Samenvatting (Summary in Dutch)

Veel belangrijke chemische reacties vinden plaats in de vloeibare fase. 'Transition state' modellen met een enkele reactiecoördinaat worden vaak gebruikt om dat soort reacties te modelleren, maar de reacties worden in werkelijkheid benvloed door de complexe dynamica van de vloeistof. Diffusie bepaalt bijvoorbeeld de snelheid waarmee de reactanten samen worden gebracht om een mogelijk geactiveerd complex of 'transition state' te vormen. De stabiliteit van zo'n complex en de tijd die het neemt om het in producten om te zetten wordt sterk benvloed door de dynamica van de omringende vloeistof. Dit betekent dat de vloeistofbewegingen met lage frequenties, die verbonden zijn met diffusie en intermoleculair beweging, een belangrijk onderwerp zijn om te onderzoeken.

De vloeistofbeweging kan worden bestudeerd in 'real time' in plaats van als resonanties in tijdsdomein derde-orde Raman spectroscopie, die met de gepulste laser ter beschikking kwam. Dit wordt gedaan door de vloeistof te exciteren met een tweetal pulsen waarmee bewegingen met lage frequenties worden opgewekt. Na een wachttijd wordt de genduceerde beweging gemeten met een derde laserveld. Dit experiment laat de bewegingen met lage frequenties zien in het tijdsdomein en geeft informatie over de reorientatie van moleculen en de intermoleculaire trillingen in de vloeistof. Helaas is het niet mogelijk de verschillende soorten lijn-verbredings / relaxatie-mechanismen te onderscheiden in dit spectrum. Daarom hebben Tanimura en Mukamel in 1993 het meer complexe vijfde-orde Raman experiment voorgesteld. [35] Hier wordt de vloeistof eerst geŒxciteerd door een paar pomp pulsen. Na een vertraging t_1 wordt een paar mengpulsen aangelegd, en ten slotte wordt na nog een vertraging t_2 het signaal gemeten met een vijfde puls. Op deze manier wordt een tweedimensionaal spectrum gemeten, dat niet alleen informatie over de relaxatie-mechanismen van de vloeistofbeweging bevat, maar ook informatie over de koppeling tussen verschillende soorten beweging en over de anharmoniciteit.

Verschillende groepen hebben de vijfde-orde Raman respons van vloeibaar koolstofdisulfide (CS_2) geprobeerd te meten. [38, 39, 81, 84] Deze respons is naar verwachting relatief

sterk vanwege de grote polariseerbaarheid en polariseerbaarheidsanisotropie van een indivicueel molecuul. Toen dit onderzoek begon, werd de experimenteel gemeten respons niet goed begrepen en het leek niet mogelijk de resultaten te interpreteren met gebruik van //n van de bekende, voor dit doel ontwikkelde, modellen. Het idee van deze studie was de vloeistofbewegingen te simuleren met gebruik van moleculaire dynamica in plaats van met harmonische oscillatormodellen zoals in alle eerdere studies. [35, 58, 72] Het zou mogelijk moeten zijn een beter begrip van het waargenomen spectrum te krijgen met gebruik van de volledige moleculaire dynamica simulaties.

Alle eerdere berekeningen van de (derde- en) vijfde-orde respons waren op klassieke tijdscorrelatiefuncties gebaseerd. De correlatiefunctie verbonden met de vijfde-orde respons bevat een Poisson haak, die erg veel tijd kost om te berekenen, [55, 57] behalve als de beweging op een analytische manier kan worden beschreven, zoals bijvoorbeeld in de harmonische oscillator modellen. De waardebepaling van de Poisson haak houdt de berekening in van het effect van elke storing van de faseruimtecoördinaten op een moment op alle coördinaten een bepaalde tijd later. [57, 58] In deze studie is een andere aanpak ontwikkeld, die er op gebaseerd is het experiment direct te simuleren. Deze aanpak wordt de finite field methode genoemd omdat de (pomp) laser velden die in het experiment worden aangelegd ook in de niet-evenwichts moleculaire dynamica direct worden toegepast. Het voordeel van deze aanpak is dat alleen het effect van de speciale storing van de faseruimtecoördinaten verbonden met de Raman excitatie op de faseruimtecoördinaten op latere momenten wordt berekend en waardoor het probleem aanzienlijk wordt vereenvoudigd. [55]

De finite field aanpak is in een bestaand moleculaire dynamica programma geimplementeerd en er zijn simulaties uitgevoerd op koolstofdisulfide, met gebruik van parameters ontwikkeld in tijdcorrelatiefunctieberekeningen van de derde-orde respons. De derde-orde respons werd berekend met gebruik van zowel de finite field methode als de tijdcorrelatiefunctiemethode om de betrouwbaarheid van de finite field methode te onderzoeken. De resultaten van de twee methoden waren in uitstekende overeenstemming en de finite field methode bleek een betrouwbare methode te zijn om de niet-lineaire Raman respons te berekenen. [55]

Ook de vijfde-orde respons werd berekend met gebruik van de nieuwe finite field methode. In de tussentijd waren nieuwe experimenten op koolstofdisulfide uitgevoerd [41] en deze suggereerden dat de experimenteel waargenomen respons niet de echte vijfde-orde respons was, maar een combinatie van twee derde-orde processen, derde-orde cascades genoemd. Deze kunnen gegenereerd worden op twee verschillende plekken in de vloeistof. De

waargenomen respons hield daarom geen informatie in, die ook niet afgeleid kan worden van het derde-orde experiment. Het is bekend, dat het mogelijk is ten ongunste van de cascadeprocessen te discrimineren door het op de juiste manier combineren van de fasen van de laservelden, maar dit was blijkbaar niet genoeg om de cascadeprocessen te verwijderen. De intensiteitsverhouding tussen de echte vijfde-orde respons en de derde-orde cascaderespons kan bepaald worden uit de derde- en vijfde-orde berekeningen in deze studie. Dit werd gedaan en de experimentele waarneming werd bevestigd. [55] Het bleek dat de fase-combinatie de cascaderesponse met een factor van minstens een miljoen moest onderdrukken om ze dezelfde intensiteit als de echte respons te geven. De onderdrukking in de experimenten werd geschat rond drie ordes van grootte te klein te zijn, en aanzienlijke verbeteringen van de experimentele methoden zijn nodig om de echte vijfde-orde respons te meten.

De Raman respons wordt bepaald door de coördinaat-afhankelijkheid van de polariseerbaarheid of in een macroscopisch systeem de coördinaat-afhankelijkheid van de eerste-orde susceptibiliteit. Daarom moet de eerste-orde susceptibiliteit en de coördinaat-afhankelijkheid ervan bekend zijn in de gesimuleerde vloeistof om de Raman respons te kunnen berekenen. In de eerste berekeningen werd de susceptibiliteit benaderd door aan te nemen dat er geen interactie tussen de moleculaire polariseerbaarheden was. [55] Dit is een tamelijk ruwe benadering en sluit de respons ten gevolge van intermoleculaire bewegingen van de berekeningen uit. Aan de andere kant geeft het wel een goede beschrijving van de moleculaire reoriëntatie en het was voldoende om een eerste schatting van de intensiteitsverhouding tussen de echte vijfde-orde respons en de concurrerende cascadeprocessen te geven. Bovendien gaf het een test van de prestatie van de ontwikkelde finite field methode.

Als een polariseerbaar molecuul in een elektrisch veld wordt geplaatst, wordt het gepolariseerd. Deze polarisatie brengt weer een lokaal elektrisch veld voort dat andere moleculen in de buurt kunnen voelen. Een molecuul in een vloeistof voelt daarom niet alleen het aangelegde veld, maar ook de lokale velden die gegenereerd zijn door de geïnduceerde polarisatie in de buurt. Dit geeft aanleiding tot een gezamenlijke polariseerbaarheid, die coördinaat-afhankelijk is en bijdraagt tot de susceptibiliteit. Daarom dragen de intermoleculaire bewegingen ook bij aan het Raman spectrum. De lokale veldeffecten kunnen gemodelleerd worden door de aanname, dat dipolen geïnduceerd worden op het moleculaire zwaartepunt en dat deze geïnduceerde dipolen vervolgens elektrische dipoolvelden genereren. Dit model wordt het dipool-geïnduceerd dipool (DID) model genoemd. Het werd geïmplementeerd en gebruikt in de berekeningen van de derde- en vijfde-orde Raman respons. [56]

In het moleculaire polariseerbaarheidsmodel zonder invloed van interacties wordt het isotrope gedeelte van de susceptibiliteit niet benvloed door de beweging in de gesimuleerde vloeistof en is er alleen een anisotrope respons. Dit betekent ook, dat de reoriŒntatie van individuele moleculen geen bijdrage geeft aan de isotrope respons. Deze respons ontstaat alleen maar door de intermoleculaire bewegingen. In het derde-orde experiment kunnen de anisotrope en isotrope respons gescheiden worden door de polarisatierichtingen van de laservelden te veranderen. Dit maakt het bijvoorbeeld mogelijk de intermoleculaire respons waar te nemen zonder storende moleculaire respons. De isotrope derde-orde respons van koolstofdisulfide blijkt rond een orde van grootte zwakker dan de anisotrope respons te zijn. [56, 62, 75]

Deze kennis kan gebruikt worden om de derde-orde cascaderespons te onderdrukken met polarisatieselectiviteit. Deze processen kunnen worden gedwongen te verlopen via het zwakke isotrope proces, waarbij de intensiteit van het cascadeproces met een orde van grootte wordt verminderd. In het experiment wordt dit gedaan, door de polarisatierichting van //n van de opgelegde paren van laservelden met de 'magische hoek' ($54.7°$) te kantelen. [75] Dit kan zelfs effectiever worden gedaan, door de polarisatierichting van de twee eerste laserveldparen $120°$ uit elkaar te kiezen en de polarisatierichting van het laatste laserveld in de midden aan te leggen. Het speciale voordeel van deze configuratie, die de 'taartconfiguratie' wordt genoemd en door anderen namen als de 'la Cour hoek' en 'het Nederlandse kruis' heeft gekregen, is dat het alle mogelijke derde-orde cascadeprocessen evenveel onderdrukt. [56] De derde- en vijfde-orde respons werden met gebruik van het dipoolgendudeerde dipoolmodel berekend en de intensiteitsverhouding tussen de echte vijfde-orde response en de derde-orde cascades werd geschat voor verschillende polarisatieconfiguraties. De 'magische hoek' configuraties van de respons onderdrukken allemaal de derde-orde respons beter dan de configuratie, waarin de polarisatierichtingen allemaal parallel zijn. De taartconfiguratie bleek zelfs beter te zijn, maar geen van de configuraties bleek de cascaderesponse voldoende te onderdrukken om het cascadeprobleem op te lossen zonder andere verbeteringen van de experimentele technieken. [56]

In recent ontwikkelde experimentele vijfde-orde technieken waarin laservelden met verschillende optische frequenties gebruikt worden, blijkt de bijdrage van de derde-orde cascaderespons sterker onderdrukt te worden dan in de oorspronkelijke experimenten, waarin alleen gebruik wordt gemaakt van //n frequentie. Een groep uit Toronto heeft een uitgebreid experimenteel onderzoek gedaan met deze techniek. [45] Ze hebben goede kwalitatieve overeenstemming gevonden tussen hun meetresultaten en de vijfde-orde respons die

in deze studie berekend is, als het dipool-genduceerde dipoolmodel gebruikt wordt. [56] Verschillen tussen theoretische resultaten en metingen zou dan aan de beperkingen van het dipool-genduceerde dipoolmodel te wijten kunnen zijn.

Het dipool-genduceerd dipoolmodel neemt niet alle mogelijke lokale veldeffecten mee. Het modelleren van de genduceerde polarisatie in de moleculen met dipolen op het zwaartepunt is een benadering, want vanwege de uitgebreide structuur van de moleculen wordt er ook polarisatie van hogere orde (multipoolpolarisatie) genduceerd. De elektronenwolken zijn bovendien in de ruimte om de kernen uitgesmeerd en dit heeft overlap tussen de elektronenwolken op verschillende moleculen tot gevolg. Deze overlap verandert ook de totale polariseerbaarheid. Deze effecten, die vaak 'close collision' effecten worden genoemd, kunnen worden beschreven op een benaderde manier met bijvoorbeeld de 'direct reaction field' model (DRF). [60, 61, 128] In dit model wordt elk atoom als een polariseerbare eenheid van een exponentieel afnemende elektronenwolk behandeld. Dit model bevat een aantal parameters, die geoptimaliseerd kunnen worden om de beste beschrijving van een verzameling wisselwerkende moleculen te geven. Om dat te doen, werden tijdsafhankelijk-dichtheidsfunctionaaltheorie-berekeningen uitgevoerd op het koolstofdisulfide monomeer en op dimeren. Deze berekeningen gaven een heel andere wisselwerking dan de met het enkelvoudige dipool-genduceerd dipoolmodel berekende wisselwerking. Het DRF model werd aan de resultaten van de tijdsafhankelijke-dichtheidsfunctionaaltheorie-berekeningen gefit. Het genduceerde multipooleffect bleek belangrijker te zijn dan de overlap van de elektronenwolken in de berekening op CS_2 dimeren. [62]

Een berekening van het derde-orde Raman spectrum met gebruik van de DRF model voor de susceptibiliteit werd uitgevoerd om het belang van de 'close collision' effecten te onderzoeken. De genduceerde-multipooleffecten bleken de intensiteit van de respons van intermoleculaire bewegingen te verzwakken. Dit heeft vooral belangrijke gevolgen voor de isotrope respons, waar de intensiteit behoorlijk overschat wordt door het dipool-genduceerd dipool model. Vergelijkbare effecten kunnen worden verwacht in de vijfde-orde respons. Aangezien deze response gevoeliger is voor lokale veldeffecten, is het te verwachten dat de 'close collision' effecten nog belangrijker zijn dan voor de derde-orde respons. [62] In verband met deze studie hebben we een onderzoek naar de invloed van overlap tussen de elektronenwolken in vloeibaar xenon uitgevoerd. Uit dit onderzoek bleek dat de overlap tussen de elektronenwolken in dit geval een grote rol speelt in niet alleen het isotrope gedeelte van de derde-orde respons, maar ook in het anisotrope gedeelte. In xenon worden deze allebei volledig bepaald door de intermoleculaire bewegingen. [65]

De lokale veldeffecten hebben een grote invloed op het spectrum, als de vloeistof verdund wordt. Dit is omdat de lokale veldeffecten door wisselwerking tussen de moleculen ontstaan en deze many-body effecten zijn afhankelijk van de waarschijnlijkheid van het vinden van moleculen binnen de afstand, waar de wisselwerking groot is. Hoe meer moleculen er deelnemen in een bepaalde beweging, hoe sneller de Raman respons van deze beweging verdwijnt als de vloeistof verdund wordt door een andere zwakkere wisselwerkende vloeistof. Simulaties zijn uitgevoerd op een gedealiseerd mengsel van koolstofdisulfide en 'spookmoleculen' met de zelfde dynamische eigenschappen als koolstofdisulfide maar geen moleculaire polariseerbaarheid. Dit maakt een studie van het effect van verdunning op een algemene manier mogelijk. De resultaten zijn vergeleken met experimentele metingen aan mengsels van koolstofdisulfide en alkanen, die in de laserspectroscopiegroep van deze universiteit zijn uitgevoerd. Er werd een duidelijk verschil tussen de gesimuleerde en gemeten spectra waargenomen. In een eerder experimenteel onderzoek was voorgesteld, dat het bijzondere gedrag van de experimentele respons door de vorming van klontjes koolstofdisulfide samengehouden door hun quadrupoolmoment, te verklaren was. [69] Door de eigenschappen van de spookmoleculen, zoals ladingen en moleculaire massa's, zijn alle mogelijke verklaringen behalve //n weerlegd. De zwakkere van der Waals krachten van de alkanen zijn de enige mogelijke verklaring voor de veranderingen van het spectrum wanneer koolstofdisulfide verdund wordt. [64]

Verder onderzoek naar de vijfde-orde spectra van CS_2 en de invloed van 'close collision' effecten op deze spectra zijn uitgevoerd. Dit onderzoek geeft de best mogelijke berekende spectra om de experimenten mee te vergelijken en om deze experimenten te verklaren. Uit deze berekeningen blijkt dat de 'close collision' effecten een belangrijk bijdrage aan het vijfde-orde spectrum geven.

Bibliography

[1] G. D. Billing and K. V. Mikkelsen. *Introduction to Molecular Dynamics and Chemical Kinetics*. John Wiley & Sons, New York, 1996.

[2] P. Debye. *Trans. Faraday Soc.*, **82**:265, (1942).

[3] M. G. Evans and M. Polanyi. *Trans. Faraday Soc.*, **34**:11, (1938).

[4] E. Eyring. *J. Chem. Phys.*, **3**:107, (1935).

[5] J. Franck and E. Rabinowitch. *Trans. Faraday Soc.*, **30**:120, (1934).

[6] R. F. Grote and J. T. Hynes. *J. Chem. Phys.*, **73**:2715, (1980).

[7] H. A. Kramers. *Physica*, **7**:284, (1940).

[8] R. A. Marcus. *J. Chem. Phys.*, **24**:966,979, (1956).

[9] R. A. Marcus. *J. Chem. Phys.*, **43**:679, (1965).

[10] R. A. Ogg and M. Polanyi. *Trans. Faraday Soc.*, **31**:604, (1935).

[11] L. Onsager. *Phys. Rev.*, **54**:554, (1938).

[12] M. Born. *Z. Phys.*, **1**:45, (1920).

[13] R. Brown. *Phil. Mag.*, **4**:161, (1828).

[14] R. Brown. *Ann. Phys. u. Chem.*, **14**:294, (1828).

[15] M. Gouy. *J. de Phys.*, **7**:561, (1888).

[16] A. Einstein. *Ann. d. Physik*, **17**:549, (1905).

[17] M. Smoluchowski. *Ann. d. Physik*, **21**:756, (1906).

[18] P. Langevin. *C. r. hebd. S'eance Acad. Sci.*, **146**:530, (1908).

[19] W. E. Morrell and J. H. Hildebrand. *J. Chem. Phys.*, **4**:224, (1936).

[20] N. Metropolis, A. W. Rosenbluth, M. N. Rosenbluth, A. H. Teller and E. Teller. *J. Chem. Phys.*, **21**:1087, (1953).

[21] N. Metropolis and S. Ulam. *J. Am. Stat. Ass.*, **44**:335, (1949).

[22] B. J. Alder and T. E. Wainwright. *J. Chem. Phys.*, **27**:1208, (1957).

[23] B. J. Alder and T. E. Wainwright. *J. Chem. Phys.*, **31**:459, (1959).

[24] A. Rahman. *Phys. Rev.*, **136**:A405, (1964).

[25] M. P. Allen and D. J. Tildesley. *Computer Simulation of Liquids*. Oxford University Press, Oxford, 1987.

[26] R. Car and M. Parrinello. *Phys. Rev. Lett.*, **55**:2471, (1985).

[27] E. L. Hahn. *Phys. Rev.*, **80**:580, (1950).

[28] J. B. Udganokar and R. L. Baldwin. *Nature*, **335**:694, (1988).

[29] H. Roder, G. A. Elove and S. W. Englander. *Nature*, **335**:700, (1988).

[30] M. Bycroft, A. Matouschek, J. T. Kellis, L. Serrano and A. R. Fersht. *Nature*, **346**:488, (1990).

[31] R. P. Feynman, F. L. Vernon and R. W. Hellwarth. *J. Appl. Phys.*, **28**:49, (1957).

[32] N. A. Kurnit, I. D. Abella and R. W. Hartmann. *Phys. Rev. Lett.*, **13**:567, (1964).

[33] T. W. Mossberg, A. M. Flusberg, R. Kachru and S. R. Hartmann. *Phys. Rev. Lett.*, **42**:1665, (1979).

[34] K. Duppen, D. P. Weitekamp and D. A. Wiersma. *Chem. Phys. Lett.*, **106**:147, (1984).

[35] Y. Tanimura and S. Mukamel. *J. Chem. Phys.*, **99**:9496, (1993).

[36] T. Steffen and K. Duppen. *Chem. Phys. Lett.*, **290**:229, (1998).

[37] A. Tokmakoff, M. J. Lang, X. L. Jordanides and G. R. Fleming. *Chem. Phys.*, **233**:231, (1998).

[38] T. Steffen and K. Duppen. *Phys. Rev. Lett.*, **76**:1224, (1996).

[39] A. Tokmakoff and G. R. Fleming. *J. Chem. Phys.*, **106**:2569, (1997).

[40] K. Tominaga and K. Yoshihara. *J. Chem. Phys.*, **104**:4419, (1996).

[41] D. A. Blank, L. J. Kaufman and G. R. Fleming. *J. Chem. Phys.*, **111**(7):3105, (1999).

[42] O. Golonzka, N. Demirdöven, M. Khalil and A. Tokmakoff. *J. Chem. Phys.*, **113**(22):9893, (2000).

[43] V. Astinov, K. J. Kubarych, C. J. Milne and R. J. D. Miller. *Optics Letters*, **25**(11):853, (2000).

[44] A. Astinov, K. J. Kubarych, C. J. Milne and R. J. Dwayne Miller. *Chem. Phys. Lett.*, **327**:334, (2000).

[45] K. J. Kubarych, C. J. Milne, S. Lin, V. Astinov and R. J. D. Miller. *J. Chem. Phys.*, **116**:2016, (2002).

[46] R. M. Hochstrasser. *Phys. Chem. Comm.*, **3**:U1, (2002).

[47] P. Hamm, M. H. Lim and R. M. Hochstrasser. *J. Phys. Chem. B*, **102**:6123, (1998).

[48] S. Woutersen and P. Hamm. *J. Chem. Phys.*, **115**:7737, (2001).

[49] Y. R. Shen. *The Principles of Nonlinear Optics*. John Wiley & Sons, New York, U.S.A., 1984.

[50] S. Mukamel. *Principles of Nonlinear Optical Spectroscopy*. Oxford University Press, New York, 1995.

[51] J. G. Snijders. *Quantum Statistical Response Functions*. Groningen, The Netherlands, 1998.

[52] T. Steffen. *Impulsive temporally two-dimensional Raman scattering*. Ph.d., Rijksuniversiteit Groningen, 1998.

[53] A. Tokmakoff. *J. Chem. Phys.*, **105**:1, (1996).

[54] A. Tokmakoff. *J. Chem. Phys.*, **105**:13, (1996).

[55] T. l. C. Jansen, J. G. Snijders and K. Duppen. *J. Chem. Phys.*, **113**(1):307, (2000).

[56] T. l. C. Jansen, J. G. Snijders and K. Duppen. *J. Chem. Phys.*, **114**:10910, (2001).

[57] S. Mukamel, V. Khidekel and V. Chernyak. *Phys. Rev. E*, **53**:R1, (1996).

[58] S. Saito and I. Ohmine. *J. Chem. Phys.*, **108**:240, (1998).

[59] A. Ma and R. M. Stratt. *Phys. Rev. Lett.*, **85**:1004, (2000).

[60] B. T. Thole. *Chem. Phys.*, **59**:341, (1981).

[61] P. Th. van Duijnen and M. Swart. *J. Phys. Chem. A*, **102**:2399, (1998).

[62] T. l. C. Jansen, M. Swart, L. Jensen, P. Th. van Duijnen, J. G. Snijders and K. Duppen. *J. Chem. Phys.*, **116**:3277, (2002).

[63] E. Runge and E. K. U. Gross. *Phys. Rev. Lett.*, **52**:997, (1984).

[64] T. l. C. Jansen, A. Pugzlys, G. D. Crînguş, J. G. Snijders and K. Duppen. *J. Chem. Phys.*, **116**:9383, (2002).

[65] N. H. Boeijenga, A. Pugzlys, T. l. C. Jansen, J. G. Snijders and K. Duppen. *J. Chem. Phys.*, **117**:1181, (2002).

[66] C. V. Raman. *Indian J. Phys.*, **2**:387, (1928).

[67] C. V. Raman and K. S. Krishnan. *Nature*, **121**:501, (1928).

[68] D. McMorrow, N. Thantu, J. S. Melinger, S. K. Kim and W. T. Lotshaw. *J. Phys. Chem.*, **100**:10389, (1996).

[69] T. Steffen, N. A. C. M. Meinders and K. Duppen. *J. Phys. Chem. A*, **102**:4213, (1998).

[70] S. Ruhman, L. R. Williams, A. G. Joly and K. A. Nelson. *J. Phys. Chem.*, **91**:2237, (1987).

[71] A. Waldman, U. Banin, E. Rabani and S. Ruhman. *J. Phys. Chem.*, **96**:10840, (1992).

146

[72] T. Steffen, J. T. Fourkas and K. Duppen. *J. Chem. Phys.*, **105**:7364, (1996).

[73] M. Born and J. R. Oppenheimer. *Ann. der Phys.*, **84**:457, (1927).

[74] D. A. Blank, L. J. Kaufman and G. R. Fleming. *J. Chem. Phys.*, **113**(2):771, (2000).

[75] L. J. Kaufman, D. A. Blank and G. R. Fleming. *J. Chem. Phys.*, **114**:2312, (2001).

[76] N. W. Ashcroft and N. D. Mermin. *Solid State Physics*. Saunders College, Philadelphia, 1987.

[77] K. Kiyohara, K. Kamada and K. Ohta. *J. Chem. Phys.*, **112**(14):6338, (2000).

[78] D. A. Kleinman. *Phys. Rev.*, **126**:1977, (1962).

[79] P. N. Butcher and D. Cotter. *The Elements of Nonlinear Optics*, volume 9 of *Cambridge Studies in Modern Optics*. Cambridge University Press, Cambridge, 1990.

[80] R. N. Zare. *Angular Momentum*. John Wiley & Sons, New York, 1987.

[81] K. Tominaga and K. Yoshihara. *Phys. Rev. Lett.*, **74**:3061, (1995).

[82] T. Steffen and K. Duppen. *J. Chem. Phys.*, **106**:3854, (1997).

[83] L. J. Kaufman, J. Heo, G. R. Fleming, J. Sung and M. Cho. *Chem. Phys.*, **266**:251, (2001).

[84] T. Steffen and K. Duppen. *Chem. Phys. Lett.*, **273**:47, (1997).

[85] A. Tokmakoff, M. J. Lang, D. S. Larsen and G. R. Fleming. *Chem. Phys. Lett.*, **272**:48, (1997).

[86] R. A. Denny and D. R. Reichman. *Phys. Rev. E.*, **63**:065101, (2001).

[87] R. L. Murry, J. T. Fourkas and T. Keyes. *J. Chem. Phys.*, **109**:7913, (1998).

[88] D. J. Ulness, J. C. Kirkwood and A. C. Albrecht. *J. Chem. Phys.*, **108**:3897, (1998).

[89] J. C. Kirkwood, D. J. Ulness and A. C. Albrecht. *Chem. Phys. Lett.*, **293**:417, (1998).

[90] R. C. Weast, editor. *CRC Handbook of Chemistry and Physics*. CRC Press, Boca Raton, 63th edition, 1983-1984.

[91] Y. Tanimura and T. Steffen. *J. Phys. Soc. Jp.*, **69**(12):4095, (2000).

[92] T. Steffen and Y. Tanimura. *J. Phys. Soc. Jp.*, **69**(9):3115, (2000).

[93] K. Okumura and Y. Tanimura. *J. Chem. Phys.*, **106**:1687, (1997).

[94] K. Okumura and Y. Tanimura. *J. Chem. Phys.*, **107**:2267, (1997).

[95] L. C. Geiger and B. M. Ladanyi. *J. Chem. Phys.*, **87**:191, (1987).

[96] L. C. Geiger and B. M. Ladanyi. *Chem. Phys. Lett.*, **159**:413, (1989).

[97] B. M. Ladanyi. *Chem. Phys. Lett.*, **121**:351, (1985).

[98] P. A. Madden. Interaction-induced, subpicosecond phenomena in liquids. D. H. Auston and K. B. Eisenthal, editors, *Ultrafast Phenomena*, volume IV, page 244. Springer, Berlin, (1985).

[99] A. Ma and R. M. Stratt. *J. Chem. Phys.*, **116**:4962, (2002).

[100] J. Cao, J. Wu and S. Yang. *J. Chem. Phys.*, **116**:3760, (2002).

[101] S. Saito and I. Ohmine. *Phys. Rev. Lett.*, **88**:207401, (2002).

[102] R. M. Stratt. *Acc. Chem. Res.*, **28**(5):201, (1995).

[103] R. L. Murry, J. T. Fourkas and T. Keyes. *J. Chem. Phys.*, **109**:2814, (1998).

[104] X. Ji, H. Alhborn, B. Space, P. B. Moore, Y. Zhou, S. Constantine and L. D. Ziegler. *J. Chem. Phys.*, **112**:4186, (2000).

[105] T. Keyes. *J. Chem. Phys.*, **106**:46, (1997).

[106] T. Keyes and J. T. Fourkas. *J. Chem. Phys.*, **112**:287, (2000).

[107] A. Ma and R. M. Stratt. *J. Chem. Phys.*, **116**:4972, (2002).

[108] J. Cao, J. Wu and S. Yang. *J. Chem. Phys.*, **116**:3739, (2002).

[109] R. van Zon and J. Schofield. *Phys. Rev. E*, **65**:011106, (2002).

[110] R. van Zon and J. Schofield. *Phys. Rev. E*, **65**:011107, (2002).

[111] W. Gadomski and B. Ratajska-Gadomska. *Phys. Rew. A*, **34**:1277, (1986).

[112] B. Ratajska-Gadomska, W. Gadomski, P. Wiewior and C. Radzewicz. *J. Chem. Phys.*, **108**:8489, (1998).

[113] B. Ratajska-Gadomska. *J. Chem. Phys.*, **116**:4563, (2002).

[114] H. Goldstein. *Classical Mechanics*. Addison-Wesley Publishing Company, Inc., Reading, Massachusetts, 1950.

[115] G. Ma, L. Guo, J. Mi, Y. Liu, S. Qian, J. Liu, G. He, Y. Li and R. Wang. *Physica B*, **305**:147, (2001).

[116] G. Placzek. E Marx, editor, *Handbuch der Radiologie*, volume VI, Pt. 2. Academische Verlagsgesellschaft, Leipzig, (1934).

[117] C. Kalpouzos, D. McMorrow, W. T. Lotshaw and G. A. Kenney-Wallace. *Chem. Phys. Lett.*, **150**:138, (1988).

[118] C. Kalpouzos, D. McMorrow, W. T. Lotshaw and G. A. Kenney-Wallace. *Chem. Phys. Lett.*, **155**:240, (1989).

[119] J. A. Bucaro and T. A. Litovitz. *J. Chem. Phys.*, **54**:3846, (1971).

[120] T. Hattori and T. Kobayashi. *J. Chem. Phys.*, **94**(5):3332, (1991).

[121] A. Idrissi, M. Ricci, P. Bartolini and R. Righini. *J. Chem. Phys.*, **111**(9):4148, (1999).

[122] D. McMorrow, N. Thantu, V. Kleiman, J. S. Melinger and W. T. Lotshaw. *J. Phys. Chem. A*, **105**(34):7960, (2001).

[123] F. Jensen. *Introduction to Computational Chemistry*. Wiley & Sons., Chicester, UK, 1999.

[124] P. Moore, A. Tokmakoff, T. Keyes and M. D. Fayer. *J. Chem. Phys.*, **103**(9):3325, (1995).

[125] P. Moore and B. Space. *J. Chem. Phys.*, **107**:5635, (1997).

[126] X. Ji, H. Alhborn, B. Space and P. B. Moore. *J. Chem. Phys.*, **113**(19):8693, (2000).

[127] C. J. F. Böttcher and P. Bordewijk. *Theory of electric polarization*. Elsevier, Amsterdam, 1978.

[128] M. Swart, P. Th. van Duijnen and J. G. Snijders. *J. Mol. Struct. (THEOCHEM)*, **458**:11, (1999).

[129] W. H. Press, S. A. Teukolsky, W. T. Vetterling and B. P. Flannery. *Numerical Recipes in C*. Cambridge University Press, Cambridge, second edition, 1992.

[130] J. Applequist, J. R. Carl and K. Fung. *J. Am. Chem. Soc.*, **94**:2952, (1972).

[131] J. Applequist. *Chem. Phys.*, **85**:279, (1984).

[132] J. Applequist. *J. Chem. Phys.*, **83**:809, (1985).

[133] H. Stassen, Th. Dorfmüller and B. M. Ladanyi. *J. Chem. Phys.*, **100**(9):6318, (1994).

[134] J. A. C. Rullmann and P. Th. van Duijnen. *Mol. Phys.*, **63**:451, (1988).

[135] F. Kootstra, P. L. de Boeij and J. G. Snijders. *J. Chem. Phys.*, **112**(15):6517, (2000).

[136] S. J. A. van Gisbergen, J. G. Snijders and E. J. Baerends. *Comp. Phys. Comm.*, **118**:119, (1999).

[137] S. J. A. van Gisbergen, F. Kootstra, P. R. T. Schipper, O. V. Gritsenko, J. G. Snijders and E. J. Baerends. *Phys. Rev.*, **A57**:2556, (1998).

[138] R. Telesca, H. Bolink, S. Yunoki, G. Hadziioannou, P. Th. van Duijnen, H. T. Jonkman, J. G. Snijders and G. A. Sawatzky. *Phys. Rev. B*, **63**:155112, (2001).

[139] M. Puranik, S. Umapathy, J. G. Snijders and J. Chandrasekhar. *J. Chem. Rhys.*, **115**:6106, (2001).

[140] S. J. A. van Gisbergen, J. G. Snijders and E. J. Baerends. *J. Chem. Phys.*, **109**(24):10657, (1998).

[141] S. J. A. van Gisbergen, J. G. Snijders and E. J. Baerends. *J. Chem. Phys.*, **109**(24):10644, (1998).

[142] V. P. Osinga, Gisbergen. S. J. A. van, J. G. Snijders and E. J. Baerends. *J. Chem. Phys.*, **106**:5091, (1996).

[143] F. Kootstra, P. L. de Boeij and J. G. Snijders. *Phys. Rev. B*, **62**:7071, (2000).

[144] N. H. Boeijenga. *Finite Field Calculations of the Nonlinear Raman Response of Liquid Xenon.* Master thesis, Rijksuniversiteit Groningen, 2001.

[145] C. Hättig, H. Larsen, J. Olsen, P. Jørgensen, H. Koch, B. Fernández and A. Rizzo. *J. Chem. Phys.*, **111**:10099, (1999).

[146] H. Koch, C. Hättig, H. Larsen, J. Olsen, P. Jørgensen, B. Fernández and A. Rizzo. *J. Chem. Phys.*, **111**:10108, (1999).

[147] G. Maroulis and A. Haskopoulos. *Chem. Phys. Lett.*, **349**:335, (2001).

[148] E. J. Baerends, D. E. Ellis and P. Ros. *Chem. Phys.*, **2**:41, (1973).

[149] G. te Velde and E. J. Baerends. *J. Comput. Phys.*, **99**:41, (1992).

[150] C. F. Guerra, O. Visser, J. G. Snijders, G. te Velde and E. J. Baerends. Parallelisation of the amsterdam density functional programme. E. Clementi and C. Corongiu, editors, *Methods and Techniques in Computational Chemistry, METECC-5.* STEF, Cagliari, Italy, (1995).

[151] S. H. Vosko, L. Wilk and M. Nusair. *Can. J. Phys.*, **58**:1200, (1980).

[152] G. te Velde, F. M. Bickelhaupt, E. J. Baerends, C. Fonseca Guerra, S. J. A. van Gisbergen, J. G. Snijders and T. Ziegler. *J. Comp. Chem.*, **22**:931, (2001).

[153] R. van Leeuwen and E. J. Baerends. *Phys. Rev.*, **A49**:2421, (1994).

[154] M. P. Bogaard, A. D. Buckingham, R. K. Pierens and A. H. White. *J. Chem. Soc. Faraday Trans.*, **74**:3008, (1978). Gasphase polarizabilities for numerous molecules.

[155] J. P. Perdew, J. A. Chevary, S. H. Vosko, K. A. Jackson, M. R. Pederson, D. J. Singh and C. Fiolhais. *Phys. Rev. B*, **46**:6671, (1992).

[156] A. J. Stone. *The theory of intermolecular forces*, volume 32 of *International series of monographs on chemistry.* Oxford University Press, Oxford, 1996.

[157] H. Torii. *Chem. Phys. Lett.*, **353**:431, (2002).

[158] V. Chernyak and S. Mukamel. *J. Chem. Phys.*, **108**:5812, (1998).

[159] H. J. C. Berendsen, D. van der Spoel and R. van Drunen. *Comput. Phys. Commun.*, **91**:43, (1995).

151

[160] R. W. Hockney. *Methods Comput. Phys.*, **9**:136, (1970).

[161] L. Verlet. *Phys. Rev.*, **159**:98, (1967).

[162] H. J. C. Berendsen, J. P. M. Postma, W. F. van Gunsteren, A. DiNola and J. R. Haak. *J. Chem. Phys.*, **81**:3684, (1984).

[163] G. Herzberg. *Molecular spectra and Molecular Structure II. Infrared and Raman spectra.* D. van Nostrand Company, INC., Princeton, 1964.

[164] J. P. Ryckaert, G. Ciccotti and H. J. C. Berendsen. *J. Comp. Phys.*, **23**:327, (1977).

[165] D. J. Tildesley and P. A. Madden. *Mol. Phys.*, **42**:1137, (1981).

[166] E. Burgos and R. Righini. *Chem. Phys. Lett.*, **96**:584, (1983).

[167] P. Th. van Duijnen, F. Grozema and M. Swart. *J. Mol. Struct.*, **464**:191, (1999).

[168] P. Th. van Duijnen. Private communication, (2001).

[169] D. J. Tildesley and P. A. Madden. *Mol. Phys.*, **48**:129, (1983).

[170] J. Etchepare, G. A. Kenny-Wallace, G. Grillon, A. Migus and J. P. Chambaret. *IEEE J. Quant. Electron.*, **QE-18**:1826, (1982).

[171] J. Etchepare, G. Grillon, J. P. Chambaret, G. Hamoniaux and A. Orszag. *Optical Commun.*, **63**:329, (1987).

[172] S. Kinoshita, Y. Kai and Y. Watanabe. *Chem. Phys. Lett.*, **301**:183, (1999).

[173] S. Kinoshita, Y. Kai, Y. Watanabe and J. Watanabe. *J. Luminescence*, **87-89**:706, (2000).

[174] D. McMorrow, W. T. Lotshaw and G. A. Kenney-Wallace. *IEEE J. Quantum Elec.*, **24**(2):443, (1988).

[175] Q.-H. Xu, Y.-Z. Ma and G. R. Fleming. *Chem. Phys. Lett.*, **338**:254, (2001).

[176] R. L. Murry, J. T. Fourkas, W.-X. Li and T. Keyes. *Phys. Rev. Lett.*, **83**:3550, (1999).

[177] P. A. Madden and D. J. Tildesley. *Mol. Phys.*, **55**:969, (1985).

[178] P. Moore and T. Keyes. *J. Chem. Phys.*, **100**(9):6709, (1994).

[179] P. B. Moore, X. Ji, H. Ahlborn and B. Space. *Chem. Phys. Lett.*, **296**:259, (1998).

[180] M. C. C. Ribeiro and P. S. Santos. *J. Mol. Liquids*, **68**:33, (1996).

[181] H. Stassen and W. A. Steele. *J. Chem. Phys.*, **110**:7382, (1999).

[182] S.-B. Zhu, J. Lee and G. W. Robinson. *Phys. Rev. A*, **38**:5810, (1988).

[183] T. Nakagawa, H. Urakawa, K. Kajiwara and S. Hayashi. *J. Mol. Struc.*, **429**:23, (1998).

[184] M. Khalil, N. Demirdöven, O. Golonzka, C. J. Fecko and A. Tokmakoff. *J. Phys. Chem. A*, **104**:5711, (2000).

[185] M. Khalil, O. Golonzka, N. Demirdöven, C. J. Fecko and A. Tokmakoff. *Chem. Phys. Lett.*, **321**:231, (2000).

[186] T. Steffen and K. Duppen. *Chem. Phys.*, **233**:267, (1998).

[187] K. J. Kubarych, C. J. Milne, S. Lin and R. J. D. Miller. *Diffractive optics based heterodyne detected Dutch Cross fifth-order Raman. 13th International Conference on Ultrafast Phenomena*, volume XIII of *Ultrafast Phenomena*, Vancouver, 2002. Springer Verlag.

[188] K. Kubarych, C. J. Milne, S. Lin and R. J. D. Miller. *Appl. Phys. B*, (submitted).

[189] L. J. Kaufman, J. Heo, L. D. Ziegler and G. R. Fleming. *Phys. Rev. Lett.*, **88**:207402, (2002).

[190] M. Neelakandan, D. Pant and E. L. Quitevis. *Chem. Phys. Lett.*, **265**:283, (1997).

[191] A. Idrissi, P. Bartolini, M. Ricci and R. Righini. *J. Chem. Phys.*, **114**(15):6774, (2001).

[192] D. McMorrow and W. T. Lotshaw. *Chem. Phys. Lett.*, **201**:369, (1993).

[193] U. Mittag, J. Samios and Th. Dorfmüller. *Mol. Phys.*, **66**(1):51, (1989).

[194] U. Mittag, J. Samios and Th. Dorfmüller. *Mol. Phys.*, **81**(5):1143, (1994).

[195] D. McMorrow and W. T. Lotshaw. *Chem. Phys. Lett.*, **174**:85, (1990).

[196] D. McMorrow and W. T. Lotshaw. *J. Phys. Chem.*, **95**:10395, (1991).

[197] D. J. Kane and R. Trebino. *IEEE J. Quantum Electron.*, **29**:571, (1993).

[198] R. Trebino and D. J. Kane. *J. Opt. Soc. Am.*, **A10**:1101, (1993).

[199] P. van der Ploeg and H. J. C. Berendsen. *J. Chem. Phys.*, **76**:3271, (1982).

[200] W. S. Gornall, H. E. Howard-Lock and B. P. Stoicheff. *Phys. Rev. A*, **1**:1288, (1970).

[201] L. Frommhold, K. H. Hong and M. H. Proffitt. *Mol. Phys.*, **35**:691, (1978).

[202] P. A. Fleury, J. M. Worlock and H. L. Carter. *Phys. Rev. Lett.*, **30**:591, (1973).

[203] B. I. Greene, P. A. Fleury, H. L. Carter, Jr. and R. C. Farrow. *Phys. Rev. A*, **29**(1):271, (1984).

[204] E. Radzio and J. Andzelm. *J. Comp. Chem.*, **8**:117, (1987).

[205] S. Faas, J. H. van Lenthe and J. G. Snijders. *Mol. Phys.*, **98**:1467, (2000).

[206] N. Runeberg and P. Pyykkö. *Int. J. Quantum Chem.*, **66**:131, (1998).

[207] C. H. Change, M. Pelisser and P. H. Durand. *Physica Scripta*, **34**:394, (1986).

[208] J. L. Heully, I. Lindgren, E. Lindroth, S. Lundquist and Mårtensson-Pendrill. *J. Phys. B*, **19**:2799, (1986).

[209] E. van Lenthe, E. J. Baerends and J. G. Snijders. *J. Chem. Phys.*, **99**:4597, (1993).

[210] E. van Lenthe, E. J. Baerends and J. G. Snijders. *J. Chem. Phys.*, **101**:1272, (1994).

[211] C. Chui and F. B. Canfield. *Trans. Faraday Soc.*, **67**:2933, (1971).

[212] A. Tortschanoff and S. Mukamel. *J. Chem. Phys.*, **116**:5007, (2002).

[213] M. Cho. *PhysChemComm*, **5**:40, (2002).

[214] T. l. C. Jansen, K. Duppen and J. G. Snijders. The finite field approach to the third- and fifth-order raman response of liquids. M. Papadopoulos, editor, *The NLO properties of materials (gases, liquids, solids)*.
(accepted).

List of publications

This is a list of papers published or prepared during the work on this thesis. The reference nunmber of each paper in this thesis and the chapters, where the material from each paper can be found, is given. Furthermore, literature citing the given paper is listed.

T. l. C. Jansen, J. G. Snijders, and K. Duppen, J. Chem. Phys. **113**, 307 (2000),
The 3rd- and 5th-order nonlinear Raman response of liquid CS_2 calculated using a finite field nonequilibrium Molecular Dynamics method
(Ref. 55, Chapters 2,3,4,6,7, Cited in Refs. $45, 56, 62, 64, 75, 91, 92, 99-101, 107, 108, 189, 212, 213$)

T. l. C. Jansen, J. G. Snijders, and K. Duppen, J. Chem. Phys. **114**, 10915 (2001),
Interaction induced effects in the nonlinear Raman response of liquid CS_2: a finite field nonequilibrium molecular dynamics approach
(Ref. 56, Chapters 2,3,4,6,7, Cited in Refs. $45, 62, 64, 101, 107, 189, 212, 213$)

T. l. C. Jansen, M. Swart, L. Jensen, P. T. van Duijnen, J. G. Snijders, and K. Duppen, J. Chem. Phys. **116**, 3277 (2002),
Collision effects in the nonlinear Raman response of liquid carbon disulfide
(Ref. 62, Chapters 4,5,7, Cited in Ref. $64, 65$)

T. l. C. Jansen, A. Pugzlys, G. D. Grînguş, J. G. Snijders, and K. Duppen, J. Chem. Phys. **116**, 9383 (2002),
Many-body effects in the stimulated Raman response of binary mixtures: A comparizon between theory and experiment
(Ref. 64, Chapter 8)

N. H. Boeijenga, A. Pugzlys, T. l. C. Jansen, J. G. Snijders, and K. Duppen, J. Chem. Phys. **117**, 1181 (2002),
Liquid xenon as an ideal probe for many-body effects in impulsive Raman scattering
(Ref. 65, Chapter 9)

T. l. C. Jansen, J. G. Snijders, and K. Duppen, accepted.
The finite field approach to the third- and fifth-order Raman response of liquids in *The NLO properties of materials (gases, liquids, solids)*, edited by M. Papadopoulos
(Ref. 214)

T. l. C. Jansen, K. Duppen and J. G. Snijders, in preparation.
Close collisions in the fifth-order Raman response of liquid Carbon disulfide
(Chapter 7)

Acknowledgement / Dankwoord

This thesis is the result of almost four years work in the theoretical chemistry group at Rijksuniversiteit Groningen. Working on this project has been exciting, interesting and sometimes frustrating, the last especially when the experimental truth seemed to change from time to time. Here I wish to thank everybody, who has contributed directly or indirectly to this work and made my stay in Groningen unforgettable.

Allereerst wil ik mijn promotor Jaap G. Snijders bedanken. Ik ben erg blij, dat ik de mogelijkheid kreeg om hier in Groningen mijn promotieonderzoek te doen. Ik ben ook erg blij met Jaap's grote vertrouwen in me en met de vrijheid die hij me heeft gegeven. Het lenen van zijn creditcard en auto was ook een grote hulp in het begin. Promotor Koos Duppen ben ik dankbaar voor zijn altijd zorgvuldige en uitgebreide correcties van onze artikels en het proefschrift. Zijn ervaring en inzicht in de niet-lineaire spectroscopie is ook een hele grote hulp geweest.

Jeg er min tidligere specialevejleder Sten Rettrup taknemmelig, der ikke blot introducerede mig til Jaap, men har ogs' fungeret som kontaktperson til Forskerakademiet under mit ph.d. forl¿b. Jeg tror heller ikke vi glemmer vores f$\leq llesbusturetilogiGroningenligemeddetsamme.Der deafatbes > geStenogLaboratorietiK > benhavn, hvordetharv \leq retenstorforn > jelseatfort \leq lleomudviklingenimitprojekt.$

Prof. dr. J. Knoester, prof. dr. W. J. Briels en prof. dr. H. Berendsen wil ik danken voor het zitting nemen in de leescommissie, en het goed bestuderen van het manuscript en het maken van correcties en suggesties.

I would like to thank Yoshitaka Tanimura for the fantastic treatment he gave me during my visit in Japan. He was an excellent guide not only in the city of Nara, but also in the original Japanese dishes. I am grateful to Shinji Saito for inviting me to visit the University of Nagoya to discuss my work. Thomas Steffen, mijn voorganger in Groningen, hoewel voornamelijk experimentalist, ben ik dankbaar voor de contacten, die hij me heeft geholpen te maken. Ik ben ook dankbaar voor de gedachten en ideeŒn over verschillende

aspecten van het werk, die hij met me heeft gedeeld. I would like to thank Shaul Mukamel for his invitation to come to Rochester and for our discussions about the Finite Field approach.

Ik ben Freddie Kootstra erg dankbaar voor de hulp en steun, die hij me heeft gegeven vanaf mijn eerste dag in Groningen, toen ik onder zijn dak sliep, tot de laatste periode, waarin hij me op de weg door de bureaukratie van de universiteit heeft geholpen. Bovendien heb ik veel leuke mensen door Freddie kennen geleerd en zonder hem zou mijn tijd in Groningen minder mooi zijn geweest. Mijn studente Nienke Boeijenga, die hard heeft gewerkt met vloeibaar xenon, verdient ook mijn uiterste dankbaarheid. Ze heeft ook naast wetenschappelijke inspanningen leven in onze kamer gebracht met haar creativiteit en de goudvissen. Ik ben ook blij, dat ze me als paranimf bijstaat tijdens de verdediging van dit proefschrift. Audrius Pugzlys, je hebt vele uren in het laboratorium voor me gestaan en jouw optimisme heeft ons ver gebracht samen met Gheorghe Dan Crînguş. Paul de Boeij en Lasse Jensen, ben ik jullie niet alleen dankbaar voor vele leuke spelletjes en bioscoopavonden, maar ook voor jullie bijdrage met ideeŒn en discussies, die me verder heeft gebracht met mijn projekt op moeilijke momenten. Ik ben Lasse ook dankbaar, dat hij me als paranimf bijstaat tijdens de verdediging van dit proefschrift. Mijn kamergenoot, Marcel Swart, ben ik dankbaar voor zijn hulp op computergebied, speciaal in het begin, en voor het gezelschap. I would like to thank Rosanna Telesca for her fruit- and tireless efforts setting me up with the local beauties and for teasing me as if I was her own brother.

De aio's van Theoretische Chemie, Alexandrina Stoyanova, Arjan Berger, Liviu Hozoi en Meta van Faassen, wil ik ook bedanken voor hun bijdrage aan de goede sfeer in onze groep. En tak skal der ogs' lyde til Alex de Vries for de hyggelige samtaler b'de p' Dansk og p' Hollandsk. Van de vaste staf binnen de Basisenheid wil ik de volgende mensen bedanken: Robert van Leeuwen, Ria Broer, Piet van Duijnen en Johan Heijnen. Verder ben ik onze secretaresse Henriette van Mil-Boddeveld dankbaar voor haar hulp met het regelen van reizen en financiŒle zaken. I would like to thank some of our foreign visitors. Especially Mrinalini Puranik, who cooked original indian food for me and with who I shared many interresting conversations. I also want to thank her for the guided tour in Princeton. Markus Pernpointer shared office with me as well as some of his experiences from New Zealand.

Anton Feenstra van de MD groep ben ik dankbaar voor zijn hulp met het gebruik van GROMACS in het begin van het onderzoek.

Buiten de kring van scheikunde wil ik ook mijn Unihockey vrienden in Groningen en de

rest van Nederland bedanken. Bedankt voor de vele leuke toernooien en borrels. Ik hoop dat onze club U.C. Faceoff vele nieuwe leden zal krijgen ook zonder mij in de PR-commissie, en dat onze website 'www.ucfaceoff.nl' ook goed bezocht zal worden.

Verder wil ik de 'aio dames' bedanken voor de vele leuke activiteiten en speciaal mijn zwemvriendinnen, Joanneke Prenger en Maaike Pulles. De leuke uren in de kroeg of op het terras met Laura Sabourin zal ik niet vergeten. Pytsje van der Veen ben ik erg dankbaar voor onze leuke gespreken, het goede gezelschap en haar correctie van de Nederlandse samenvatting.

Mine danske venner, vil jeg ogs' takke for ikke at have glemt mig, n'r der skulle inviteres til fest og komsammen i det danske, selvom jeg langtfra altid kunne komme.

Gennem min tid som ph.d. studerende har min familie ogs' $v \leq rettiluvurderligst >$ $tte.Minmormor, Marie-Louise, hars'ledess > rgetforkostoglogip'minebes > giK >$ $benhavn.Minefor \leq ldreKimogAnneerjegtaknemmeligforderesst > ttegennemdesidstefire'rogfor$ $sningenp'detdanskeresum/.Mins > sterLouiseoghendesfamilieSara, FridaogJensharogs'v \leq$ $rettilstorst > tteselvom'yndlingsonkel'harsiddetidetstoreudland.$

Tilsidst vil jeg gerne takke Forskerakademiet, senere kaldet Forskeruddannelsesr'det, for ph.d.-stipendiet til de f¿rste tre 'r af mit ph.d.-forl¿b samt $d\leq kningafuddannelsesm \leq$ $ssigeudgifterialle fire'r.BirgitChristensen, TinnaMeyerogAnjaE.Rasmussenskalogs'havetakforde$

Bedankt allemaal

<div align="right">
Thomas la Cour Jansen

Juli 2002
</div>

Curriculum vitae

25 nov 1974   Geboren te Gentofte.

1990 - 1993   Vooropleiding:
              Gymnasium,
              VUC,
              Vordingborg.

1993 - 1998   Academische opleiding:
              Scheikunde,
              Københavns Universitet,
              København.

1998 - 2002   Promotie onderzoek:
              Theoretische Chemie,
              Rijksuniversiteit Groningen,
              Groningen.